The dynamics of charge-density waves

G. Grüner

Department of Physics and Solid State Science Center, University of California, Los Angeles, California 90024

In many materials with a highly anisotropic band structure, electron-phonon interactions lead to a novel type of ground state called the charge-density wave. The condensate is pinned to the underlying lattice by impurities and by boundary effects, but can, even for small electric fields, carry current in a fashion originally envisioned by Fröhlich. This review discusses some of the underlying theories and the main experimental observations on this new collective transport phenomenon. The frequency- and electric-field-dependent conductivity, current oscillations, electric-field-dependent transport coefficients and elastic properties, together with nuclear-magnetic-resonance experiments, provide clear evidence for a translational motion of the condensate. Various theories, involving classical and quantum-mechanical concepts, are able to account for a broad variety of experimental findings, which were also made in the presence of combined dc and ac fields.

CONTENTS

I. INTRODUCTION

More than 30 years have elapsed since the basic concepts of the phenomenon which is the subject of this review have surfaced. It was first pointed out by Peierls (1955) that a one-dimensional metal coupled to the underlying lattice is not stable at low temperatures. The ground state of the coupled electron-phonon system is characterized by a gap in the single-particle excitation spectrum and by a collective mode formed by electron-hole pairs involving the wave vector $q=2k_F$. The charge density associated with the collective mode is given by

$$\rho(\mathbf{r})=\rho_0+\rho_1\cos(2\mathbf{k}_F\cdot\mathbf{r}+\varphi)\ , \tag{1.1}$$

where ρ_0 is the unperturbed electron density of the metal, and the condensate is called the charge-density wave (CDW). As in superconductors, the order parameter is complex and the phase φ of the condensate is of fundamental importance; its time and spatial derivatives are related to the electric current and to the condensate density. As noted by Fröhlich (1954), in the absence of pinning and damping, the condensate can carry current leading to superconductivity.

These early ideas resurfaced when the first materials with highly anisotropic crystal and electronic structures became available. The formation of charge-density-wave ground states is by now well documented in a broad range of so-called low-dimensional solids. While some evidence for collective dynamical effects has been found by optical and dielectric measurements in certain organic materials, and also in the pseudo-organic compound potassium platinocyanide called KCP (see, for example, Devreese, Evrard, van Doren, 1979), transport phenomena clearly associated with the dynamics of the collective mode have been found to date mainly in various inorganic linear-chain compounds. Moving CDW's were perhaps first observed by Fogle and Perlstein (1972), who found nonlinear electrical conduction at low electric fields in the compound $K_{0.3}MoO_3$, called the blue bronze, at temperatures below a metal-insulator transition. While this observation received little attention, experiments on nonlinear conduction in the material $NbSe_3$, together with the strongly anomalous microwave conductivity (Monceau *et al.*, 1976), clearly demonstrated the collective nature of the electrical conduction process simply because the energy scale associated with the applied dc field or ac frequency was orders of magnitude smaller than those which would lead to E- and ω-dependent single-particle conduction.

In contrast to superconductors, the phase excitations of the collective mode are gapless. Consequently, electrostatic potentials (due to impurities, grain boundaries, surface effects, etc.) break the translational symmetry and lead to the pinning of the collective mode. This results in a nonconducting but highly polarizable ground state and,

in the case of random impurity distributions, in the absence of long-range order. For weak pinning, the response of the system to dc and ac excitations is dominated by the dynamics of the collective mode with single-particle effects occurring only at optical frequencies. This leads to a strongly frequency-dependent response in the radio frequency to millimeter wave range and, in moderate dc electric fields, to a current-carrying state as originally envisioned by Fröhlich. The discovery of other inorganic linear-chain compounds with a CDW ground state and with an anomalous response to combinations of dc and ac excitations led to the rapid development of the field and to a dazzling variety of experimental observations, only partially accounted for by various theories at present.

This paper gives an overview of the experimental state of affairs, starting with a description of the charge-density-wave ground state, and a short overview of the materials and phase transitions. This is followed by a summary of the fundamental experimental observations on electrical conductivity, other transport coefficients, elastic properties, and experiments involving local probes. Pinning is a central concept that leads to the absence of a dc conduction and to the nonlinear and frequency-dependent phenomena; the broad variety of pinning centers is responsible for the large variation of observations concerning the details of the nonlinear *I-V* characteristics, and, most probably, for differences in the observed ac response and interference phenomena. The various pinning mechanisms will be discussed in depth, and this is followed, after a short review of theories, by the detailed discussion of the frequency- and field-dependent response and various phenomena that occur in the presence of joint ac and dc excitations. Sections VII and VIII discuss two special topics where the dynamics of charge-density waves were also used to address broader questions concerning the dynamics of driven, many-degrees-of-freedom systems. The two sections, when contrasted, also point to the breadth of phenomena that are observed and that are related to the dynamics of charge-density waves.

Several reviews have appeared recently that discuss the early developments and various aspects of the field (Fleming, 1981; Grüner, 1983a, 1983b, 1983c; Ong, 1983; Grüner and Zettl, 1985; Gill, 1986a, 1986b; Monceau, 1986) which is also the subject of a recent monograph (Monceau, 1986) and proceedings (*Charge Density Waves in Solids,* edited by Gy. Hutiray and J. Sólyom, 1985; *Proceedings of the XV Yamada Conference on Physics and Chemistry of Quasi-One-Dimensional Conductors,* edited by S. Tanaka and K. Uchinokura, 1986).

II. THE CHARGE-DENSITY-WAVE GROUND STATE

While charge-density waves also occur in materials with two- or three-dimensional band structures, they are predominantly a one-dimensional phenomenon. Consequently, most of the discussions concerning the ground state and the phase transition are based on idealized, one-dimensional models.

Due to the particular geometry of the Fermi surface, a one-dimensional (1D) electron gas is not stable at $T=0$, and correlation effects lead to phase transitions and to different collective modes at low temperatures. Depending on the details of the electron-electron and electron-phonon interactions, various ground states (such as singlet and triplet superconducting), spin-density wave (SDW), and CDW may occur. These (with the exception of triplet superconductivity) have been widely observed in various solids where the Fermi surface is strongly anisotropic. Several recent reviews (Berlinski, 1979; Heeger, 1979; Sólyom, 1979) discuss the nature of the CDW ground state and its thermodynamic and static properties in detail. Therefore only the main features of the phase transition and of the collective charge-density-wave mode will be discussed here, together with the evidence for CDW formation in various inorganic linear-chain compounds.

A. The Peierls transition: Theory

We consider a one-dimensional metal at $T=0$. In the absence of electron-electron or electron-phonon interaction, the ground state corresponds to the situation shown in Fig. 1(a): The electron states are filled up to the Fermi level ε_F; the lattice is a periodic array of atoms with lattice constant a. In the presence of an electron-phonon

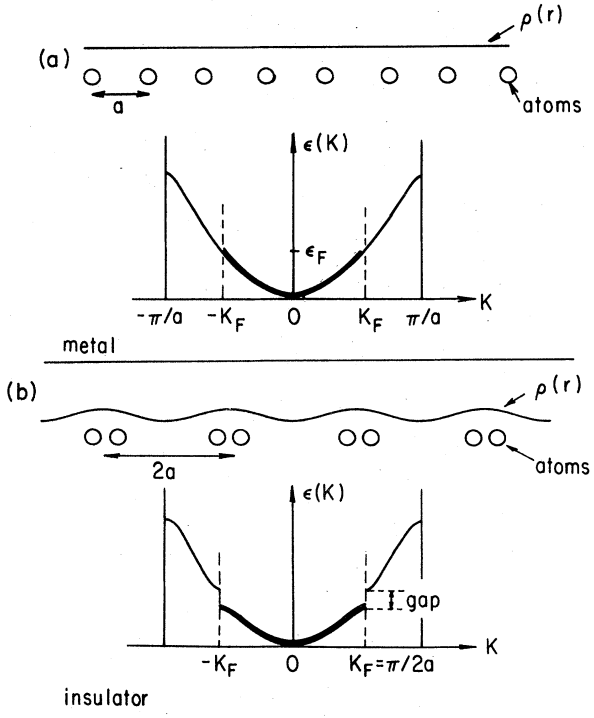

FIG. 1. Peierls distortion in a one-dimensional metal with a half-filled band: (a) undistorted metal; (b) Peierls insulator.

interaction, it is energetically favorable to introduce a periodic lattice distortion with period λ related to the Fermi wave vector k_F by

$$\lambda=\frac{\pi}{k_F} . \tag{2.1}$$

This distortion opens up a gap at the Fermi level as shown in Fig. 1(b), where the situation appropriate for a half-filled band is displayed. Since states only up to $\pm k_F$ are occupied, the development of a gap leads to a lowering of the electronic energy. In one dimension the single-particle gap Δ is proportional to the amplitude of the periodic lattice distortion u, and the decrease of the electronic energy is for small displacements proportional to $u^2 \ln u$. The distortion leads also to an increase of the elastic energy proportional to u^2 (Rice and Strässler, 1973). Consequently, for a small distortion, the total energy of the coupled electron-phonon system is smaller than that of the undistorted metal. The size of the gap and the magnitude of the distortion can be found from the condition for the maximum energy gain. The modification of the dispersion relation also leads to a position-dependent electron density much in the same way as in the nearly-free-electron theory of metals. The density will be a periodic function of the position x with the period also given by Eq. (2.1). (In the following, the direction along which the CDW develops shall in general be called the x direction, and the lattice constant in this direction shall be called a.) For an arbitrary band filling, the period of the charge-density wave (and also the accompanying periodic lattice distortion) is incommensurate with the underlying lattice, i.e., λ/a is irrational.

At finite temperatures normal electrons excited across the single-particle gap screen the electron-phonon interaction. This in turn leads to the reduction of the gap (Kuper, 1955) and of the magnitude of the lattice distortion, and eventually to a second-order transition at the so-called Peierls temperature T_p. The material is a metal above the transition while it is a semiconductor below T_p with a temperature-dependent gap $\Delta(T)$. The main features of this so-called Peierls transition and of the collective mode can be described by the mean-field treatment of the 1D electron-phonon Hamiltonian

$$\mathcal{H}=\sum_{k,\sigma}\varepsilon_k c^+_{k\sigma}c_{k\sigma}+\sum_{k,\sigma}\hbar\omega^0_q b^+_q b_q + \sum_{k,q,\sigma} g(k)c^+_{k+q,\sigma}c_{k,\sigma}(b_q+b^+_{-q}) , \tag{2.2}$$

where $c^+_k(c_k)$, $b^+_q(b_q)$ are the electron and phonon creation (annihilation) operators with momenta k and q, σ denotes the spin, ε_k and ω^0_q are the electron and phonon dispersions, and $g(k)$ is the electron-phonon coupling constant.

Defining a complex order parameter

$$\Delta e^{i\varphi}=g(2k_F)\langle b_{2k_F}+b^+_{-2k_F}\rangle , \tag{2.3}$$

where Δ and φ are real, the displacement field of the ions is given by

$$\langle b_{2k_F}+b^+_{-2k_F}\rangle e^{2ik_Fx}+\text{c.c.}=\frac{2\Delta}{g(2k_F)}\cos(2k_Fx+\varphi) . \tag{2.4}$$

One can diagonalize the electronic part of the Hamiltonian by setting up a self-consistent equation in a mean-field approximation by replacing b_{2k_F} by $\langle b_{2k_F}\rangle$ and using a linear dispersion relation to describe the electron band near ε_F,

$$\varepsilon_k=v_F(|k|-k_F) , \tag{2.5}$$

where v_F is the Fermi velocity. The thermodynamics of the CDW state closely resembles that of a superconducting ground state (Sólyom, 1979; Kuper, 1955). The gap Δ in terms of the dimensionless electron-phonon coupling constant $\lambda'=g^2(2k_F)(\omega^0_{2k_F}\varepsilon_F)^{-1}$ is given by the BCS gap equation, and at $T=0$,

$$\Delta=2D\exp(-1/\lambda') , \tag{2.6}$$

where the cutoff energy D is the one-dimensional bandwidth. The temperature dependence of Δ also has the characteristic BCS form and vanishes at the transition temperature $T_P=\Delta(T=0)/1.76k_B$.

The temperature-dependent carrier concentration in the condensate $n_c(T)$ is also related to $\Delta(T)$, and close to T_p:

$$\frac{n_c(T)}{n_c(T=0)}=\frac{\pi\Delta(T)}{4k_BT_p} , \tag{2.7}$$

while at $T=0$, n_c is equal to the number of electrons in the metallic state. The spatially dependent electron density can also be evaluated, and at $T=0$,

$$\rho(x)=\rho_0+\frac{\Delta\rho_0}{\lambda' v_F k_F}\cos(2k_Fx+\varphi) =\rho_0+\rho_1\cos(2k_Fx+\varphi) , \tag{2.8}$$

where ρ_0 is the electron density in the absence of electron-phonon interaction, and is given in one dimension by $\rho_0=\pi/k_F$. The appearance of a gap in the single-particle excitation spectrum, together with the collective mode described by a complex order parameter [see Eq. (2.3)], is a feature reminiscent of superconductivity. The collective mode here, however, is formed by electron-hole pairs, involving the wave vector $2k_F$ as electrons and holes on the opposite side of the Fermi surface are combined to lead to the CDW and to the accompanying lattice distortion. Furthermore, due to the large cutoff frequency D, which appears in the gap equation (compared to the characteristic phonon frequency, which enters into the superconducting gap), the transition temperatures are considerably larger than superconducting transition temperatures. The fact that in 1D the CDW state is stable at $T=0$ for whatever small electron-phonon coupling constant λ', is the consequence of the logarithmically divergent response function

$$F(q,\omega)=\sum_k \frac{f_{k+q}-f_k}{\varepsilon_k-\varepsilon_{k+q}+\hbar\omega} \sim \frac{1}{\pi v_F}\frac{2k_F}{q}\ln\left|\frac{1+q/2k_F}{1-q/2k_F}\right|, \quad (2.9)$$

where f is the Fermi distribution function. Consequently, there is an enhanced tendency for CDW formation in materials with highly anisotropic band structure; the latter is in general the consequence of a crystal structure where chains in the x direction are formed.

The mean-field (MF) description neglects the important role of one-dimensional fluctuations and, consequently, leads to a finite transition temperature T_{MF}, even for a strictly one-dimensional metal. Fluctuations strongly suppress the transition (Sólyom, 1979), and for a single 2D metallic chain a phase transition does not occur at finite temperatures. For a system of coupled chains, with coupling due either to the overlap of the electronic wave functions or to Coulomb interactions between the electrons on the neighboring chains, the phase transition is restored at $T\neq 0$ with most of the 1D correlations preserved in the ordered state below the phase transition temperature (Lee *et al.*, 1973; Rice and Strässler, 1973). The general picture that emerges, then, is that materials that are composed of chains and are metals at high temperatures show strong 1D correlations along the chain direction even above a three-dimensional (3D) transition T_{3D}, leading to a wide fluctuating region for the transition, $T_{3D} < T_p < T_{MF}$. Below T_{3D} the correlations on neighboring chains couple together, leading to three-dimensional long-range order (Sólyom, 1979). The CDW under such circumstances develops along the chain direction. Perpendicular to the chains, the periodic change and lattice modulation are either in-phase or out-of-phase on neighboring chains, depending on the relative magnitude of the perpendicular bandwidth and Coulomb correlations (Sólyom, 1979; Barisic, 1986).

B. The Peierls transition: Materials and experiment

Because of the enhanced tendency for nesting Fermi surfaces and, consequently, strongly singular response functions in lower dimensions, materials in which CDW transitions are readily observed have chain or layer structures. Organic conductors, of which tetrathiafulvalene-tetracyanoquinodimethane (TTF-TCNQ) is the prototype of one group of solids, have been widely studied (see, for example, Heeger, 1979). Another group of compounds with a CDW ground state are inorganic layer compounds (Wilson *et al.*, 1975) where two-dimensional (2D) charge-density waves develop. Materials discussed in this review are inorganic chain compounds, where the basic structural units form chains with strongly overlapping electronic wave functions along the chains and weak overlap in the perpendicular directions. This leads to a quasi-one-dimensional electronic band structure with relatively wide bands in the chain direction, the necessary prerequisites for a Peierls transition.

The first inorganic linear-chain material in which CDW transitions were found is $NbSe_3$, the structure of which is shown in Fig. 2. The $NbSe_3$ units form infinite and relatively well-separated chains. They are linked together with Nb—Se bonds in the perpendicular direction. The main features of this structural arrangement are also found in the other members of this tri-chalcogenide group, $TaSe_3$, TaS_3 (both orthorhombic and monoclinic forms, o-TaS_3 and m-TaS_3), and in the different modifications of NbS_3 (Meerschaut, 1983). While the bonding both within the chain and between the chains varies from compound to compound, this influences only the single-particle properties, such as the conductivity anisotropy, single-particle bandwidth, and the Peierls transition temperature. These differences, however, do not play an important role in the dynamics of the collective mode aside from that of setting an overall energy scale and correlation length. For a strictly one-dimensional band, the electron configuration in $NbSe_3$ would correspond to a quarter-filled band (0.5 e/at.), but the overlap of the wave functions between neighboring chains leads to a slight deviation from this value (Monceau *et al.*, 1982; Monceau, 1986). Nearly-quarter-filled bands are also expected for other members of this family of compounds. Materials, called the halogen transition-metal tetrachalcogens $(MX_y)_n$, where the transition metal M = Nb or Ta, X = S or Se, and h = I, Br, or Cl, represent another group of materials where transitions to CDW ground states were observed. Here chains of (MX_y) units are separated by halogen chains. While

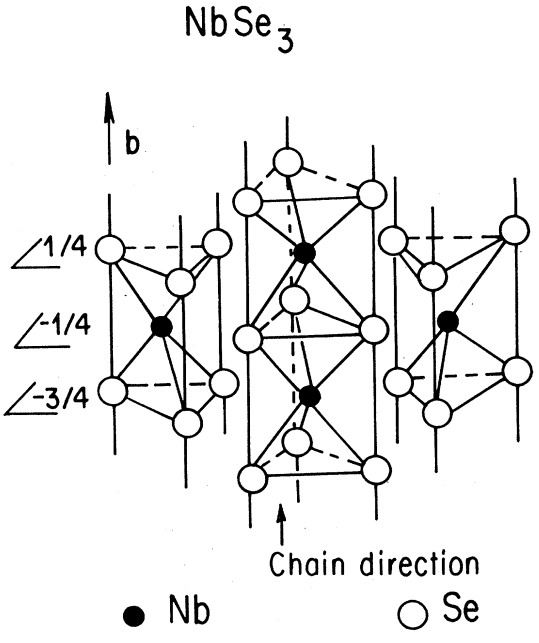

FIG. 2. Crystal structure of $NbSe_3$.

most of the members of this group are semiconductors (Rouxel, 1982), $(TaSe_4)_2I$ (Wang, Monceau, *et al.*, 1983; Zettl and Grüner, 1983c), $(NbSe_4)_{3.33}I$ (Wang, Monceau *et al.*, 1983), and $(NbSe_4)_2I$ (Fujishita *et al.*, 1984) undergo Peierls transitions below room temperature.

Another group of linear-chain compounds, of which $K_{0.3}MoO_3$ and $Rb_{0.3}MoO_3$ are the prime examples, also develop charge-density-wave ground states below room temperature. The MoO_6 octohedra form chains, separated by chains of alkali-metal atoms (Fogle and Perlstein, 1972), leading to a quasi-two-dimensional crystal structure, but to nearly a one-dimensional band structure (Schlenker and Dumas, 1986).

In all of these compounds the highly anisotropic single-particle band is the consequence of not only the chain structure but also of the strong overlap of the *d* orbitals along the chain direction, with no direct *d-d* overlap perpendicular to the chains. Consequently, the materials are relatively good metals along the chain directions with room-temperature conductivities parallel to the chains, $\sigma_{\parallel}$ on the order of $\sim 10^3-10^4\ \Omega^{-1}\text{cm}^{-1}$. The conductivity perpendicular to the chains is between 10 and 10^3 times smaller (Fogle and Perlstein, 1972; Ong and Monceau, 1977; Ong and Brill, 1978). As σ is (in tight-binding approximation) proportional to the square of the transfer integral, this suggests a band with anisotropy between 3 and 30. Both the magnetic susceptibility (Johnston, 1984; Johnston *et al.*, 1985) and the thermoelectric power are small in these materials and are metallic at room temperature and above. Moreover, both can be analyzed using standard formulas appropriate for a narrow one-dimensional band. Such analysis leads to bandwidths of the order of 1–3 eV, typical to *d*-band metals, and Fermi velocities of the order of 3×10^7 cm/sec. Detailed analysis of these features demonstrates that electron-electron interactions are not important in these compounds (Grüner and Zettl, 1985).

The above materials undergo a second-order metal-to-insulator (or metal-to-semimetal) transition at below room temperature, as evidenced by a wide range of transport, magnetic, and specific-heat studies. Furthermore, detailed structural studies demonstrate that these transitions are associated with the development of periodic lattice distortions that are incommensurate with the underlying lattice. The compound $NbSe_3$ shows sharp increases of the resistivity $\rho(T)$ (measured along the chain direction) at $T=144$ K and $T=59$ K (Haen *et al.*, 1975), as shown in Fig. 3. This indicates a partial destruction of the Fermi surface at these temperatures, which is confirmed by Hall-effect (Ong and Monceau, 1977) and by magnetoresistance (Ong and Brill, 1978) studies. The two phase transitions, and the metalliclike character of $\rho(T)$ is believed to be the consequence of three structurally slightly different chains in the material (Wilson, 1979). One chain remains metallic down to low temperatures, while the two phase transitions reflect the development of lattice distortions in the remaining two chains. Direct evidence for such distortions are obtained from electron

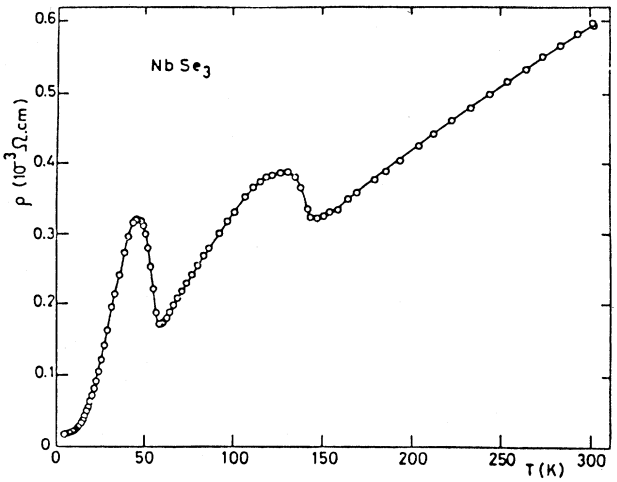

FIG. 3. Temperature dependence of the electrical resistance of $NbSe_3$. Sharp increases of $\rho(T)$ at 144 and 59 K signal the onset of two phase transitions involving different chains.

(Tsutsumi *et al.*, 1978) and x-ray (Fleming *et al.*, 1978, 1984) diffraction studies. Both phase transitions are associated with the development of incommensurate lattice distortions along the chain direction. For approximately 0.5 *e*/at. in $NbSe_3$, the band is approximately quarter-filled with k_F close to $\pi/4a$. In both CDW states the experimentally determined period is indeed close to $\lambda=4b$ (the chain direction is denoted by *b* in this compound) but not exactly equal to 4 times the lattice period, i.e., the charge-density wave and periodic lattice distortion are incommensurate with the underlying lattice.

Another member of the group, TaS_3, occurs in two modifications, orthorhombic (o-TaS_3) and monoclinic (m-TaS_3). The former has one type of chain (this has not been determined by structural studies, but is suggested by the observation of a single phase transition) and one phase transition at $T_P=220$ K, the latter two transitions at $T_1=240$ K and at $T_2=160$ K. In o-TaS_3, the whole Fermi surface is removed by the transition; consequently, the material is a semiconductor below T_P, as indicated by the temperature dependence of the dc conductivity measured along the chain direction. This is also the case for $(TaSe_4)_2I$ and for $K_{0.3}MoO_3$, with the former having a Peierls transition at $T=265$ K and the latter at $T=180$ K. Besides the semiconducting behavior of the dc conductivities (all measured along the chain direction), other transport coefficients such as the thermoelectric power or Hall effect confirm that for low dc electric fields, the conductivity is due to carrier excitations across the single-particle gap. They all can be described consistently in terms of standard formulas appropriate for band semiconductors. The materials, for which the conductivity is displayed in Fig. 4, are more anisotropic than $NbSe_3$. Consequently, 1D fluctuations play an important role above the three-dimensional ordering temperature, and

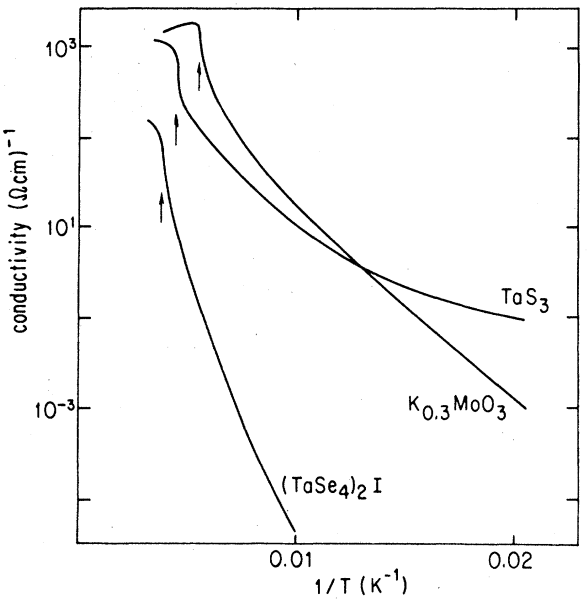

FIG. 4. Temperature dependence of the electrical conductivity in o-TaS_3, in $(TaSe_4)_2I$, and in $K_{0.3}MoO_3$. The arrows represent the Peierls transition temperatures; they are evident by examining the temperature derivatives dR/dT.

the anomalies in the transport and magnetic properties can be well described (Johnston, 1984) in terms of theories that treat these fluctuation effects (Lee *et al.*, 1973; Rice and Strässler, 1973).

The single-particle gaps have also been determined directly by optical measurements (Brill and Herr, 1983; Challener and Richards, 1984; Geserich *et al.*, 1986). They agree in general with the gaps that are determined from the temperature dependence of the dc conductivity below T_P. In all cases the ratio $2\Delta/k_BT_p$ is significantly larger than the mean-field BCS value of $2\Delta/k_BT_p=3.5$, most probably because of the large anisotropy that leads to a three-dimensional ordering temperature significantly smaller than the mean-field transition temperature. Large gap values have been observed also in $NbSe_3$ (Fournel, Sorbier, Konczykowski, and Monceau, 1986). Here strong-coupling effects have been suggested to be important. The gaps that have been obtained by tunneling are different from the single-particle gaps evaluated from optical studies (Challener and Richards, 1984); the reason for this difference is not clear.

The metal-to-semiconductor transition is also associated with the development of incommensurate CDW's in these compounds [TaS_3: Tsutsumi *et al.*, 1978, Roucau, 1983; $(TaSe_4)_2I$: Fujishita *et al.*, 1984; $K_{0.3}MoO_3$: Pouget *et al.*, 1983, Sato *et al.*, 1983, Tamegai *et al.*, 1985], with periods in qualitative agreement with those inferred from valence structure arguments. Below the phase transition, the phase-phase correlation length is extremely long, exceeding 1μ along the chain direction. This has been most thoroughly established by high-resolution synchrotron radiation studies in $NbSe_3$ (Fleming *et al.*, 1984) and in $K_{0.3}MoO_3$ (Fleming *et al.*, 1985c). Perpendicular to the chains, long correlation length was found in $K_{0.3}MoO_3$ (Fleming *et al.*, 1985c); in other materials this could not be measured due to the mosaic structure of the crystals investigated. The temperature dependence of the amplitude of the superlattice reflections gives directly the order parameter Δ. The intensity of the reflections (proportional to Δ^2) as a function of temperature is shown in Fig. 5 for some of the

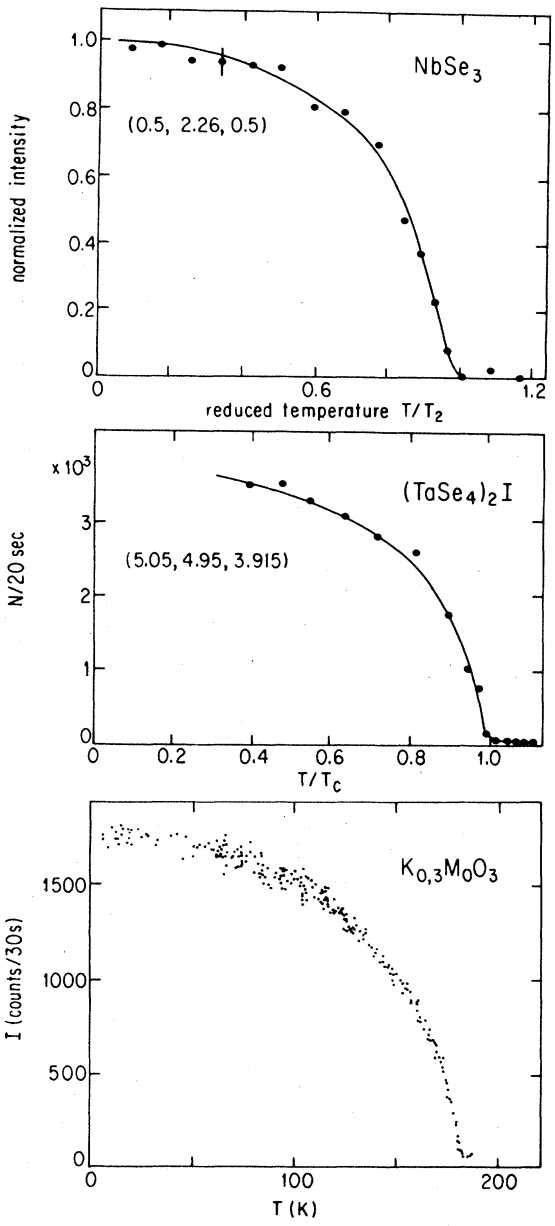

FIG. 5. Temperature dependence of the superlattice reflection intensities in $NbSe_3$ (lower transition) (Fleming, 1980), in $(TaSe_4)_2I$ (Fujishita *et al.*, 1984), and in $K_{0.3}MoO_3$ (Sato *et al.*, 1983).

compounds. While a fit to a BCS-type temperature dependence for $\Delta(T)$ has not been attempted, it is evident that in all cases a description in terms of a temperature-dependent gap that goes to zero at the second-order phase transition is appropriate.

While in $NbSe_3$ and in $(TaSe_4)_2I$ the wave vector of the CDW is independent of the temperature and the lattice distortion remains incommensurate, in *o*-TaS_3 (Wang *et al.*, 1983c) and in $K_{0.3}MoO_3$ (Sato *et al.*, 1983; Fleming, Schneemeyer, and Moncton, 1985) the charge-density wave becomes commensurate with $\lambda=4a$ at low temperatures. This has been firmly established in $K_{0.3}MoO$, but in *o*-TaS_3 the evidence for lock-in at wave vector $\lambda=4a$ is weaker. This is expected to have important consequences for the dynamics of the collective mode.

Unusual domain structures associated with the CDW superlattice have been found in $NbSe_3$ (Fung and Steeds, 1980) and in *o*-TaS_3 (Chen and Fleming, 1983). These were studied by examining the dark field electron microscope images associated with the superlattice reflections in the CDW state. Although many of the details are not entirely reproducible, a domain structure with a typical size of 1μ along the chain direction and approximately 300 Å perpendicular to the chains has been observed in both compounds. Superimposed on this large-scale domain pattern are smaller domains of the size of 20×20 Å. The images are time dependent and the domains appear in constant motion, with a characteristic time scale on the order of seconds. The origin of this domain pattern has not been explained yet, although it is evident that it represents some kind of instability in the CDW superlattice. Slight changes in the direction of the wave vector $2k_F$, which characterizes the CDW distortion, may explain the observations (Fung and Steeds, 1980). It has also been suggested (Wilson, 1979; Bak, 1982a) that the small domains reflect discommensurations. As λ is close to $4a$ both in $NbSe_3$ and in TaS_3, the CDW's may become commensurate with the lattice over a macroscopic region by breaking into domains separated by phase slips between domains of commensurate CDW sections. The observed domain structure, however, has no clear relation to the dynamical behavior of charge-density waves. While the pattern is time dependent, an applied electric field that leads to a current-carrying CDW state does not induce any changes in the size or in the time dependence of the domain pattern. Although several observations concerning the response of CDW's to applied electric fields can be explained tentatively in terms of the dynamics of coupled domains, a direct correlation between these observations and those made by dark field electron microscope studies has not been attempted yet.

III. THE DYNAMICS OF THE COLLECTIVE MODE: SOME BASIC RESULTS

In the Peierls state the material is expected to be a semiconductor, with the various properties determined by carrier excitations across the single-particle gap. The dc resistivity due to these excitations displays an exponential temperature dependence, with deviations from Ohm's law only at rather high electric field. The optical properties are also determined by the gap, which, in general, corresponds to $\hbar\omega$ in the visible-to-infrared spectral range. In addition to these single-particle phenomena, the coupled electron-phonon system can contribute to charge transport by moving the CDW rigidly, while the ions that are involved in the periodic lattice distribution execute only oscillatory motion. The energy of an incommensurate CDW is independent of the phase φ; consequently, the translational motion could be induced by small dc electric fields. In the absence of damping, this would also lead to a supercurrent, as described by Fröhlich (1954).

No evidence for such anomalous conductivity is found when the experiments are performed in small dc fields; under such circumstances all transport coefficients can be described in terms of standard single-particle transport theories appropriate for a band semiconductor. It has been emphasized first by Lee, Rice, and Anderson (1974) that, in contrast to superconductors, the phase of the CDW condensate can be pinned to the lattice through the interaction with impurities, lattice imperfections, grain boundaries, etc. Consequently, the collective-mode contribution to the dc conductivity measured at low electric fields is zero. However, the pinning energy per electron can be much smaller than the single-particle energies Δ and ε_F, and, consequently, the response to finite amplitude dc and to ac excitations is dominated by the dynamics of the collective mode.

A. Fundamental concepts

The dynamics of the collective mode is described in terms of a position- and time-dependent order parameter $\Delta(x,t)$. As $\Delta(x,t)$ is complex [see Eq. (2.3)], both amplitude and phase fluctuations occur. These can be described by assuming that the two types of fluctuations are decoupled and

$$\Delta(x,t)=(\Delta_0+\delta)e^{i\varphi'} , \tag{3.1}$$

where Δ_0 is the equilibrium order parameter, and δ and φ' are the fluctuations from the equilibrium value. Then to lowest order in δ and φ' the amplitude mode corresponds to $\Delta_{2k_F}+\Delta_{-2k_F}=2\Delta_0+2\delta$, and the phase mode corresponds to $\Delta_{2k_F}-\Delta_{-2k_F}=2\Delta_0\Delta\varphi'$. The dispersion relations of these modes were evaluated first by Lee, Rice, and Anderson (1974), using the electron-phonon Hamiltonian (2.2). The electron-phonon interaction transforms the acoustic phonons near the zone boundary into an optical and an acoustic branch with frequencies

$$\Omega_+^2=\lambda'(\omega_{2k_F})^2+\frac{1}{3}\left[\frac{m}{m^*}\right](v_Fq)^2 , \tag{3.2a}$$

$$\Omega_-^2=\left[\frac{m}{m^*}\right](v_F q)^2=(c_0 q)^2 , \tag{3.2b}$$

where the effective mass m^* is given in terms of fundamental parameters of the problem λ', ω_{2k_F} and Δ_s by

$$\frac{m^*}{m}=1+\frac{4\Delta_s^2}{\hbar^2\lambda'(\omega_{2k_F})^2} \tag{3.3}$$

at $T=0$. Both modes soften with increasing temperature, while the temperature dependence of the effective mass is given by

$$\frac{m^*}{m}=1+\frac{4\Delta_s^2}{\hbar^2\lambda'(\omega_{2k_F})^2}\frac{n_c(T)}{n_c(T=0)} \tag{3.4}$$

with the temperature-dependent carrier density given by Eq. (2.7). While the amplitude mode has a gap, the phase mode is gapless; the $q=0$ translational mode corresponds to zero excitation energy. The dispersion relation for Ω_+ and Ω_- are shown in Fig. 6. The large effective mass m^* is the consequence of the coupled dynamics of the electrons and phonons: in the case of the $q=0$ translational mode, the total kinetic energy includes both that of the electrons that execute translational motion and the ions that oscillate about their equilibrium positions. The amplitude mode Ω_+ is expected to be Raman active, while the phase mode carries a dipole moment as it involves the motion of condensed electrons across the background of the position changes of the ions. Consequently, the $q=0$ phase mode carries a current. Equation (3.2) is appropriate in the long wavelength $q^{-1}\gg\lambda$ limit. For short-wavelength fluctuations, deviations from the above dispersion relation occur that are similar to those that arise for optical and acoustic phonons near a zone boundary. In addition, Coulomb interactions may shift the Ω_- branch up to optical frequencies. Uncondensed electrons, however, most likely screen the Coulomb interactions, and Eq. (3.2) is expected to be appropriate.

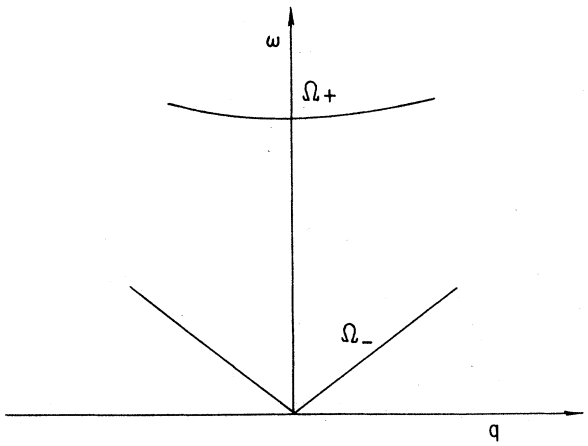

FIG. 6. Phase and amplitude mode dispersion relations.

With a characteristic Fermi energy $\varepsilon_F\sim 1$ eV, single-particle gap $\Delta_s\sim 0.1$ eV, and phonon frequency $\omega_{2k_F}\sim 10^{-2}$ eV, the electron-phonon coupling constant λ' is of the order of 0.5 [see Eq. (2.6)]. With these values, Ω_+ $(q=0)\sim 5\times 10^{-3}$ eV, which is smaller than Δ_s, and the effective mass is of the order of $m^*/m\sim 10^3$. Several attempts have been made to observe the amplitude mode by Raman scattering, but the mode has not yet been unambiguously determined (Tsang *et al.*, 1978; Travaglini *et al.*, 1983). Due to the gap in the dispersion relation for the amplitude mode, amplitude fluctuations do not play an important role at temperatures $kT\ll\Omega_+$. Therefore most of the descriptions of dynamical collective phenomena are in terms of the dynamics of the phase only. Such a description may be appropriate at low temperatures, but close to the Peierls transition important effects coming from the dynamics of the amplitude mode are expected to occur. By treating the phase as a classical field, the Lagrangian density in one dimension can be written (Brazovskii and Dzyaloshinskii, 1976; Fukuyama, 1976; Fukuyama and Lee, 1978)

$$\mathcal{L}=\frac{n_c}{4\pi}\left[\frac{m^*}{mv_F}\left[\frac{d\varphi}{dt}\right]^2-\kappa^2\left[\frac{d\varphi}{dx}\right]^2\right] \tag{3.5}$$

to lowest order in the derivatives, and n_c is the carrier density along the chain direction. This form follows from the elimination of the electronic degrees of freedom from the Hamiltonian (2.2) (Brazovskii and Dzyaloshinskii, 1976). The first term on the right-hand side corresponds to the kinetic energy of a line mass m^*n_c per unit length. The second term represents the potential energy associated with the distortions of the collective mode, with a phenomenological elastic constant κ. The equation of motion corresponding to the above Lagrangian is

$$\frac{d^2\varphi}{dt^2}=\frac{m}{m^*}\kappa^2\frac{d^2\varphi}{dx^2} . \tag{3.6}$$

The solutions for Eq. (3.6) are of the form $\exp[i(\omega t-qx)]$ with the dispersion relation

$$\Omega_-^2=\frac{m^*}{m}\kappa^2(kq)^2 ; \tag{3.7}$$

comparison with Eq. (3.2b) gives the phenomenological elastic constant in terms of v_F as

$$\kappa=V_F . \tag{3.8}$$

The plane-wave solutions represent the periodic compression and expansion of the CDW; these excitations are called phasons. The dispersion relations (3.2) and (3.7) also define a phason velocity

$$c_0=\left[\frac{m}{m^*}\right]^{1/2}v_F , \tag{3.9}$$

in which, for $v_F\sim 3\times 10^7$ cm/sec and for $m^*/m\sim 10^3$, c_0 is approximately 10^6 cm/sec.

As in a superconductor, the phase $\varphi(x,t)$ plays an important role in the dynamics of the collective mode. The $q=0$ phase mode corresponds to the translational motion of the condensed electrons, with the ions oscillating around their equilibrium positions. A rigid displacement of the CDW leads to an electric current, and the current density per chain $j_{\rm CDW}=-n_c e v_d = -n_{\rm CDW} e(d\varphi/dt)$. With $\varphi=2k_F x$ and $\lambda=\pi/k_F$,

$$j_{\rm CDW}=\frac{e}{\pi}\frac{d\varphi}{dt} . \tag{3.10}$$

A compression of the wave leads to a change of the electronic density, and therefore

$$n_c=\frac{e}{\pi}\frac{d\varphi}{dx} \tag{3.11}$$

at zero temperature. The cross derivatives of the above equations lead to the equation of continuity

$$\frac{dj_{\rm CDW}}{dx}+\frac{dn_c}{dt}=0 . \tag{3.12}$$

Equation (3.12) is more general than implied by its deviation above and is valid to all orders in the derivative expansion of the phase (Horovitz, 1986). Here and in the previous formulas, the subscript refers to the current carried by the CDW. Subsequently, the subscript will be used only if the effect of normal electrons leading to normal current is also important. Otherwise all quantities (current, current density, cordial and differential conductivity, etc.) refer to transport carried by the collective mode.

The above relations can also be derived by considering the modification of the dispersion relation of electrons in momentum space (Allender *et al.*, 1974; see also Bjelis, 1987). As in a superconductor for a slowly varying $\varphi(x,t)$ (on the time scale much less than $\hbar/\Delta s$) the Fermi surface is tied to the position- and time-dependent condensate. We consider first a slowly varying $\varphi(x)$, for which $(1/k_F)(d\varphi/dx)\ll 1$. This can be described as a change in the wave vector $2k_F+d\varphi/dx$; consequently, the single-particle gap is shifted from $\pm k_F$ to $\pm[k_F+\frac{1}{2}(d\varphi/dx)]$, as shown in Fig. 7. If the electrons do not change their density, then the gap is removed from the Fermi surface. This leads to electrons in states above the gap and to a large increase of the total electronic energy. A change in the electron density, by tying the gap to the Fermi surface, involves less energy. As $\rho(x)=2k_F(x)/2\pi$, the gap is at the Fermi level if

$$\rho(x)=\rho_0+\frac{1}{\pi}\frac{d\varphi}{dx} , \tag{3.13}$$

the same relation as Eq. (3.11).

For a time-dependent phase $\varphi(t)$, with $d\varphi/dt = 2k_F v_{\rm CDW}$, the inversion symmetry is broken and the dispersion relation becomes asymmetric, as shown in Fig. 7(b). The electronic energies are given by (Allender *et al.*, 1974)

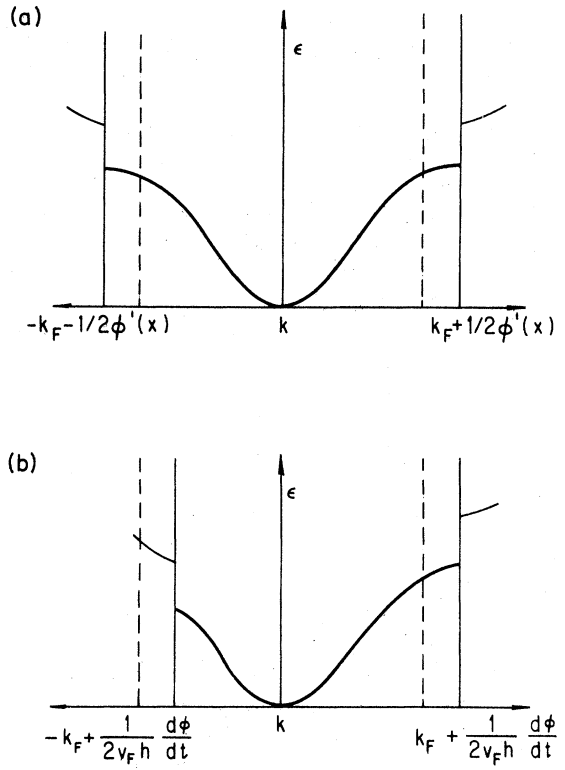

FIG. 7. Displaced Fermi surface for a position- (a) and for a time-dependent (b) phase. The states are filled up to the Fermi level, $\pm\{k_F+\frac{1}{2}[d\phi(x)/dx]\}$ in (a), and up to $\pm[k_F \pm(1/2v_f h)(d\phi/dt)]$ in (b) indicated in both cases by the solid lines. The dotted lines refer to the original Fermi surface at $\pm k_F$.

$$\varepsilon_{\pm k}=\left[\varepsilon(k)\pm\frac{1}{2}\left[\frac{d\varphi}{dt}\right]^2+\Delta_s^2\right]^{1/2} . \tag{3.14}$$

The energies corresponding to the displacement Fermi surface are different for positive and negative momenta, leading to different occupation numbers for positive and negative k values. This then leads to a total current

$$j_{\rm CDW}=2e\int\frac{d\varepsilon}{dk}\frac{dk}{2\pi}=\frac{e(\varepsilon_{+k}-\varepsilon_{-k})}{\pi}=-\frac{e}{\pi}\frac{d\varphi}{dt} \tag{3.15}$$

(where the integration is over all occupied states), the same as Eq. (3.10). This relation, and also Eq. (3.13), breaks down for strong local distortions of the condensate. In such cases both the amplitude and the phase perturbations have to be included. The relation that connects the electric current and condensate density to the time and spatial derivative of the phase $\varphi(x,t)$ of the condensate is different from the relations that are appropriate for a superconductor,

$$p_s=i\hbar\frac{d\varphi}{dx} \quad \text{and} \quad \mu=i\hbar\frac{d\varphi}{dt} ,$$

where p_s and μ are the momentum and the chemical potential. This arises because, in contrast to the superconducting ground state, the charge-density-wave condensate is formed by electron-hole pairs, and pairing also involves the wave vector $2k_F$.

In the presence of an applied electric field $E(\omega)=E_0e^{i\omega t}$, the equation of motion becomes

$$\frac{d^2\varphi}{dt^2}+\frac{m}{m^*}\hbar v_F^2\frac{d^2\varphi}{dx^2}=\frac{2k_FeE(\omega)}{m^*}\ , \tag{3.16}$$

and the frequency-dependent conductivity

$$\sigma(\omega)=\frac{j(\omega)}{E(\omega)}=\frac{m}{m^*}\frac{i\omega_p^2}{4\pi(\omega+i\delta)}\ , \tag{3.17}$$

where $\omega_p^2=8v_Fe^2$ is the plasma frequency. The real part of the conductivity

$$\mathrm{Re}\sigma(\omega)=\frac{m}{4m^*}\omega_p^2\delta(0) \tag{3.18}$$

has a Dirac δ singularity at $\omega=0$, with an oscillator strength

$$f=\frac{\pi ne^2}{m^*}\ . \tag{3.19}$$

Because of the gap Δ_s in the single-particle excitation spectrum, the ω-dependent response due to single-particle processes also displays a gap resulting in $\sigma(\omega)=\sigma_{\mathrm{CDW}}(\omega)+\sigma_{\text{single particle}}(\omega)$ displayed in Fig. 8. The oscillator strength that appears at zero frequency is removed from the single-particle excitations that appear at $\omega>2\Delta_s$. As a consequence, the one-dimensional singularity, which has the form of $(\omega-2\Delta_s)^{-1/2}$, is removed, and $\sigma(\omega)$ becomes rounded, as shown in Fig. 8(a).

The appearance of a single-particle gap together with the zero-frequency collective mode is reminiscent of superconductivity. Here the $\omega=0$ mode corresponds to the translationally invariant CDW which, in the absence of damping, would lead to a supercurrent. Various interactions between the CDW and the underlying lattice, however, remove the translational invariance and lead to pinning of the phase of the condensate. Such pinning is brought about by the local distortions of the condensate around pinning centers. When described in terms of a restoring force, pinning effects shift the collective-mode conductivity to finite frequencies (Rice and Strässler, 1973; Lee *et al.*, 1974). With pinning represented by an average pinning frequency ω_0, and also including a phenomenological damping term $\Gamma(d\varphi/dt)$, the equation of motion becomes, for small amplitude displacements,

$$\frac{d^2\varphi}{dt^2}+\frac{1}{\tau}\frac{d\varphi}{dt}+\omega_0^2\varphi=\frac{2k_FeE}{m^*}\ . \tag{3.20}$$

The frequency-dependent conductivity that corresponds to Eq. (3.20) is given by

$$\sigma(\omega)=\frac{n_ce^2}{i\omega m^*}\frac{\omega^2}{\omega_0^2-\omega^2-i\omega/\tau} \tag{3.21}$$

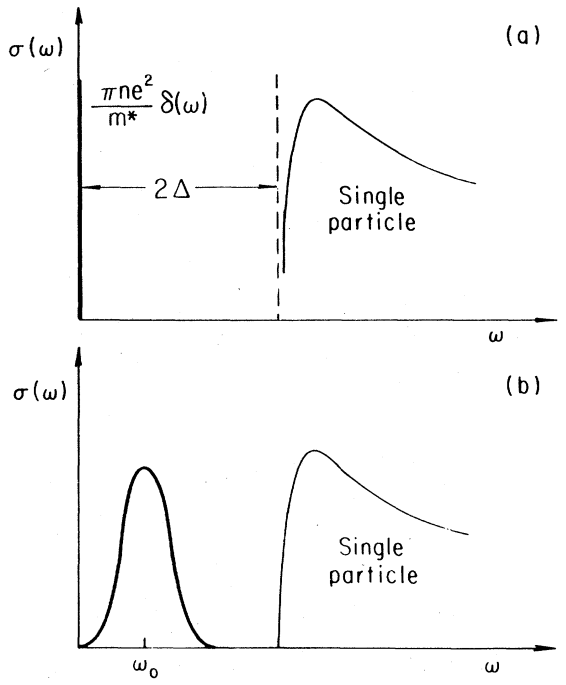

FIG. 8. Frequency-dependent response of the collective mode (a) without pinning, and (b) with pinning and damping. The response at frequencies $\omega>2\Delta/h$ is due to single-particle excitations.

and is that of an optical mode centered around the frequency ω_0. The dc conductivity, $\mathrm{Re}\sigma_{\mathrm{CDW}}(\omega=0)=0$, and the zero-frequency dielectric constant is given (including the contribution from excitations across the gap Δ) as

$$\varepsilon(\omega=0)=1+\frac{4\pi n_ce^2}{m^*\omega_0^2}+\frac{4\pi ne^2\hbar^2}{m\Delta^2}\ . \tag{3.22}$$

The second term on the right-hand side describes the contribution of the collective mode; the third term represents the contribution of single-particle excitations. For weak pinning, where $\hbar\omega_0\ll\Delta$, Eq. (3.21) leads to the conductivity shown in Fig. 8(b), with the contribution of the pinned mode appearing well within the single-particle gap. This also leads to a giant dielectric constant at low frequencies and to a zero crossing at $\omega=\omega_0$.

Coulomb interactions have been completely neglected in the above analysis; consequently, the picture is expected to be appropriate near the Peierls transition, where the normal electrons are available to screen the Coulomb effects associated with the phason excitations.

B. Frequency- and electric-field-dependent conductivity

For band semiconductors the electrical conductivity is independent of frequencies for $\omega<\Delta/\hbar$ and is also independent of electric field for applied fields $eEl<\Delta$, where l is the mean free path. For a typical gap of the

order of 0.1 eV, nonlinear conduction occurs in the kV range, with frequency-dependent conduction observed at optical (infrared) frequencies. In contrast, in the materials discussed before, in the CDW ground state σ is both strongly nonlinear and frequency dependent. In Fig. 9, the frequency-dependent conductivity $\mathrm{Re}\sigma(\omega)$ measured along the chain direction is displayed in several compounds. Only experimental results in the region of the single-particle gaps (shown by solid lines) and in the dc to millimeter wave spectral range are displayed for clarity. The solid lines are the results of optical experiments, and the strong decrease of the conductivity with decreasing frequency demonstrates the existence of the single-particle gaps. The gap values evaluated from the optical experiments (Zeller, 1974; Geserich *et al.*, 1986; Herr *et al.*, 1986; Travaglini and Wachter, 1984) compare, in general, favorably with the gaps evaluated from the dc conductivity below T_p. The strong resonances observed in the millimeter wave spectral range (Ng *et al.*, 1986; Reagor and Grüner, 1986; Reagor, Sridhar, and Grüner, 1986; Sridhar *et al.*, 1986) indicate a collective response associated with the charge-density-wave ground state, as it is evident that the frequency-dependent response such as that displayed in the figure cannot arise from a single-particle transport mechanism. The energy that corresponds to the frequency where $\mathrm{Re}\sigma(\omega)$ has a maximum is orders of magnitude smaller than the single-particle gap

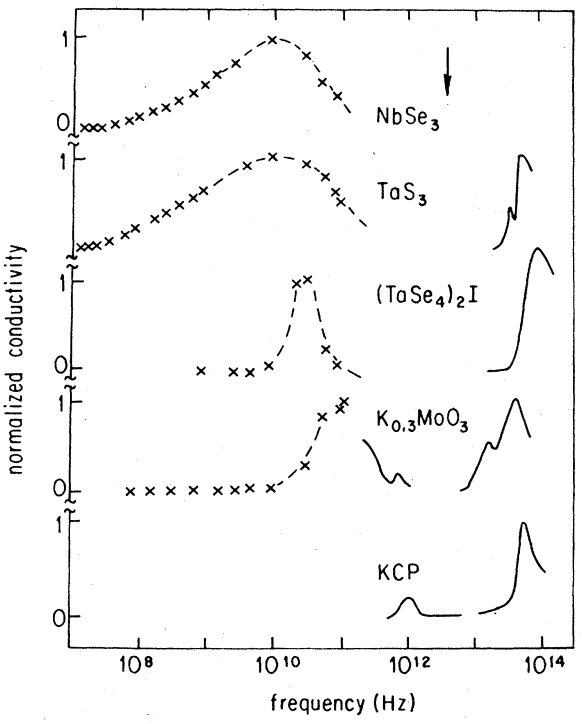

FIG. 9. The frequency-dependent conductivity of $NbSe_3$, o-TaS_3 and $(TaSe_4)_2I$, and $K_{0.3}MoO_3$. The solid lines represent the regions where the drop signals the single-particle gaps; the strong peaks in the millimeter wave spectral range are due to the response of the pinned collective mode.

and also the thermal energy kT. The oscillator strength that appears at finite frequency (in contrast to what is observed in a superconductor) suggests that the collective mode is pinned to the underlying lattice. This is borne out by detailed investigations on specimens where the impurity concentration is varied. The peak frequency ω_0 can be associated with the pinning frequency ω_0, as discussed in Sec. III. The finite width of the resonances observed may be due to damping effects associated with the dynamics of the collective mode, or, alternatively, can be the consequence of inhomogeneous broadening brought about by randomly positioned impurity pinning centers. Alternatively, a band of heavy carriers with a small gap would also lead to an overall behavior, which is displayed in Fig. 9.

The low-frequency dielectric constant is enormous, in general of the order of 10^7 or more, and this is the consequence of the large oscillator strength which occurs at low frequencies. The zero-frequency dielectric constant is given by

$$\varepsilon(\omega)=\frac{4\pi e^2}{m^*}\int_0^\infty \frac{\mathrm{Re}\sigma(\omega)}{\omega^2}d\omega \ ,$$

which for a narrow resonance reduces to $\varepsilon\sim 4\pi ne^2/m^*\omega_0^2$, in agreement with Eq. (3.22). Details of $\sigma(\omega)$ and also $\varepsilon(\omega)$ will be discussed later.

The small pinning energy associated with the collective mode suggests that for a small dc electric field, the collective mode can be driven into a current-carrying state with possibly nonlinear current-voltage characteristics. Indeed, nonlinear conductivity has been observed in all the materials discussed before, with a sharp onset field, called the threshold E_T, for the nonlinear conductivity. The detailed form of the nonlinear conduction varies depending on external factors such as temperature, impurity concentration, or macroscopic inhomogeneities (such as grain boundaries) in the specimen.

The dc conductivity, defined as j/E where j is the total current density and E is the applied electric field, is shown in orthorhombic TaS_3 in Fig. 10. Below, a threshold field E_T, approximately 300 mV/cm, the conductivity obeys Ohm's law, and the temperature dependence of this component reflects the exponential freezing out of the electrons excited across the single-particle gap. The onset of nonlinear conduction is smooth, as evidenced by the current-voltage characteristics displayed in the figure. A behavior, similar to that displayed in Fig. 10, is found, in general, for the other compounds; the existence of the sharp threshold field E_T is well established. The behavior in the figure can be described in terms of a two-fluid model involving electrons excited across the gap and electrons concerned in the collective mode. The former has an Ohmic contribution; the other, a nonlinear response. The total current can be written as

$$I_{\mathrm{tot}}=I_n+I_{\mathrm{CDW}} \ , \qquad (3.23)$$

where the subscripts n and CDW refer to current carried by the uncondensed and condensed electrons. The validi-

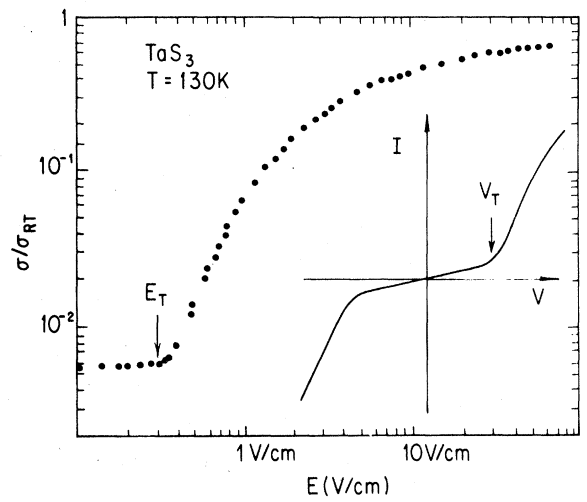

FIG. 10. Electric-field-dependent conductivity $\sigma(E)$ in o-TaS_3. The data are normalized to the room-temperature conductivity. The inset shows typical dc I-V characteristics on the same material.

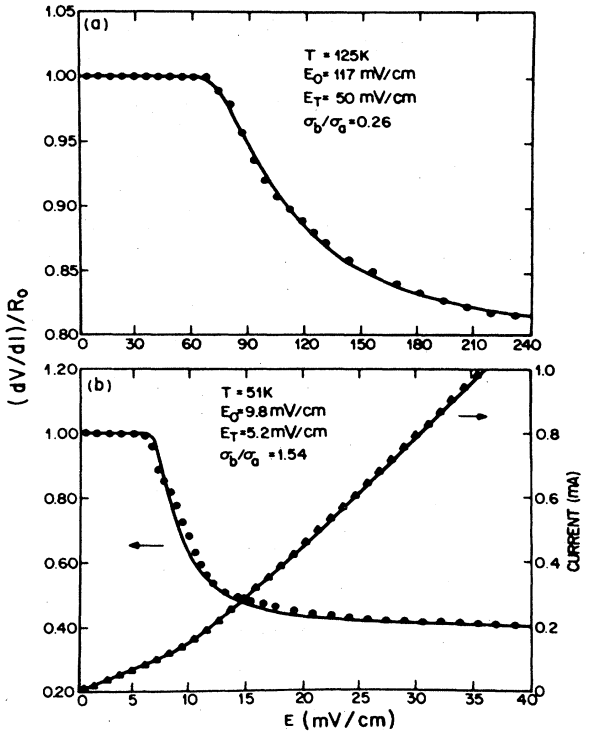

FIG. 11. Normalized differential resistance as a function of dc bias field for the upper (a) and lower (b) CDW states of $NbSe_3$. A threshold field for the onset of nonlinear conduction is clearly observed. The field dependence of the current is also shown for the low-temperature CDW state. The solid lines correspond to Eq. (5.1) using parameters indicated on the figure.

ty of such a two-fluid description has been clearly demonstrated recently by generating nonlinear current-voltage characteristics in an open circuit configuration ($I_{\rm tot}=0$), where the voltage was generated through the thermoelectric effect (Beyermann *et al.*, 1986).

The current-voltage characteristics are also often explored by measuring the differential resistance dI/dV, employing low-frequency lock-in techniques. While the method cannot be used at high fields because of heating effects, it is advantageous to study the behavior near threshold. The first such measurements where a well-defined E_T was evident is shown in Fig. 11.

The frequency- and field-dependent response is strongly related, and a smaller pinning frequency, and, consequently, a larger dielectric constant, leads to a smaller threshold field, suggesting that both are related to an overall energy that characterizes the pinning of the collective mode.

The conductivities of various materials, when extrapolated to the infinite electric field limit or measured at frequencies $\omega_{\rm max}$ where $\mathrm{Re}\sigma(\omega)$ is maximum, are finite, and are close to the conductivities that would be observed in the absence of the phase transitions. In terms of a relaxation time τ, the conductivity at high fields or frequencies is written as

$$\sigma_{\rm CDW}(E\rightarrow\infty \text{ or } \omega_{\rm max})=\frac{ne^2\tau}{m}\ , \tag{3.24}$$

suggesting that the ratio of the relaxation time to the mass is approximately the same for the uncondensed and condensed electrons, and

$$\frac{\tau_N}{m}\sim\frac{\tau}{m^*}\ , \tag{3.25}$$

where m is the band mass. This is approximately obeyed in $NbSe_3$ (Ong and Monceau, 1977), in o-TaS_3 (Sridhar *et al.*, 1986), in $(TaSe_4)_2I$ (Reagor, Sridhar, and Grüner, 1985; Reagor, Sridhar, Maki, and Grüner, 1985), and in $K_{0.3}MoO_3$ (Reagor and Mozurkewich, 1985) at temperatures where the CDW's are incommensurate with the lattice. The high-field conductivity is weakly depressed by small amounts of impurities in $NbSe_3$ (Oda and Ido, 1982); in o-TaS_3 the high-frequency conductivity is also fairly insensitive to impurity effects (Reagor and Grüner, 1986). Both suggest that even for a "perfect" crystal, without impurities, sliding charge-density waves would lead to a finite conductivity.

The onset of nonlinear conduction is often rather dramatic and is accompanied by switching and hysteresis effects. These have been observed in $NbSe_3$ (Zettl and Grüner, 1982a), TaS_3 (Mihály and Grüner, 1984), and $K_{0.3}MoO_3$ (Maeda, Furuyama, and Tanaka, 1986; Maeda, Furuyama, Uchinokura and Tanaka, 1986); such effects usually become more pronounced with decreasing temperature. An example is shown in Fig. 12, where I-V curves recorded in $NbSe_3$ at two different temperatures are displayed. At higher temperatures the onset of nonlinear conduction is accompanied by an oscillatory instability, which, by lowering the temperature gradually, evolves into a hysteretic current-voltage characteristic. The behavior is due to extended pinning centers in the

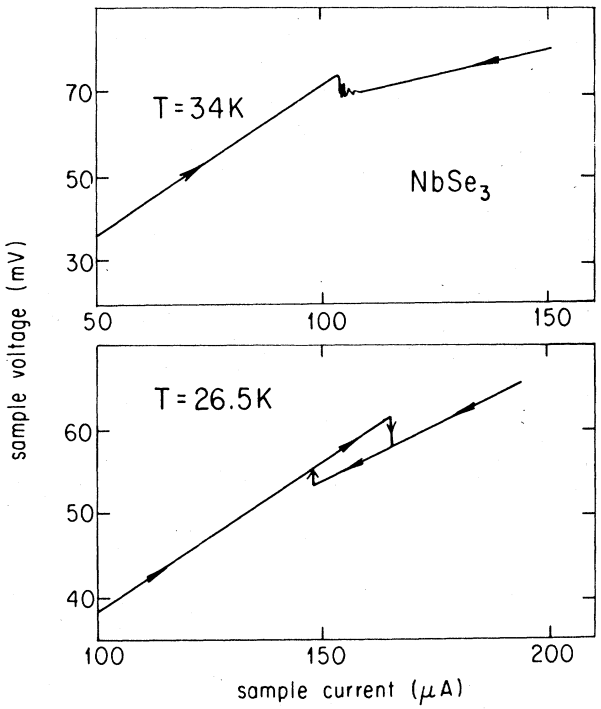

FIG. 12. Current-voltage characteristics observed in $NbSe_3$ at two different temperatures (Zettl and Grüner, 1982a, 1982b, 1982c).

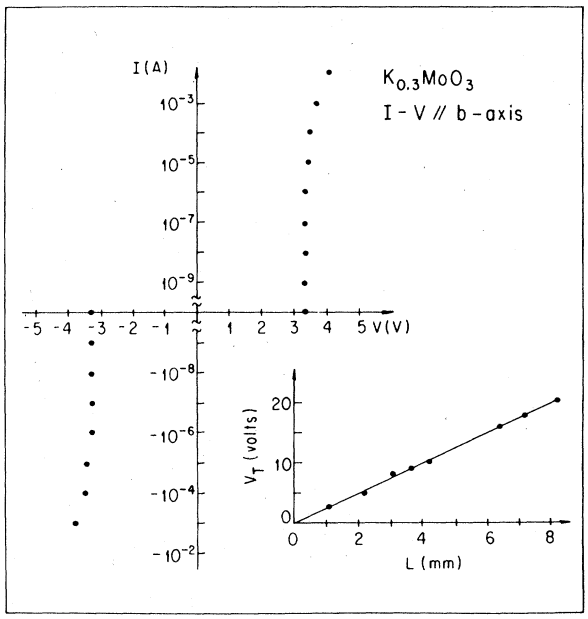

FIG. 13. Current-voltage characteristics measured in $K_{0.3}MoO_3$ at low temperatures. Beyond V_T a small change in the applied voltage leads to orders-of-magnitude increase of the current.

materials, and this has been demonstrated directly by locating (by using moving contacts) the exact positions where such behavior is generated (Brown and Mihály, 1985; Hall *et al.*, 1986). At very low temperatures $T \ll T_p$ still a different type of nonlinearity, a rather steep current-voltage characteristic is observed (Mihály and Tessema, 1986), with a threshold field 1 or 2 orders of magnitude larger than E_T where the smooth nonlinear conduction such as that displayed in Fig. 11 occurs. The overall behavior of the current-voltage characteristics, shown in Fig. 13, and the threshold field are similar to those observed in ordinary semiconductors where the effect is due to hot electrons. Consequently, the behavior may be of single-particle origin and not related to the onset of charge-density-wave-transport. However, strong polarization effects, certainly due to deformations of the CDW, are observed below V_T. This would suggest that the nonlinear conduction and charge-density-wave dynamics are intimately related.

The fact that the charge-density wave is not destroyed, but contributes to the dc current for $E > E_T$, in experiments such as those displayed in Figs. 10–12 has been demonstrated by performing x-ray experiments in the nonlinear conduction region (Fleming *et al.*, 1978, 1984). The superlattice reflections were found in the current-carrying region with intensities equal to those measured without an applied field. The observation demonstrates that the charge-density wave executes a translational motion in the presence of an applied electric field. This has been confirmed by a series of NMR experiments performed in various materials.

Other types of experiments also suggest that the CDW is, by the application of electric fields, driven out of the pinned configuration, and, furthermore, that the dynamics of the internal deformation of the mode is important. Here, the relaxation back to a pinned state is monitored through the measurement of the normal (Ohmic) resistance. Making the natural assumption that local changes of the CDW phase around pinning centers also lead to the changes in the resistance R_n of the normal electrons that are excited across the gap, the time evolution of this quantity can be used as a measure of the above relaxation process. Figure 14 shows R_n as a function of time after an applied electric field larger than E_T is removed (Mihály and Mihály, 1984). A slow, logarithmic time decay

$$R_n(t) - R_n(0) = A_0 \ln \frac{t}{t_0}$$

is observed over many decades in o-TaS_3, with similar sluggish time response in other materials. Here R_{n0} is the normal electron resistance for an "equilibrium" configuration achieved as $t \to \infty$. The observation is qualitatively similar to those made on spin glasses after an applied magnetic field. This similarity is not accidental and suggests the absence of long-range order (and, consequently, a broadly defined "glassy" behavior) for a CDW that is pinned by randomly positioned impurities. More complicated phenomena, such as remanent dielectric polarization, are related to the above observation.

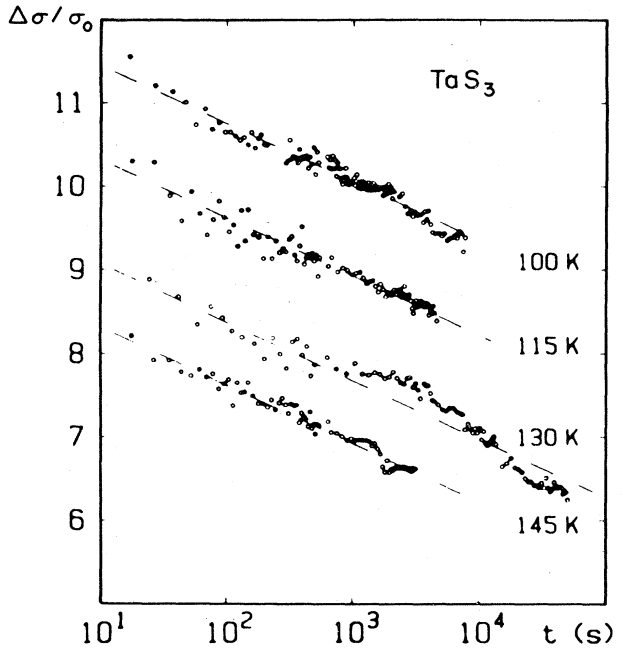

FIG. 14. Time dependence of the low-field dc conductivity after a thermal quench. The temperatures refer to the base temperature where the reaction is monitored (from Mihály and Mihály, 1984).

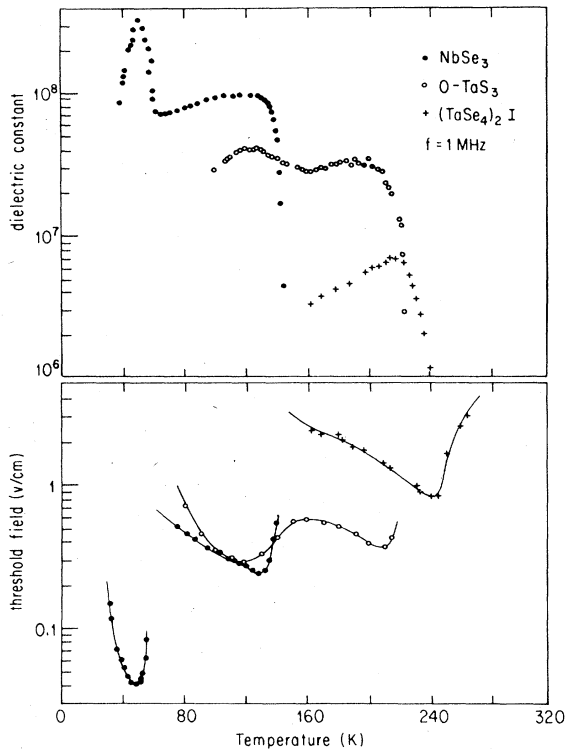

FIG. 15. Temperature dependence of the threshold electric field E_T and low-frequency dielectric constant (ε measured at $f=4$ MHz) in various materials. The solid lines are guides to the eye.

The long-time effects associated with these relaxation phenomena may also play a role in the details of the depinning process, and therefore also in determining current-voltage characteristics in the nonlinear conductivity region.

The parameters that characterize the frequency- and field-dependent conductivity vary from material to material, and they also display a characteristic temperature dependence. While in the majority of cases, pinning by impurities plays the most important role (except in rather pure specimens with small dimensions where boundary effects may be important), as a rule the threshold electric field E_T is smaller, and the low-frequency dielectric constant ε is larger in materials with smaller Peierls transition temperature. In Fig. 15 these two parameters are displayed for various materials as a function of temperature. The decrease of ε and increase of E_T near T_P is most probably related to the strongly temperature-dependent condensate density, but the low-temperature behavior of these parameters is unexplained. The decreasing ε and increasing E_T with decreasing temperature may be related to the local thermal oscillation of the impurities, but alternatively to temperature-induced local excitations of the collective mode. In o-TaS_3 and in $K_{0.3}MoO_3$, which become commensurate below about $T\sim 100$ K, pinning by the lattice may be important, but such effects presumably do not play an important role in the other compounds where the CDW remains incommensurate with the underlying lattice. It has also been suggested that temperature-driven fluctuations of the phase (a phenomenon similar to the Debye-Waller effect) lead to the temperature-dependent threshold field (Maki, 1986).

C. Other transport coefficients

While the low-field dc conductivity provides clear evidence for the metal-to-semiconductor transition associated with the development of the CDW ground state, other transport coefficients, such as thermoelectric power (TEP) and Hall effect, also reflect the removal of the Fermi surface by the transition. A small, metalliclike TEP above T_P is usually followed by a strong rise below the transition. This is accompanied by similar changes in the Hall constant. At temperatures below T_P these parameters can, in general, be accounted for by formulas developed for ordinary band semiconductors, with a temperature-dependent gap $\Delta_s(T)$ having the BCS form and disappearing at the transition. At low temperatures, where also the dc conductivity deviates from the exponential form, anomalies in the TEP (Allgeyer *et al.*, 1982; Fisher, 1983; Johnston *et al.*, 1983) and Hall effect (Ong, 1982) can also be found. It is likely these reflect the contribution of impurity states to the transport coefficients.

Equation (3.23) implies a two-band model where the normal electrons and electrons in the CDW condensate

provide separate and independent channels for the conduction process. While this description suggests a collective transport carried by the CDW when electric fields exceed threshold, other transport measurements performed in the nonlinear conductivity region provide direct evidence that the current at high fields is carried by a ground-state condensate.

Early measurements (Dee *et al.*, 1979) of the thermoelectric power in $NbSe_3$ are in apparent conflict with the Fröhlich conduction mechanism. Detailed measurements on *o*-TaS_3 (Stokes *et al.*, 1984) and subsequently on other materials indicate that no, or very little, entropy is associated with the nonlinear electrical conduction as expected for a current carried by a ground-state condensate. Both the measurement and the analysis of TEP experiments, when extended to investigate nonlinear phenomena, require special care. First, conventional experiments use an open circuit, $J=0$ configuration. In order to detect a contribution to the thermopower in the nonlinear regime, a finite current has to be applied. Second, conventional discussions of thermoelectric effects consider only small thermal and electric gradients in cases of systems initially in thermal equilibrium. For a system initially in a nonequilibrium steady state (driven by an electric field E) at a uniform temperature T, the electric and heat current densities δJ and δU are given by

$$\delta J(E)=\left.\frac{dJ}{dE}\right|_{E=E_0}\delta E+\frac{L_{12}(E_0)}{T^2}\nabla T\ ,$$
$$\delta U(E)=\left.\frac{dU}{dE}\right|_{E=E_0}\delta E+\frac{L_{22}(E_0)}{T^2}\nabla T\ , \tag{3.26}$$

where ∇T is the applied (small) temperature gradient, and L_{12} and L_{22} are Onsager coefficients. The thermoelectric power, for constant current density is given by

$$S(E_0)=\frac{-L_{12}}{T^2\left.\frac{dJ}{dE}\right|_{E=E_0}}\ . \tag{3.27}$$

For a two-fluid model of the normal electrons and the CDW condensate as suggested by Eq. (3.23), the TEP is given by

$$S(E_0)=\frac{S_N\left.\frac{dJ}{dE}\right|_{\text{normal}}+S_{\text{CDW}}\left.\frac{dJ}{dE}\right|_{\text{CDW}}}{\left.\frac{dJ}{dE}\right|_{\text{normal}}+\left.\frac{dJ}{dE}\right|_{\text{CDW}}}\ , \tag{3.28}$$

where the subscripts refer to the differential conductivities for the normal and condensed electrons. For the case $S_{\text{CDW}}=0$, the above equation reduces to

$$\frac{S(E_0)}{S_N}=\frac{\sigma'_N(E)}{\sigma'_N(E)+\sigma'_{\text{CDW}}(E)}\ . \tag{3.29}$$

Here $\sigma'=dJ/dE$ is the differential conductivity. Therefore, for $S_{\text{CDW}}=0$, the electric field dependence of the total measured thermopower S is expected to be the same as that of the inverse differential conductivity. In Fig. 16 these parameters measured in *o*-TaS_3 are displayed as a function of electric field. Within experimental error Eq. (3.29) is obeyed over a wide range of applied fields confirming that (to within the experimental error) $S_{\text{CDW}}=0$.

The Peltier heat is related to the thermoelectric power by

$$\Pi(E)=TS(E_0)\{\sigma'(E_0)E_0[J(E_0)]^{-1}\}\ , \tag{3.30}$$

and consequently $\Pi(E)$ associated with the nonlinear conduction is also close to zero. This analysis suggests that, in contrast to single-particle transport where the Wiedeman-Franz law applies, no or very little entropy transport is associated with the nonlinear electric conduction. The slight deviation from Eq. (3.28) observed at low temperatures can be accounted for by phonon-drag phenomena (Stokes *et al.*, 1983). Similar conclusions are reached for $(TaSe_4)_2I$ and in the upper transition of $NbSe_3$, while at the lower phase transition in $NbSe_3$ the anomalous behavior (Dee *et al.*, 1979) suggests that phonon-drag effects may be dominant. Such effects were studied subsequently by Kriza and Mihály (1987), who extended the early experiments on TaS_3 higher electric fields and found deviations from Eq. (3.29) that became more important at lower temperatures. The reason for this behavior is not clear at present, but it may signal the breakdown of a simple two-fluid model for large CDW velocities.

Within the framework of the two-fluid model, the Hall voltage V_H, for a magnetic field H perpendicular to the chain direction, is given by

$$V_H=\frac{\sigma_N\mu_{N\perp}+\sigma_{\text{CDW}}\mu_{\text{CDW}\perp}}{(\sigma_N+\sigma_{\text{CDW}})_\perp}HE\ , \tag{3.31}$$

where E is the electric field applied along the chain direc-

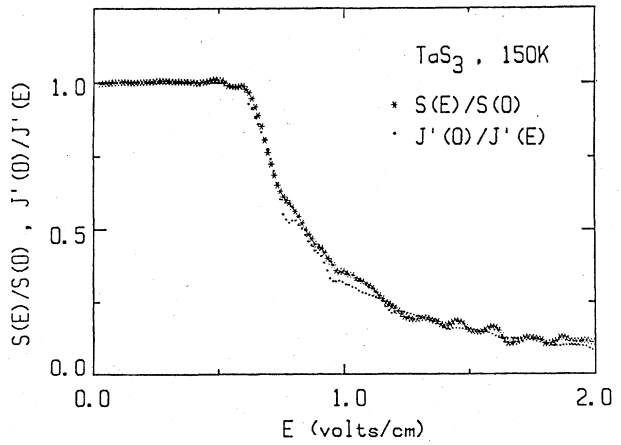

FIG. 16. Electric field dependence of the thermopower S and differential conductivity $I'=dI/dV$ in *o*-TaS_3 (Stokes *et al.*, 1984).

tion. $\mu_{N\perp}$ and $\mu_{\mathrm{CDW}\perp}$ are the contributions of the normal and CDW electrons, respectively, to the mobility perpendicular to the chain direction at electric field E, while $(\sigma_N+\sigma_{\mathrm{CDW}})_\perp$ refers to the total perpendicular conductivity that corresponds to the Hall voltage. Measurements performed in $NbSe_3$ (Kawabata *et al.*, 1981; Tessema and Ong, 1981) lead to a Hall voltage that is proportional to the electric field up to fields of $E\sim 2E_T$; for such electric field values V_H is smaller than the threshold field E_T. Consequently, the current associated with the nonlinear conduction is extremely anisotropic and is not influenced by the Lorentz force. While this was subsequently confirmed in TaS_3 (Artemenko *et al.*, 1984) for electric fields slightly exceeding E_T, for larger electric fields deviations from $V_H\sim E$ are found, the effect being more apparent at low temperatures. The most detailed experiments were performed recently on $K_{0.3}MoO_3$ (Forró *et al.*, 1985) and in $NbSe_3$ (Everson *et al.*, 1984); both point to the apparent breakdown of the two-fluid description at low temperatures and at high magnetic fields. In the former compound the CDW current is accompanied by normal electron backflow, while in $NbSe_3$ there is a conversion between the CDW and normal carriers by the magnetic field.

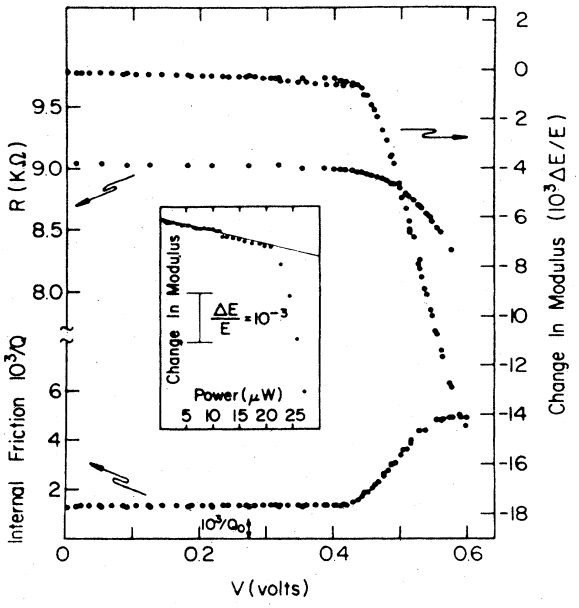

FIG. 17. Resistance, 1/(quality factor), and relative change in modulus $\Delta E/E_0=2\Delta f/f_0$ vs voltage at 149 K in TaS_3. O_0 is the quality factor in vacuum at zero voltage. Inset: $\Delta E/E_0$ vs power dissipated in sample at 149 K. The line shows the proportionality below threshold (Brill and Roark, 1984).

D. Elastic properties

The metal-to-semiconductor transition is associated with pronounced anomalies of the elastic properties. The Young's modulus has a large dip, and the internal friction increases at T_P (Brill and Ong, 1978; Brill, 1982; Mozurkewich *et al.*, 1985a, 1985b). These anomalies, not unexpected for a structural phase transition, are related to specific-heat anomalies within the framework of the Clausius-Clapeyron equation (see, for example, Testardi, 1975), which account for the changes in the elastic constant. Corresponding changes in the internal friction remain unexplained.

Both the Young's modulus and the internal friction show large anomalies in the nonlinear conductivity region. This was first investigated in *o*-TaS_3 (Brill and Roark, 1984; Brill *et al.*, 1986), in *o*-TaS_3, $(TaSe_4)_2I$, and $NbSe_3$ (Mozurkewich *et al.*, 1985b; Xiang and Brill, 1988), and in $K_{0.3}MoO_3$ (Bourne *et al.*, 1986). Experimental results for the electric field dependence of the elastic modulus $\Delta E'/E'$ and internal friction $\delta'\sim Q^{-1}$ (where Q is the quality factor of the elastic resonance) measured in TaS_3 are displayed in Fig. 17. The onset of nonlinear conduction leads to a decrease of E' and an increase of δ'. Similar behavior was found in $NbSe_3$ and in $(TaSe_4)_2I$ (Mozurkewich *et al.*, 1985b; Suzuki *et al.*, 1986), but no effect was observed in $K_{0.3}MoO_3$ (Bourne *et al.*, 1986). The shear modulus was also measured recently, showing significant anomalies as the function of applied electric field (Xiang and Brill, 1988).

While the detailed underlying mechanism for the observed effect is not clear, it is expected that a pinned CDW would contribute to the elastic constant while, for a completely unpinned mode, such contribution would be negligible. Moreover, damping effects associated with the dynamics of the internal modes can be responsible for the increased internal friction observed. The change of the elastic constant can be estimated by a mode coupling approach, where the phonon and phason branches are coupled through Coulomb forces (Mozurkewich *et al.*, 1985b), or by calculating the longitudinal sound velocity (Coppersmith and Varma, 1984) and taking the internal degrees of freedom explicitly into account (Sneddon, 1986; Maki and Virosztek, 1988; Zeyher, 1988). Such calculations lead to the softening of the lattice in the sliding conductivity region. These models also give specific predictions concerning the electric field dependence of the bulk modulus and attenuation; these are in broad semiquantitative agreement with experiments performed mainly in TaS_3.

E. Nuclear magnetic resonance

The most direct evidence for moving charge-density waves comes from NMR experiments. Transitions to the CDW state have profound influence on the NMR spectrum, mainly because of the inhomogeneous broadening caused by the charge-density-wave modulation through quadrupole effects.

The development of the periodic modulation of the charge density leads to a periodic modulation of the electric-field-gradient tensor, and the frequency associated with the transitions between the nuclear levels is given by (Berthier and Ségranson, 1987)

$$\Delta v_{m\to m+1}(\mathbf{R}G)=\Delta v^{0}_{m\to m+1}(T\mathbf{C})+\frac{\omega_1}{2\pi}\cos(2k_F\mathbf{r}+\varphi)$$
$$+\frac{\omega_2}{2\pi}\cos^2(2k_F\mathbf{r}+\varphi)\ , \qquad (3.32a)$$

where the numerical factors ω_1 and ω_2 depend on the amplitude of the CDW and on the quadrupole moment. For an incommensurate CDW, Eq. (3.32a) leads to a line broadening, which can be calculated and contrasted with the experimentally found broadening. Such studies have clearly established the development of charge-density modulation below the Peierls transition. This has been studied in detail in $NbSe_3$ (Devreux, 1982; Wada *et al.*, 1984) and in $Rb_{0.3}MoO_3$ (Butaud *et al.*, 1985).

The NMR line shape in the presence of uniform CDW velocity has been worked out in detail (Kogoj *et al.*, 1984) as the function of the velocity v. The solution leads to a motional narrowing and the appearance of a central line at the unperturbed Larmor frequency. While early studies (Douglass *et al.*, 1985) did not reveal any motional narrowing, subsequent experiments in $NbSe_3$ (Ross *et al.*, 1986) and in $Rb_{0.3}MoO_3$ (Nomura *et al.*, 1986; Ségranson *et al.*, 1986) clearly established the motional narrowing associated with moving charge-density waves. A detailed analysis and the reevaluation of CDW velocity require the calculation of NMR line shapes, with the added complication that often only part of the sample is involved in the nonlinear conduction process. Such analysis leads to CDW velocities in good agreement with those expected from studies summarized in the next section. The results suggest a distribution of CDW velocities in $Rb_{0.3}MoO_3$ (Berthier and Ségranson, 1987); such effects are much less evident in $NbSe_3$ (Ross *et al.*, 1986).

F. Current oscillations

Perhaps the most spectacular observation in the field is the detection of current oscillations in the nonlinear conductivity region. The phenomenon, which has been studied both in the time and in the frequency domain, is often referred to as "narrow-band noise." The term "noise," however, is misleading. Consequently, we refer to the phenomenon as current oscillations.

Depending on the experimental arrangement, either an oscillating current or an oscillating voltage is detected; the former for a constant voltage, the latter for a constant current drive. Due to the presence of normal electrons that lead to a normal component to the total current and thus contribute to the voltage drop across the specimen, the usual experimental configuration represents an intermediate situation. To first approximation, the current oscillation amplitude Δj_1 and the oscillating voltage ΔV_1 are related by $\Delta J_1=\Delta V_1/R$, where R is the measured resistance of the specimen at a frequency that corresponds to the frequency of the oscillations.

Figure 18 shows the first observation by Fleming and Grimes (1979) made on $NbSe_3$, where the Fourier spectrum of the time-dependent voltage, recorded by a spectrum analyzer, is displayed. Only a structureless broadband noise is observed for electric fields below threshold, but for $E>E_T$ sharp peaks superimposed on a large amplitude broadband noise are evident. The spectrum consists of a fundamental frequency and of several harmonics with slowly decaying intensity. For increasing electric fields, the amplitude and the frequencies increase. The spectra shown in Fig. 18 indicate a time-dependent current with a periodic but nonsinusoidal time dependence. This was subsequently confirmed by studies in real time domain, following a pulse applied to the specimens (Bardeen *et al.*, 1982; Fleming, 1982). Spectra, similar to those shown in Fig. 18, have been subsequently observed in all materials where nonlinear conduction occurs—in TaS_3 (Grüner, Zettl, Clark, and Thompson, 1981), in $(TaSe_4)_2I$ (Wang, Monceau *et al.*, 1983), in $(NbSe_4)_{3.33}I$ (Wang, Saint-Lager *et al.*, 1983), and in $K_{0.3}MoO_3$ (Dumas *et al.*, 1983)—and consequently is a characteristic overall feature that accompanies the non-

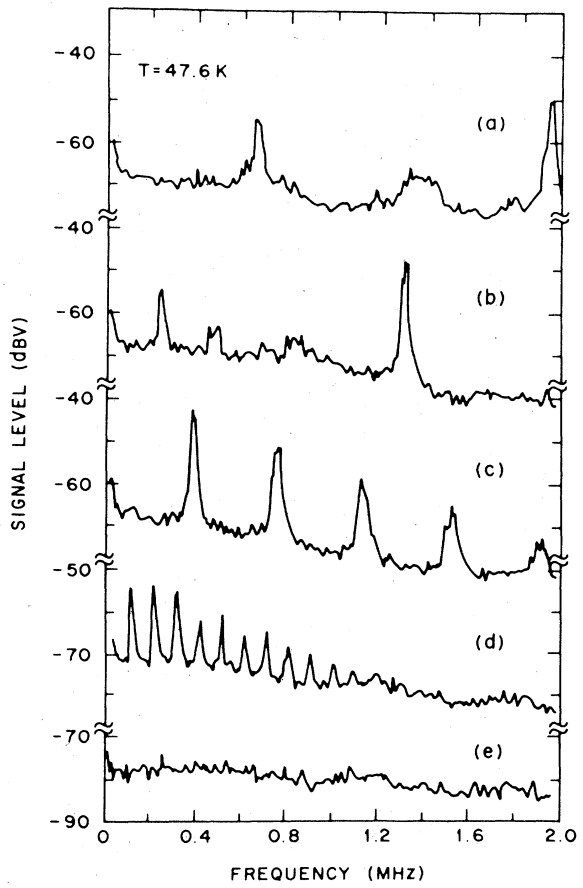

FIG. 18. Fourier transform of the time-dependent current in $NbSe_3$ or various applied currents. Narrow-band "noise" results if the current exceeds the threshold value for nonlinear conduction. Currents and dc voltages are (a) $I=270\ \mu A$, $V=5.81$ mV; (b) $I=219\ \mu A$, $V=5.05$ mV; (c) $I=154\ \mu A$, $V=4.07$ mV; (d) $I=123\ \mu A$, $V=3.40$ mV; (e) $I=V=0$. The sample cross-sectional area $A\approx 136\ \mu m^2$ (Fleming and Grimes, 1979).

linear conduction process.

The frequency of the oscillations is approximately proportional to the excess current carried by the CDW (Monceau *et al.*, 1980); furthermore, the ratio of the excess current to the frequency varies with temperature, approximately as the number of condensed electrons n_c (Bardeen *et al.*, 1982). Figure 19 displays the linear relation between $I_{\rm CDW}$ and f_0 in a wide frequency range for a pure $NbSe_3$ specimen (Bardeen *et al.*, 1982), with the ratio $I_{\rm CDW}/f_0$ as the function of T in the inset. Normalizing to CDW current for one chain, the above observations can be described as

$$\frac{j_{\rm CDW}}{f_0}=\text{const}\times e\times\frac{n_c(T)}{n_c(T=0)}\ , \tag{3.32b}$$

where $j_{\rm CDW}$ refers to the current per chain. While the precise value of the constant in Eq. (3.32b) is still debated, it is between 1 and 2 for a broad range of materials.

The above relation between the current and oscillation frequency is associated with the fundamental periodicity associated with the phase φ. The CDW current, described in terms of drift velocity v_d of the (rigidly moving) condensate, is given by $j_{\rm CDW}=n_c e v_d$. Associating the fundamental frequency with a CDW displacement by one period, $f_0=v_d/\lambda$, leads to

$$\frac{j_{\rm CDW}}{f_0}=n_c(T)e\lambda\ , \tag{3.33}$$

with $\lambda=\pi/k_F$ and $n_c=2k_F/\pi$. Equation (3.32b) with a constant $c=2$ is then recovered. Alternatively, the fundamental frequency can be related to the energy difference ΔE between the two sides of the displaced Fermi surface shown in Fig. 7(b). With

$$\Delta E\sim\frac{\partial E}{\partial v}v_d=\frac{\partial E}{\partial k}\frac{\partial k}{\partial v}v_d=2v_F v_d\ , \tag{3.34}$$

$\Delta E=hf_0$ and $j_{\rm CDW}=n_c e v_d$ also leads to Eq. (3.32) with $c=2$. The strictly linear relation between $j_{\rm CDW}$ and f_0 as displayed in Fig. 19 suggests that the CDW velocity is constant throughout the specimen. Indeed $j_{\rm CDW}$ is proportional to f_0 over a broad range of currents and frequencies only in high-quality specimens. In materials where evidences suggest that disorder plays an important role, deviations from the linear relation between $j_{\rm CDW}$ and f_0 are observed (likely related to finite velocity-velocity correlation lengths).

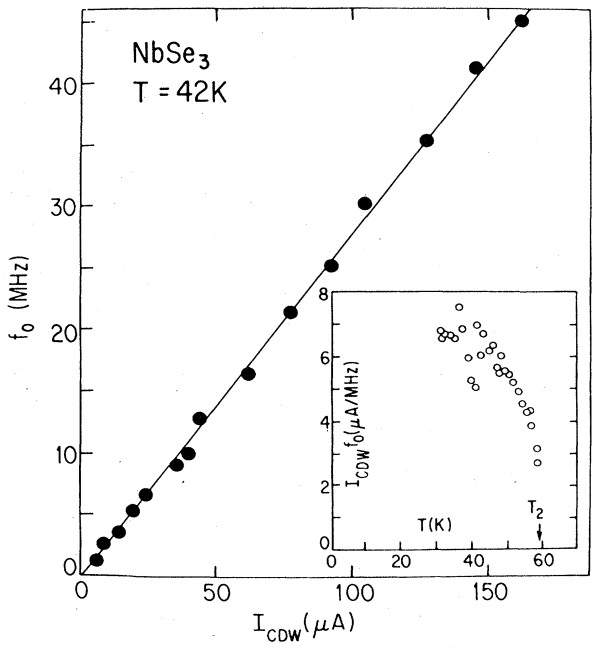

FIG. 19. Relation between the CDW current and fundamental oscillation frequency in $NbSe_3$. The inset shows $I_{\rm CDW}/f_0$ vs temperature (Bardeen *et al.*, 1982).

The question of whether current oscillations are generated in the bulk or at boundaries, like current contact, has been hotly debated, and a variety of experiments have been designed to test the validity of both assumptions. While it is generally agreed that current oscillations are a finite-size effect and do not occur in the thermodynamic limit, the issue of current generation has not yet been resolved. Experiments where the noise amplitude was measured as the function dimensions of the specimens (Mozurkewich and Grüner, 1983a; Ong, Verma, and Maki, 1984) led to contradictory results. Experiments involving nonperturbative contacts that also can be moved along the length of the specimens favor bulk noise generation (Brown and Mihály, 1985). Various experiments have also been performed in the presence of a temperature gradient, which leads to different temperatures T_1 and T_2 at the site of the current contacts, placed, in general, at the ends of the specimens. In case of oscillating current generation at the contacts, under certain circumstances a splitting of the oscillation frequencies is expected. While the first experiments (Zettl *et al.*, 1984) did not show such splitting in subsequent measurements (Ong, Verma and Maki, 1984; Ong and Maki, 1985), such splitting has indeed been detected. It has, however, been shown that a further increase of the temperature gradient leads to further splitting of the oscillation frequencies (Brown, Mozurkewich, and Grüner, 1985; Lyding *et al.*, 1986). The multiple splittings suggest the formation of velocity coherent regions with a minimum length of the order of 100 μm. Similar conclusions have been reached by Monceau *et al.* (1986) by employing temperature gradients large enough to heat the contact regions above the transition temperature. The current oscillations were present under such circumstances, indicating that they are not generated exclusively by carrier injection at the contacts. While these experiments do not give a clear answer to the question of current generation, they do raise the important question of topological defects in charge-density waves and the possibility of phenomena associated with the dynamics of the amplitude of the order parameter (Gorkov, 1983; Batistic *et al.*, 1984; Ong, 1984; Ong and Maki, 1985).

In addition to the current oscillations, the nonlinear

conduction is also accompanied by a substantial broad band noise with an effective noise temperature of several thousand degrees (Richard, Monceau, Popoular *et al.*, 1982; Grüner and Zettl, 1983). The spectral dependence can be well described by an $f^{-\alpha}$ behavior (Bhattacharya *et al.*, 1985; Maeda, Furuyama, and Tanaka, 1986), and the amplitude of the noise voltage is inversely proportional to the square-root volume, suggestive of fluctuations generated by independent pinning centers in the bulk (Richard, Monceau, and Renard, 1982; Bhattacharya *et al.*, 1985). It has also been suggested, on the basis of experiments on intentionally damaged specimens (Thorne *et al.*, 1987), that broad band noise is either generated by macroscopic defects or is mainly reflective of the distribution of various current oscillation components. The $1/f^{\alpha}$ spectrum may then represent the distribution of heat frequencies between various coherent regions separated by macroscopic defects. The phenomena have also been interpreted as due to a current noise, generated at various pinning centers (Wonneberger and Breymayer, 1984)

The amplitude, and also the phase of the current oscillation, displays characteristic time dependences (Brown *et al.*, 1985b; Bhattacharya *et al.*, 1987; Link and Mozurkewich, 1988). Fluctuations of both the position and the amplitude of the peaks in the Fourier-transformed spectrum are indicative of noise generation in various regions in the specimens, which then are weakly coupled through the nonlinear medium. Such weak coupling may lead to temporal locking of oscillations in the various regions of the specimens, with locking-unlocking effects leading to low-frequency fluctuations. The time-average width of the Fourier-transformed "narrow-band noise" scales with the observed broad band noise amplitude, indicating that the two are intimately related.

IV. THE MECHANISMS OF PINNING

Both the frequency- and the electric-field-dependent conduction observed in materials with incommensurate charge-density-wave ground state are the consequence of the interaction between the collective mode and the lattice irregularities. The interaction leads to a finite pinning energy; this in turn shifts the oscillator strength to finite frequencies and also results in a finite dc threshold for nonlinear conduction. Pinning effects, together with the fundamental $2k_F$ periodicity of the problem, are also responsible for the current oscillation phenomena.

In contrast to superconductors, the relevant collective mode, the phason mode with the dispersion relation (3.2b), is gapless. The collective mode can distort around potentials represented by $V(\mathbf{r})$, thus lowering the total energy of the collective mode. The Ginzburg-Landau Hamiltonian for a potential that couples directly to the phase of the CDW is (Fukuyama and Lee, 1978)

$$\mathcal{H}=\frac{n_c\hbar v_F}{4\pi}\int(\nabla\varphi)^2 d\mathbf{r}+\int\rho_1 V(\mathbf{r})\cos[2\mathbf{k}_F\cdot\mathbf{r}+\varphi(\mathbf{r})]d\mathbf{r}\ . \tag{4.1}$$

The first term on the right-hand side represents the elastic energy associated with the long-wavelength phase deformations; the second represents the interaction of the collective mode with the pinning potential. It is assumed that the amplitude of the collective mode is not perturbed by the interaction between the collective mode and the potential $V(\mathbf{r})$. Consequently, Eq. (4.1) is expected to be appropriate for relatively weak potentials, which are substantially smaller than the band gap Δ_s. The combined effect of elastic and potential-energy terms in Eq. (4.1) is a decrease of the total energy. Because the potential depends on the position $V(\mathbf{r})$, the interaction also leads to pinning of the collective mode. For small amplitude displacements the pinning energy is given by $E_{\rm pin}=K(x-x_0)^2/2$, where K is the restoring force constant and $(x-x_0)$ is the rigid displacement of the mode from the equilibrium position x_0, which is established as a result of the potential $V(\mathbf{r})$. In terms of a purely classical description of the small amplitude oscillations of the collective mode, the pinning frequency is $\omega_0^2=K/m^*$, and the dc dielectric constant is given by

$$\varepsilon=1+\frac{4\pi n_c e^2}{K}\ , \tag{4.2}$$

which can be substantial for a small restoring force. A dc electric field leads to the translational motion of the condensate and, consequently, to a current-carrying state when the energy provided by the dc field over one period λ is larger than $E_{\rm pin}$. The condition that follows from this argument leads to a threshold field

$$E_T=\frac{\lambda K}{2e}\ . \tag{4.3}$$

The ω- and E-dependent responses of the pinned mode are strongly related. By taking $K=m^*\omega_0^2$, the relation between E_T and the characteristic pinning frequency ω_0 is

$$E_T=\frac{\lambda m^*\omega_0^2}{2e}\ , \tag{4.4}$$

and the dielectric constant is related to E_T through the relation

$$E_T\varepsilon(\omega\rightarrow 0)=4\pi e n_\perp\ , \tag{4.5}$$

where $n_\perp$ is the number of chains per unit area. At $T=0$, $n_{\rm CDW}=2n_\perp/\lambda$. These arguments completely neglect the role played by the internal modes of the condensate in the dynamics. It is assumed that after the long-wavelength deformations around the pinning potentials are established, the response to external dc and ac driving forces is accounted for by considering the time dependence of the average phase. The internal deformations, however, remain unchanged when going from the

pinned to the current-carrying state.

Since the restoring force drops out in Eqs. (4.4) and (4.5), they are expected to be appropriate for any pinning mechanism. Impurities, grain boundaries, lattice defects, and even the boundaries of the specimens may contribute to the overall restoring force. Because of early experimental evidences suggesting that impurities play an important role in pinning the collective mode, only impurity pinning has been considered in detail. Recently it has become increasingly more evident, however, that pinning by macroscopic defects and surfaces may also be important under certain circumstances.

A. Impurity pinning

The interaction between impurities and the CDW has fundamental consequences on both the static and dynamic properties. As first argued by Sham and Patton (1976), Imry and Ma (1975), and Efetov and Larkin (1977), long-range order is destroyed by randomly positioned impurities, and, in less than four dimensions, the phase-phase correlation function has the form

$$e^{i[\varphi(\mathbf{r})-\varphi(0)]} \approx e^{-r/L_0} , \tag{4.6}$$

where the characteristic length scale L_0 depends on the strength of the impurity potential and on the elastic properties of the condensate. L_0 can be evaluated using scaling arguments (Fukuyama and Lee, 1978). For a random impurity distribution, with impurity potentials $V(\mathbf{r})=V_0\delta(\mathbf{r})$, Eq. (4.1) reads

$$\mathcal{H}=\frac{n_c\hbar v_F}{4\pi}\int(\nabla\varphi)^2 d\mathbf{r}+V_0\rho_1\sum_i \cos[2\mathbf{k}_F\cdot\mathbf{r}_i+\varphi(\mathbf{r}_i)] , \tag{4.7}$$

with i referring to random impurity sites. In Eq. (4.7) it is assumed that spatial fluctuations of the phase $\varphi(\mathbf{r})$ occur for wavelengths large compared to the amplitude coherence length $\xi_a=hv_F/kT_p$, on the order of 100 Å for typical materials. Also, amplitude fluctuations of the collective mode, together with quantum and finite-temperature effects, are neglected. The first term favors a spatially homogeneous phase, while the second term favors local distortions of the condensate where the phase is fully adjusted at every impurity site to obtain a maximum decrease of the potential energy. The ratio

$$\varepsilon'=\frac{V_0\rho_1}{\pi\hbar v_F} \tag{4.8}$$

tells whether the potential energy on elastic distortions is more important; $\varepsilon'>1$ is called strong impurity pinning and $\varepsilon'<1$ is called weak impurity pinning. For $\varepsilon'\gg 1$, where the elastic energy can be totally neglected, the pinning energy is simply due to total energy gain due to the electrostatic interaction with the impurities in $\varepsilon=V_0\rho_1 n_i$ and, consequently, the pinning energy (Fukuyama and Lee, 1978; Lee and Rice, 1979)

$$\varepsilon_{\rm pin}=V_0\rho_1 n_i\frac{\lambda_2}{2} \tag{4.9}$$

and the restoring force constant $K=V_0\rho_1 n_i$. All the arguments advanced earlier apply, and Eq. (4.3) with Eq. (4.9) leads to a threshold field proportional to the impurity concentration. The phase-phase correlation length is expected to be of the order of the distance between impurities, as each impurity completely breaks the phase of the condensate.

The case of $\varepsilon\ll 1$ (weak impurity pinning) is more interesting, and scaling arguments can be used to evaluate the phase-phase correlation length. In d dimensions one can define a volume $(L_0)^d$ over which the phase is constant but is adjusted to impurity fluctuations to have a maximum decrease of the potential energy. This argument (Fukuyama, 1978; Fukuyama and Lee, 1978) leads to the potential-energy density

$$\varepsilon_{\rm pot}=-V_0\rho_1\left[\frac{n_i}{L_0^d}\right]^{1/2} . \tag{4.10}$$

The elastic energy of the domain, using Eqs. (4.7) and (3.8), is given by

$$\varepsilon_{\rm elastic}=\frac{n_\perp\hbar v_F}{4\pi}L_0^d\left[\frac{\pi}{L_0}\right]^2 d , \tag{4.11}$$

where $n_\perp$ is the number of chains per unit area. Minimizing the total energy density of the domain with respect to L_0 leads to a finite phase-phase correlation length for any dimension $d<4$. In three dimensions

$$L_0^{-1}=\left[\frac{V_0\rho_1}{\pi\hbar v_F}\right]n_i \tag{4.12}$$

and the pinning energy

$$\varepsilon_{\rm pin}=-\tfrac{1}{4}\varepsilon_{\rm pin}=-\frac{1}{4}\frac{(V_0\rho_1)^4}{(\pi\hbar v_F n_\perp)^3}n_i^2 . \tag{4.13}$$

An anisotropic band structure also leads to an anisotropic phase-phase correlation length. As L_0 is proportional to v_F, see Eq. (4.12), the correlation length in the various directions scales with the anisotropy of v_F. With typical band anisotropies of the order of 10, L_0 is expected to be approximately 10 times larger along the chain direction than it is perpendicular to the chains. The anisotropy of L can be included in equations of $\varepsilon_{\rm pin}$ and E_T by appropriate scaling. Such a procedure leads to additional numerical factors of the order of $(v_z v_y/v_x^2)$, where x refers to the chain direction. The concentration dependence of the parameter remains, however, unchanged. Arguments similar to those used before lead to ω_0, to $\varepsilon(\omega\to 0)$, and to E_T with the following results:

$$\omega_0=2\pi\left[\frac{m}{m^*}\right]^{1/2}v_F L_0^{-1} , \tag{4.14}$$

$$\varepsilon(\omega\to 0)=1+\frac{n_\perp^4\hbar^4\pi n^3 v_F^2 n_{\rm CDW}e^2}{m^* V_0^4\rho_1^4 n_i^2} , \tag{4.15}$$

$$E_T = \frac{\pi\hbar v_F}{8e}\left[\frac{V_0\rho_1}{\pi\hbar v_F n_\perp}\right]^4 n_i^2 . \quad (4.16)$$

In contrast to the strong pinning case, E_T is proportional to the square of the impurity concentration, while $\varepsilon(\omega\to 0)\sim n_i^{-2}$.

For a typical impurity potential of $V_0 = 10^{-2}$ eV, with $v_F = 3\times 10^7$ cm/sec, and a CDW amplitude $\rho_1 = 0.1$, an impurity concentration of 1000 ppm leads to $\varepsilon'' \sim 2$, suggesting that for relatively pure specimens, strong impurity pinning is appropriate, while for alloys, with a substantial amount of impurities, the weak impurity pinning limit occurs. From Eq. (4.12) the phase-phase correlation length $L_{0x} \sim 1$ mm in three dimensions, comparable with the length of the specimens investigated. With a typical bandwidth anisotropy of approximately 10, the correlation length perpendicular to the chain direction is of the order of 0.1 mm, which is also comparable to the dimensions of typical specimens in this direction. This suggests that for pure specimens the phase is approximately constant over the volume, and that pinning by sources other than impurities (such as the surface or contacts) may also contribute. The pinning energy, for strong impurity pinning [see Eq. (4.14)], is on the order of 10^{-2} K with the above parameters. This is the same order of magnitude as the energy $\hbar\omega_0$, which corresponds to the peak in the frequency-dependent conductivity in various pure materials, shown in Fig. 9.

The discussion above, and the notion of weak and strong impurity pinning, is appropriate only for weak impurity potentials V_0 that do not perturb the amplitude of the collective mode considerably. The Ginzburg-Landau treatment, which leads, for example, to Eqs. (4.12) and (4.13), breaks down when $V_0 > \Delta$; in this case, bound states develop for weak impurities in the gap region, and for strong impurities outside the gap (Tüttő and Zawadowski, 1985). These, in principle, could be detected by optical experiments; however, no attempt has been made to search for the predicted features.

B. Experiments on alloys and irradiated specimens

The importance of impurity pinning is confirmed by a broad range of studies where the electric field and frequency-dependent response is investigated in alloys or on specimens where impurities are created by irradiation. Early experiments (Ong *et al.*, 1979; Brill *et al.*, 1981) on $NbSe_3$ alloys suggested that E_T is proportional to n_i^2, in agreement with weak impurity pinning.

Experiments performed on alloys in a broad concentration range (Monceau, 1982; Underweiser *et al.*, 1987), however, indicate that the situation is more complicated than that suggested by the scaling approach of Fukuyama and Lee (1978). In Fig. 20, E_T measured below the second phase transition is displayed as a function of the reciprocal residual resistivity ratio $(\mathrm{RRR})^{-1}$. The latter is proportional to the total strength of the impurity

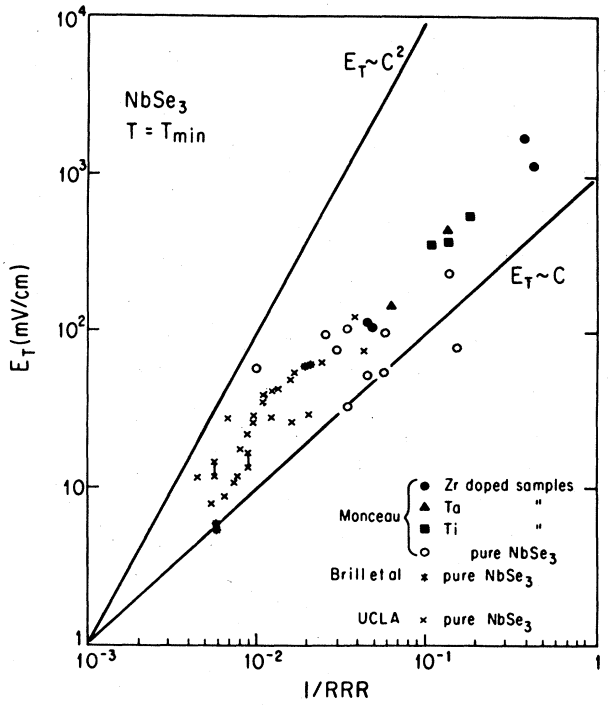

FIG. 20. Threshold electric field vs inverse residual resistivity ratio in pure $NbSe_3$ and in alloys. The straight line represents the linear and the quadratic concentration dependence of E_T, $E_T \sim n_i^m$ (Monceau, 1982; Underweiser, 1987).

scattering and can consequently be regarded as a scaled impurity concentration n_i. While E_T strongly increases with increasing n_i, the functional dependence is somewhat stronger than linear, but weaker than n_i^2. The behavior is not understood at present. It may be the consequence of a crossover between strong impurity pinning for small concentration, and weak impurity pinning for large concentration of impurities. Alternatively, finite-size effects may play an important role for small impurity concentrations where the phase-phase correlation length becomes comparable to the dimension of the specimens. The large scatter of the data for relatively pure specimens also indicates that pinning centers other than impurities may become important. In contrast, in the upper CDW state of $NbSe_3$, E_T was found to be a linear function of n_i suggesting that the strong impurity limit is appropriate even for small impurity potentials such as those represented by the Ta atoms. In materials where defects are introduced by irradiation ($NbSe_3$: Fuller *et al.*, 1981; TaS_3: Mihály, Mihály, and Mutka, 1984; $K_{0.3}MoO_3$: Mutka *et al.*, 1984), E_T is proportional to the defect concentration, suggesting strong impurity pinning. Such behavior, observed in electron-irradiated $Rb_{0.3}MoO_3$ and $K_{0.3}MoO_3$ (Mutka *et al.*, 1984), is displayed in Fig. 21; the solid line corresponding to $E_T \sim n_i$, E_T also increases with alloying for TaS_3, and this increase is proportional to the square of ΔT_P, the change of the Peierls transition temperature with alloying (Hsieh *et al.*, 1983). As ΔT_P

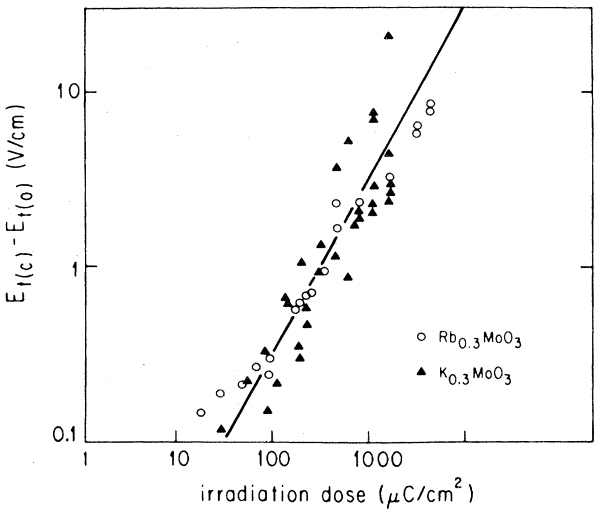

FIG. 21. Threshold electric field vs irradiation dose in $K_{0.3}MoO_3$ and $Rb_{0.2}MoO_3$ (from Mutka *et al.*, 1984).

is proportional to $n_i^{1/2}$ (Mihály, Mihály, and Mutka, 1984), E_T increases linearly with the impurity concentration. In $Rb_{0.3}MoO_3$ doping increases E_T, roughly proportional to the square of the dopant concentration, suggesting that in this material doping the Rb chain may lead to weak-impurity-pinning effects (Schneemeyer *et al.*, 1985). The strongly concentration-dependent threshold field is accompanied by corresponding changes in the frequency-dependent response. The pinning frequency has been measured directly by investigating the ω-dependent response both in TaS_3 (Reagor and Grüner, 1986) and in $(TaSe_4)_2I$ (Kim *et al.*, 1987), but in the absence of the precise impurity concentrations, the functional dependence of ω_0 on n_i could not be evaluated. The relation between $\varepsilon(\omega\rightarrow 0)$ and E_T has, however, been

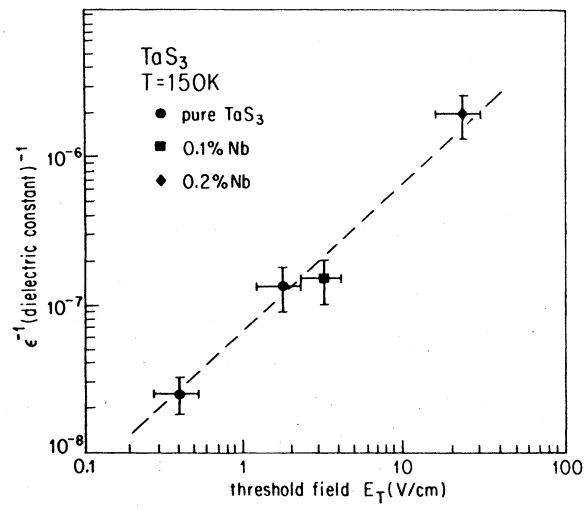

FIG. 22. Inverse low-frequency dielectric constant ε (4 MHz) vs threshold field E_T in o-TaS_3 alloys (Wu *et al.*, 1985).

investigated by measuring both parameters on the same specimens of alloys $Ta_{1-x}Nb_xS_3$ (Wu, Mozurkewich, Mihály, and Grüner, 1984). The results are shown in Fig. 22. The solid line gives

$$\varepsilon(\omega\rightarrow 0)E_T = 0.75 e n_\perp , \tag{4.17}$$

which is within an order-of-magnitude agreement with Eq. (4.5). Although the frequency-dependent response has not been investigated in detail, the relation $E_T \sim \omega_0^2$ was also confirmed by frequency-dependent studies performed at microwave frequencies in irradiated o-TaS_3 (Mihály, Hutiray, and Mihály, 1983).

With the role of impurities clearly established by experiments performed on alloys and on irradiated specimens, it is expected that various correlation lengths (determined by the strength of impurity potentials, concentration, etc.) play a fundamental role in the dynamics of the collective mode.

The static phase-phase coherence length L_0 is related to the overall pinning energy, and Eq. (4.2), which is expected to be model independent, relates L_0 to the pinning frequency ω_0. With the parameters used before, $m^*/m \approx 10^3$ and $v_F = 3\times 10^7$ cm/sec, a characteristic pinning frequency (derived from the frequency-dependent response, see Fig. 9) of approximately 10^{10} sec^{-1} leads to L_0 on the order of 10 μm. Equation (4.12) refers to the correlation length along the chain direction L_{0x}; because of the anisotropic Fermi surface, the correlation lengths in the perpendicular directions L_{0y} and L_{0z} are 1 to 2 orders of magnitude less than the above estimate.

The finite static correlation length leads to a broadening of the superlattice reflections and thus could, in principle, be determined by scattering experiments. Because of the limited resolution, such studies give only a lower bound on the range of phase correlations both parallel to the chains and in the perpendicular directions. Both in $NbSe_3$ and in $K_{0.3}MoO_3$, the diffraction peaks are resolution limited (Fleming *et al.*, 1982, 1984). This sets a lower bound of $L_{0x} > 0.4$ μm in $NbSe_3$ and > 0.7 in $K_{0.3}MoO_3$; the phase coherence perpendicular to the chains extends over a distance of approximately 0.2 μm.

While the pinning frequencies are not available in different materials and for different impurity concentrations, the measured low-frequency dielectric constants can be used to estimate L_0 in the chain direction. Equation (4.15) when combined with Eq. (4.14) leads to

$$\varepsilon(\omega\rightarrow 0) = 1 + \frac{4\pi n_c e^2 L_{0x}^2}{\pi m v_F^2} ,$$

and $\varepsilon = 4\times 10^7$ (appropriate for o-TaS_3) together with $v_F = 3\times 10^7$ cm/sec leads to $L_{0x} = 50$ μm. Similar $\varepsilon(\omega\rightarrow 0)$ values are found in other pure materials, and consequently L_{0x} is expected to be the same order of magnitude. In alloys, the concentration-dependent dielectric constants (such as those displayed in Fig. 22) can be used to estimate the concentration dependence of the correlation length.

C. Finite-size effects: Pinning by surfaces and by extended defects

For relatively pure specimens where the overall impurity potential $\sum_i V_i$ is weak, other defects such as dislocations and grain boundaries may also play an important role; in small specimens, the surface of the specimens or the contacts may act as pinning centers. The latter has been investigated in several materials by measuring the threshold field as the function of the dimension of the specimens.

The total pinning energy in the case of boundary effects may come from pinning centers in the bulk, from the surface, and also from the pinning by the contacts placed (ideally) at the end of the specimens. These have a different dependence on the sample dimensions, and in general, in terms of restoring forces which act on the collective mode, can be written as

$$K = K_{\text{bulk}} + K_{\text{surface}} + K_{\text{contact}} = t_1 AL + t_2 SL + t_3 A \ , \tag{4.18}$$

where A, L, and S refer to the cross section, length, and surface (per unit length) of the specimen. The constants t_1, t_2, and t_3 refer to the pinning strengths for unit dimensions. The threshold electric field is given in the presence of the various contributions to pinning by

$$E_T = \frac{V_T}{L} = \frac{\lambda}{2e}\frac{k}{AL} = \frac{\lambda}{2e}\left[t_1 + t_2\frac{S}{A} + \frac{t_3}{L}\right] . \tag{4.19}$$

In the thermodynamic limit with boundary effects neglected, E_T is independent of the dimensions of the specimen. For surface pinning it increases with decreasing cross section (for a square cross section $E_T \sim A^{-1/2}$), and for contact pinning it increases with decreasing length, with E_T given by Eq. (4.19). The relative importance of these effects is determined by the constants t_1, t_2, and t_3.

Various experiments indicate that pinning by the contacts is important for short specimens. The threshold field E_T has been investigated as the function of length L of the specimens in $NbSe_3$ (Zettl and Grüner, 1984; Gill, 1985; Prester, 1985) and in TaS_3 (Mihály, 1983). The results displayed in Fig. 23, can be described well by

$$E_T = E_T \frac{(L + L_0)}{L} \ , \tag{4.20}$$

with L_0 a characteristic length also given in the figure. While the experimental results can be accounted for by assuming a restoring force due to the contacts placed at the end of the specimens, or by assuming that a finite correlation length L_0 is important, recent experiments (Monceau *et al.*, 1986) suggest that contact pinning is important. Indeed, for $L_0 \sim 100\mu$ the number of sites near or at the contacts is comparable to the number of impurity sites. Thus impurity and contact pinning is comparable for comparable impurity and contact potentials.

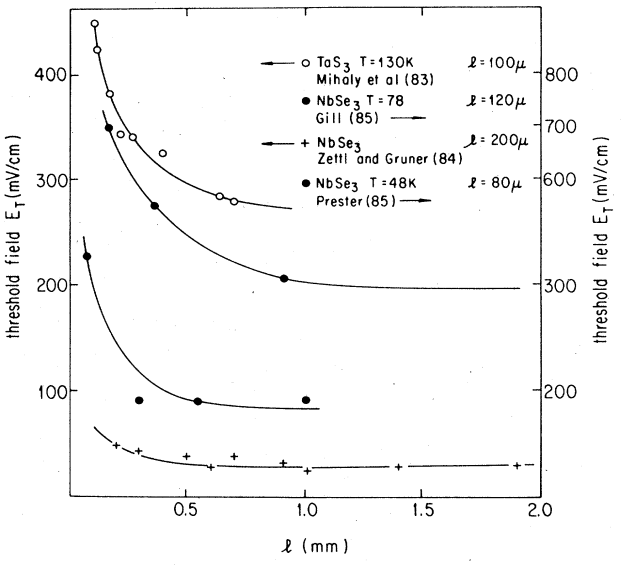

FIG. 23. Length dependence of the threshold field E_T in $NbSe_3$ and in TaS_3. The solid lines are fits to Eq. (4.19) with L_0 values given on the figure.

Careful experiments have been reported recently on specimens with small cross section (Borodin *et al.*, 1986; Gill, 1986c; see also Fig. 24). In both *o*-TaS_3 and in $NbSe_3$, the threshold field scales with the cross section of the specimens as $E_T \sim A^{-1/2}$, a clear indication for the importance of surface pinning in specimens where the cross section is smaller than approximately $100\mu^2$. A simple estimate suggests that the pinning potential due to surface is approximately the same as an impurity potential. The above critical cross section is not unreasonable. For a specimen of square cross section with $A = 100\mu^2$,

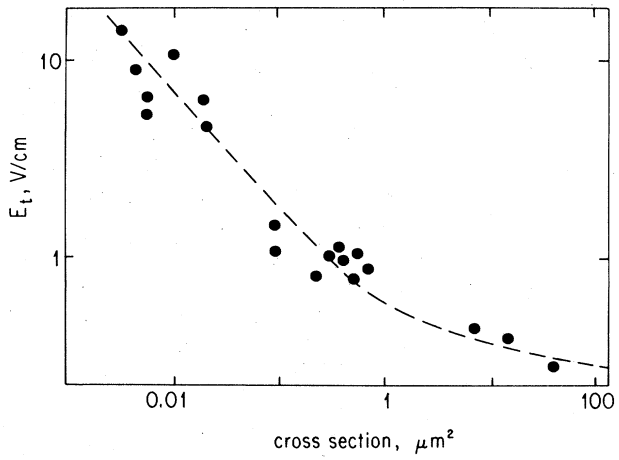

FIG. 24. Dependence of the threshold field E_T on the cross section of the specimens in the upper CDW state of $NbSe_3$.

the ratio of the surface-to-bulk atomic sites is approximately 10^2. If $t_1 \simeq t_2$, then an impurity concentration of 1% leads to an equal contribution to the pinning for impurities and for the surface. Careful experiments on specimens with different impurity concentrations are required to test the above experiments. It is clear, however, that for sample dimensions of $A \simeq 100\mu^2$ and $l \simeq 100\mu$, pinning by surfaces plays an important role.

V. MODELS: A SHORT OVERVIEW

A variety of models have been proposed to account for the main characteristics of the frequency- and electric-field-dependent conduction of the coherent current oscillations and low-frequency relaxation phenomena. They range from soliton models, which assume that commensurability effects are important (Horowitz and Krumhans, 1984; Horowitz *et al.*, 1986) through Frenzel-Kontorova-type models (Bak, 1982b; Coppersmith, 1984) to models similar to those that describe plastic deformations of crystals (Feinberg and Dumas, 1986). While they are interesting as examples of nonlinear dynamical systems, it appears that commensurability effects—required to be essential in soliton or Frenzel-Kontorova models—are not important, while other models have not been developed to an extent where a comparison with theory is appropriate.

Two rather different approaches have been advanced to account for the variety of experimental findings. Both assume that the dynamics of the phase of the order parameter is important, and pinning is provided by inhomogeneities that couple directly to the phase. In both models, the frequency- and electric-field-dependent conduction is the consequence of the translational motion of the CDW condensate, as originally envisioned by Fröhlich (1954). Both models neglect a host of factors likely to be important, such as the dynamics of the amplitude mode and finite-temperature effects, among others. Consequently, the models are not expected to account for all the observations in all of the materials that have been investigated. Neglecting inertial effects, the equation of motion for the time dependence of the phase $\varphi(\mathbf{r})$ is given by

$$\frac{1}{\tau}\frac{d\varphi(\mathbf{r})}{dt} = -\frac{\delta H}{\delta \varphi} + \frac{k_F e E}{m^*} , \tag{5.1}$$

treating the phase $\varphi(\mathbf{r})$ as a classical variable. For one dominant pinning center, or for specimens with small dimensions, the phase may be regarded as uniform throughout the specimen. The equation of motion then is

$$\frac{1}{\tau}\frac{d\varphi}{dt} + \omega_0^2 \sin\varphi = \frac{2k_F e E}{m^*} , \tag{5.2}$$

the so-called "single-particle" model (Grüner, Zawadowski, and Chaikin, 1981; Monceau *et al.*, 1986). The form of the potential has been chosen for its apparent simplicity, but other potentials have also been considered (Grüner, Zawadowski, and Chaikin, 1981). They, too, follow from an electronic circuit analog (Weger *et al.*, 1980, 1983), also proposed as a simple description of CDW transport. Equation (5.2) is that of a classical particle moving in a sinusoidal washboard potential, as shown in Fig. 25. The response to small amplitude ac fields is the same as that of a harmonic oscillator. For small applied dc fields, the particle is displaced from the bottom of the potential well; for electric fields exceeding a certain threshold field E_T, the particle starts to roll down in the washboard potential. This leads to a nonlinear time-average velocity $\langle v(t) \rangle$ and also to a time-dependent component with a frequency proportional to $\langle v(t) \rangle$.

The current-voltage characteristics depend on whether the applied electric field E or the current is constant during the experiment. For E=const, the solution of Eq. (5.2) gives (Grüner, Zawadowski, and Chaikin, 1981)

$$\langle J(t) \rangle = \begin{cases} \sigma_N E + \dfrac{n_{\mathrm{CDW}} e^2 \tau}{m^*}(E^2 - E_T^2)^{1/2}, & E > E_T , \\ \sigma_N E, & E < E_T \end{cases} \tag{5.3}$$

where $\langle\ \rangle$ refers to time average, and the threshold field for the nonlinear conduction is given by

$$E_T = \frac{\lambda}{2\pi}\frac{m^* \omega_0^2}{e} . \tag{5.4}$$

The current also has a time-dependent component in the nonlinear conductivity region, with fundamental frequency

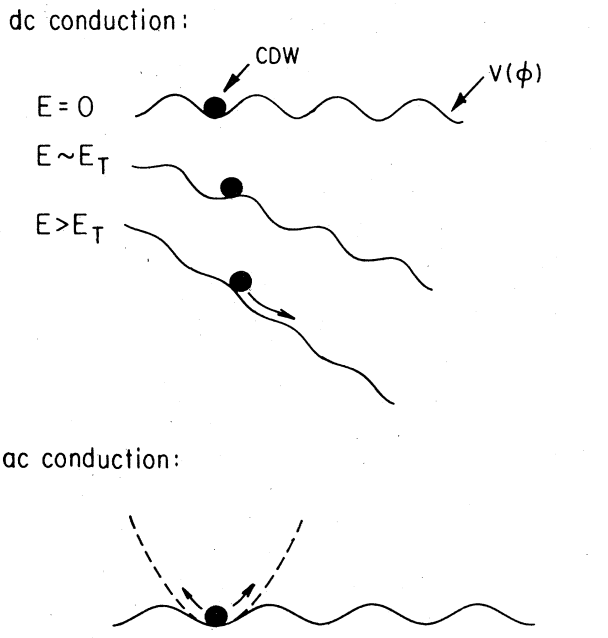

FIG 25. Classical particle model of charge-density-wave transport.

$$f_0=\frac{2e\tau}{m^*\lambda}(E^2-E_T^2)^{1/2} . \tag{5.5}$$

Combining Eqs. (5.3) and (5.5), we see that the relation between the time-average current and oscillation frequency is given by Eq. (3.33). With $\lambda=\pi/k_F$ and $n_\parallel=k_F/\pi$, for one chain

$$\langle j(t)\rangle=2ef_0=\frac{4e^2\tau}{m^*\lambda}(E^2-E_T^2)^{1/2} . \tag{5.6}$$

When the applied current is constant, the equation of motion [eliminating E from Eqs. (5.2) and (5.3)]

$$\frac{1}{\tau}[1+(n_{\rm CDW}e^2\tau/m^*)]\frac{d\varphi}{dt}+\omega_0^2\sin\varphi=\frac{2k_Fe}{m^*\sigma_N}J \tag{5.7}$$

has the same structure as Eq. (5.2) but with renormalized parameters and with a driving current replacing the applied electric field E. The measured electric field is time dependent, and the time-average electric field

$$\langle E(t)\rangle=\frac{1}{\sigma_N}\left[J-\frac{n_{\rm CDW}e}{2k_F}\frac{d\varphi}{dt}\right] \tag{5.8}$$

is given by

$$\langle E(t)\rangle=\frac{J}{\sigma_N}-\frac{(n_{\rm CDW}e^2\tau/m^*)E_T}{\sigma_N+n_{\rm CDW}e^2\tau/m^*}[(J/J_T)^2-1]^{1/2} , \tag{5.9}$$

where J_T is the threshold current corresponding to the threshold field E_T. The time-dependent component leads also to a linear relation between $j_{\rm CDW}$ and f_0 as before. The current-voltage characteristics that follow from the two descriptions are fundamentally different. While both predict sharp threshold fields for the onset of nonlinear conduction and lead to the same high electric field limit given by

$$\sigma(E\to\infty)=\frac{n_{\rm CDW}e^2\tau}{m^*}+\sigma_N . \tag{5.10}$$

A constant electric field leads to zero differential resistance, while for a constant current J an infinite negative differential resistance is obtained at threshold.

While this approach may be appropriate for rather small specimens, effects associated with the finite-phase correlation length L_0 may be important when L_0 approaches the dimensions of the specimens. Such a model was discussed by Klemm and Schrieffer (1983, 1984) and subsequently by Klemm and Robbins (1986). The equation of motion for $\delta\varphi(\mathbf{r},t)$ is treated by perturbation in terms of the impurity fluctuations. The solution gives a large number of metastable states even within a single domain of size L_0^3. A finite threshold field, comparable to that given by Eq. (5.4), is obtained, with current-voltage characteristics different from those given by the classical particle model. In particular, the differential conductivity increases with increasing electric field (except close to threshold) in contrast to the equations that describe the dynamics of a single degree of freedom. Current oscillations with features slightly different from those of the classical particle model are also recovered for a single domain. The model has also recently been extended to include finite-frequency effects (Robbins and Klemm, 1986). These become important at low frequencies and at fields close to the threshold field.

For sufficiently large specimens, close to the thermodynamic limit, a perturbation expansion in terms of impurity fluctuations breaks down, and Eqs. (4.1) and (5.1) represent a complicated nonlinear problem for which analytical solutions are not available for the full range of parameters. In the large velocity limit the effects of impurities can be treated perturbatively (Sneddon *et al.*, 1982) by a hydrodynamic approach. The average velocity is determined by dissipative processes associated with the dynamics of the local deformations, and in contrast to Eq. (5.3), the leading correction to the current is given by

$$\langle J(t)\rangle_t=\sigma_bE-A_1\sqrt{E} \tag{5.11}$$

in the infinite velocity limit. The frequency-dependent conductivity has a similar square-root behavior (Fisher, 1985; Robbins and Klemm, 1986), and in the high frequency, $\omega\gg\omega_0^2\tau$ limit

$$\sigma(\omega)=\sigma_b-\frac{A_2}{\sqrt{\omega}} . \tag{5.12}$$

Equations (5.11) and (5.12) imply a scaling between the ω- and E-dependent response in the high-velocity limit, i.e., the functional dependence on the frequency and field expected to be identical. Due to the local deformations of the charge-density wave around impurities, the velocity-velocity correlation function is finite and, consequently, the current oscillations disappear in the thermodynamic limit. The response to various joint ac and dc excitations has not been considered in detail in this limit. The dielectric constant, however, goes to zero for large velocities (Sneddon, 1984a, 1984b), and the amplitude of the Shapiro steps is independent of the volume (Sneddon *et al.*, 1982).

The perturbation treatment of the local deformations breaks down for small velocities, and a nonperturbative treatment of the large number of nonlinearly interacting degrees of freedom is required. Computer simulations can be performed by going from the continuum equation to a discrete lattice version (Weisz *et al.*, 1979; Sokoloff, 1981; Sokoloff and Horovitz, 1983; Matsukawa and Takayama, 1984) or by assuming that damping occurs only at the (discrete) lattice sites (Teranishi and Kubo, 1979; Pietronero and Strässler, 1983). In both cases the equilibrium configuration, and also the time-dependent phase at a particular site i, $\varphi(\mathbf{r}_i,t)$ is related to phases at other sites through a set of different equations. Due to the complexity of the problem, only one-dimensional models have been considered.

A different approach has been taken to treat the essential features of the dynamics in the nonperturbative re-

gime near threshold (Fisher, 1983, 1984, 1985). It is assumed that the phase-phase correlation length L_0 is much smaller than the dimensions of the specimens, and a discrete version of the Fukuyama-Lee-Rice model is proposed. The Hamiltonian on a discrete lattice is given by

$$H=\sum_{i,j}\kappa'(\mathbf{r}_i-\mathbf{r}_j)(\varphi_i-\varphi_j)^2-\sum_{i,j}V_j\cos(\varphi_i-\beta_j)\ ,$$
$$H_e=\sum eE\varphi_i\ , \tag{5.13}$$

where the first term represents the elastic energy of the charge-density wave, with elastic constant κ', the second, the interaction of the CDW with impurities at sites j, with the phase β_j a random variable between 0 and π. H_e describes the coupling of the CDW to the applied electric field. An essentially similar model has been proposed by Tua and Zawadowski (1984), where the subscripts i and j refer to macroscopic domains rather than to impurity sites. The important features of the model are the infinite number of internal degrees of freedom and the randomness due to the preferred phases β_j. The development of the current-carrying state is treated as a dynamical critical phenomenon, with several critical exponents that characterize the dynamical properties of the system. The behavior in the presence of applied fields is described using relaxational dynamics, both in the mean-field approximation (Fisher, 1983) and for short-range interactions (Fisher, 1984, 1985). The model leads to various critical exponents near E_T, among them the behavior of the average velocity. Above threshold is the most relevant to various observations. It is given by

$$\langle v(t)\rangle\sim(E-E_T)^{\xi},\quad \xi=\tfrac{3}{2}\ . \tag{5.14}$$

The exponent is different from the one that follows from the single-particle model that leads to $\xi=\frac{1}{2}$. Several frequency scales are important both above and below E_T; they determine the detailed frequency dependence in the presence of a dc bias and the amplitude of the current oscillations close to threshold (Fisher, 1985).

A rather different situation may occur when a large pinning center, such as a grain boundary, situated in the bulk of the specimen is important. This can effectively decouple the sample into two coherent domains, with weak coupling between the domains. The dynamics of the coupled phases at the two sides of the barriers may display features different from that of a single degree of freedom, or infinite degree of freedom of dynamics. In particular, switching and hysteresis effects similar to those that occur in coupled Josephson junctions may follow from such models (Mihály, Chen, and Grüner, 1987). Similar features are recovered from models that assume that the amplitude mode goes to zero at the barriers (Inui and Doniach, 1987).

While all of the above models treat the phase of the condensate as a classical variable, a rather different approach has been taken by Bardeen (1979, 1980, 1984, 1986) by assuming that tunneling processes are responsible for the advancement of the average phase $\langle\varphi\rangle$ of the condensate. Advancement of the CDW phase by tunneling in a single chain was first treated by Maki (1977, 1978). Bardeen's model, which has been used extensively to analyze experimental results, relies heavily on phase coherence between the neighboring chains. The model, which applies in the weak impurity pinning limit, has evolved hand-in-hand with the experiments and at present it is able to account for a broad variety of observations made in the presence of dc and ac electric fields (see, for example, Thorne *et al.*, 1987, and references cited therein). The model starts from the Fukuyama-Lee-Rice theory (Fukuyama and Lee, 1977; Lee and Rice, 1979) and replaces the phase-phase correlation length L_0, given by Eq. (4.12), with periodic pinning forces at distance L_0 apart. This leads to a position-dependent phase as shown in Fig. 26. Two degenerate solutions are possible for this particular pinning, and these are given by

$$\varphi_A=\frac{\pi}{2}\sin\frac{\pi x}{L_0}\ ,$$
$$\varphi_B=-\pi-\frac{\pi}{2}\sin\frac{\pi x}{L_0} \tag{5.15}$$

with both minimizing the pinning energy (Bardeen, 1986). The periodicity of the pinning fields to a pinning gap at the Fermi level and this has to be overcome by the dc field in order to induce nonlinear conduction. The pinning potential has the form of

$$V(\theta)\sim\begin{cases}-\cos\theta & \text{for } \dfrac{\pi}{2}<\theta<\dfrac{\pi}{2}\ ,\\ \cos\theta & \text{for } \dfrac{\pi}{2}<\theta<\dfrac{3\pi}{2}\ ,\end{cases}$$

which is distinctively different from the sinusoidal potential that appears in Eq. (5.2). The pinning gap is given by

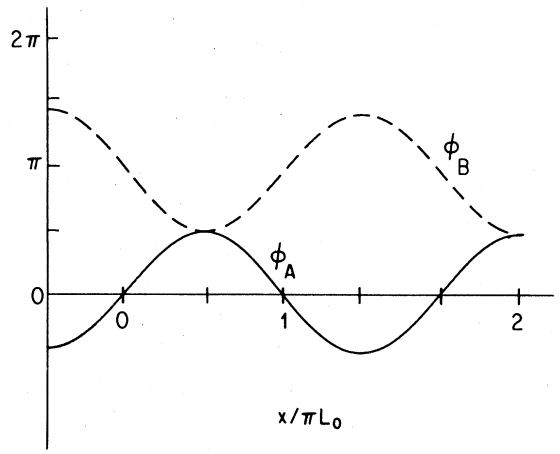

FIG 26. Phase variations that minimize the pinning energy in the tunneling model. $\phi_A(x)$ gives a minimum pinning energy when the average phase $\theta=0$, while $\phi B(x)$ gives minimum when $\theta=-\pi$ (after Bardeen, 1986).

$$E_g=\frac{2}{\pi}\left[\frac{m^*}{m}\right]^{1/2}\pi\Omega_p\ , \tag{5.16}$$

where $\Omega_p=\pi C_p/L_0$, with C_p the phason velocity given by Eq. (3.2b). The nonlinear conduction has the typical tunneling form

$$\sigma(E)=\sigma_\infty\left[1-\frac{E_T}{E}\right]\exp\left[-\frac{E_0}{E}\right]\ , \tag{5.17}$$

with

$$E_0=\frac{m^*}{m}\frac{\pi^2\omega_p^2}{V_F e} \tag{5.18}$$

similar to the equation for single-particle (Zener) tunneling. The threshold field E_T is the consequence of the finite correlation length. The frequency-dependent conduction follows from Tucker's photon-assisted tunneling (PAT) theory (Tucker, 1979), giving (Bardeen, 1984, 1986) a scaling relation between the ω- and E-dependent response,

$$\sigma\left[\frac{\omega}{\omega_p}\right]=\sigma\left[\frac{E}{E_T}\right]\ . \tag{5.19}$$

According to Eq. (5.19) the small amplitude ac conductivity as the function of frequency has the same functional form as the dc conductivity on the function of electric field. Both saturate at the high-frequency and high-field limit, and Eq. (5.19) also implies a sharp threshold frequency ω_p.

A detailed discussion of the tunneling steps and of the microscopic wave functions that characterize the pinned and current-carrying state, as well as the possible effects of disorder, can be summarized by Bardeen (1986, 1987) in several reviews.

The model does not treat the low-frequency fluctuations that are assumed to be decoupled for the tunneling that occurs at high frequencies (Tucker, 1986), nor does it treat the polarization effects that are important for processes below threshold (Miller *et al.*, 1985). Such processes are responsible for the absence of threshold frequency in contrast to Eq. (5.19).

VI. THE FREQUENCY- AND FIELD-DEPENDENT RESPONSE

Based on the models discussed above, a variety of predictions have been made concerning the small amplitude ac response $\sigma(\omega)$ and the nonlinear dc response $\sigma(E)$. Detailed comparisons between theory and experiment are also available. The models also describe various experiments performed in the presence of both dc and ac applied excitations. The fact that many of the observations can be observed for rather different approaches concerning the dynamics of the collective mode is not too surprising, as theories that are in agreement with the experimentally observed $\sigma(\omega)$ or $\sigma(E)$ are expected to account also for most of the observations on $\sigma(\omega,E)$. Many of the issues involved in analyzing the available experimental results are highly controversial at present; this is due partly to the fact that the experiments can be accounted for to a degree of accuracy using various starting points about the underlying theory, but also because the details of the nonlinear and frequency-dependent response are determined by the details of the pinning itself, and are dependent also on factors like temperature, size of the specimens, impurity concentration, etc.

A. Frequency-dependent response

The frequency-dependent response of pinned CDW condensates has been explored in detail over an extremely broad spectral range, with experiments ranging from audio to the millimeter wave frequencies. The main features of the small amplitude response are displayed in Fig. 9; such representation emphasizes the high-frequency part of the response, with important features observed in the radio-frequency spectral range and below not visible in the figure.

The simplest approach to account for the frequency-dependent conduction is to assume that the response is that of a harmonic oscillator with the equation of motion

$$\frac{dx^2}{dt}+\frac{1}{\tau}\frac{dx}{dt}+\omega_0^2 x=\frac{eE}{m^*}e^{i\omega t}\ , \tag{6.1}$$

where the pinning frequency ω_0 has been discussed before (see Sec. IV), the effective mass m^* is given in mean-field approximation by Eq. (3.4), and τ is a phenomenological damping constant. The real and imaginary part of the conductivity is given by

$$\mathrm{Re}\sigma(\omega)=\frac{ne^2\tau}{m^*}\frac{\omega^2/\tau^2}{(\omega_0^2-\omega^2)^2+\omega^2/\tau^2}\ , \tag{6.2}$$

$$\mathrm{Im}\sigma(\omega)=\frac{ne^2\tau}{m^*}\frac{(\omega_0^2-\omega^2)\omega/\tau}{(\omega_0^2-\omega^2)^2+\omega^2/\tau^2}\ . \tag{6.3}$$

Frequency-dependent-conductivity measurements have been performed in all materials that show charge-density-wave transport phenomena, and, in general, Eq. (6.27) gives a good description of the experimental findings. In Fig. 27, $\mathrm{Re}\sigma(\omega)$ and $\mathrm{Im}\sigma(\omega)$ are displayed for TaS_3 with a solid line given by Eq. (5.2) with parameters given in the figure (Sridhar *et al.*, 1986). The dotted line assumes a distribution of pinning frequencies, and the significance of this will be discussed later. The frequency-dependent response appears to be overdamped in TaS_3, and also in $NbSe_3$ (Reagor, Sridhar, and Grüner, 1986) in both CDW states, while in other materials a weakly damped response is observed—with τ, however, temperature and also impurity concentration dependent. The conductivity measured in $(TaSe_4)_2I$ and two different temperatures is shown in Fig. 28 (Kim *et al.*, 1987). While ω_0 is slightly temperature dependent, the main effect is the strongly increased damping of the higher temperature. Similar behavior has been found in

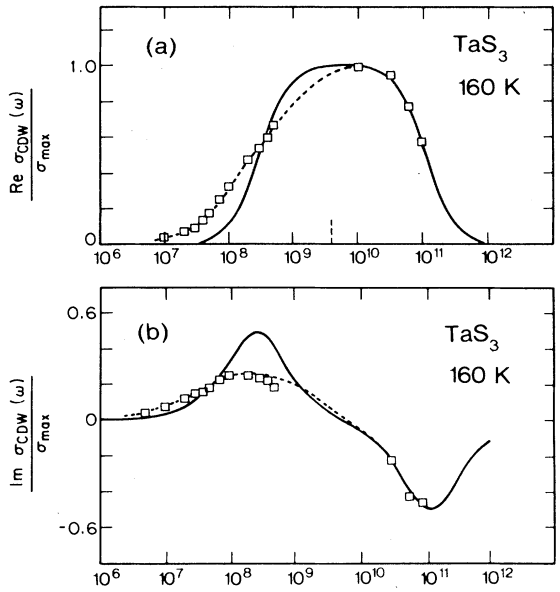

FIG. 27. Re$\sigma(\omega)$ and Im$\sigma(\omega)$ measured in nominally pure TaS_3. The solid line is a fit to a harmonic oscillator response, Eq. (6.2), with parameters given in the figure.

$(NbSe_4)_2I$ (Phillip *et al.*, 1987) and, although the data are far less complete, also in $K_{0.3}MoO_3$ (Ng *et al.*, 1986). Fits such as those displayed in Figs. 27 and 28 can be used to evaluate the basic parameters—the pinning frequency ω_0, the effective mass m^*, and the damping constant τ—and these can be compared with theory.

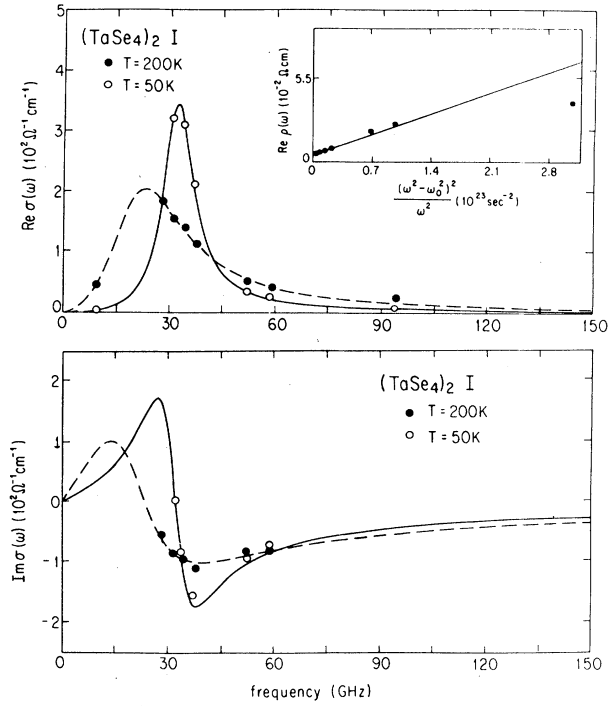

FIG. 28. Re$\sigma(\omega)$ and Im$\sigma(\omega)$ measured in nominally pure $(TaSe_4)_2I$ at two different temperatures. The solid line is a fit to a harmonic oscillator response, Eq. (6.2).

The pinning frequency ω_0 is in general of the order of 10^{11} sec^{-1} corresponding to a pinning energy $\hbar\omega_0 \sim 10^{-4}$ eV. It has also been shown, both in TaS_3 (Reagor and Grüner, 1986) and in $(TaSe_4)_2I$ (Kim *et al.*, 1987), that impurities increase ω_0 dramatically, but, due to lack of knowledge about the precise impurity concentrations, in the alloys investigated the concentration dependence could not be evaluated. In the strong pinning limit, the restoring force is given by $K = V_0\rho_1 n_i$ and, consequently, the pinning frequency

$$\omega_0 = \sqrt{\kappa/m^*} = \left[\frac{V_0\rho_1 n_i}{m^*}\right]^{1/2}, \tag{6.4}$$

giving, with $V_0 = 10^{-2}$ eV, $\rho_1 = 0.1$, $m^* = 10^3 m_c$ (the free-electron mass), and $n_i = 0.1\%$, a characteristic frequency of 10^{11} sec^{-1}, in good agreement with the experimental findings. It should be noted that ω_0 is higher for materials with high transition temperatures, and this is related to the higher threshold fields observed in materials with higher T_c (see, for example, Fig. 15). The significance of this is not clear, and the finding is surprising because ω_0 is expected to be determined by the residual impurity concentration, which certainly varies from material to material. Clearly detailed studies of ω_0 as a function of n_i in various materials would be highly desirable. The pinning frequency is also only weakly temperature dependent in the materials studied so far, in contrast to the strongly temperature-dependent threshold field E_T and dielectric constant $\varepsilon(\omega \to 0)$. This suggests that both E_T and $\varepsilon(\omega \ll \omega_0)$ are determined by processes that are not directly related to the harmonic oscillator response as given by Eq. (6.2).

The effective mass is found to be temperature independent (Reagor, Sridhar, and Grüner, 1986; Sridhar *et al.*, 1986), except close to T_p where the ratio m^*/m is (approximately) independent of temperature, in agreement with theory (Lee and Rice, 1979). m^* varies from material to material and strongly increases with increasing transition temperatures. The mean-field theory predicts that

$$\frac{m^*}{m} = 1 + \frac{4\Delta_s^2}{\lambda' \omega_{2k_F}^2}, \tag{6.5}$$

where Δ_s is the single-particle gap (not necessarily related to the transition temperature T_p, due to the anisotropic nature of these materials). The phonon frequency and the electron-phonon coupling constant are not expected to vary significantly from material to material, and, consequently, to a first approximation m^* should be proportional to Δ_s^2. Such a plot is shown in Fig. 29, where the single-particle gaps were evaluated from the optical data, from the temperature dependence of the dc resistivity below the transition, or from the analysis of the temperature-dependent magnetic susceptibility (Johnston *et al.*, 1985), and from optical (Geserich *et al.*, 1986; Herr *et al.*, 1986) and tunneling (Latyshev and Savitskaya, 1986) studies. The error bars represent ambigui-

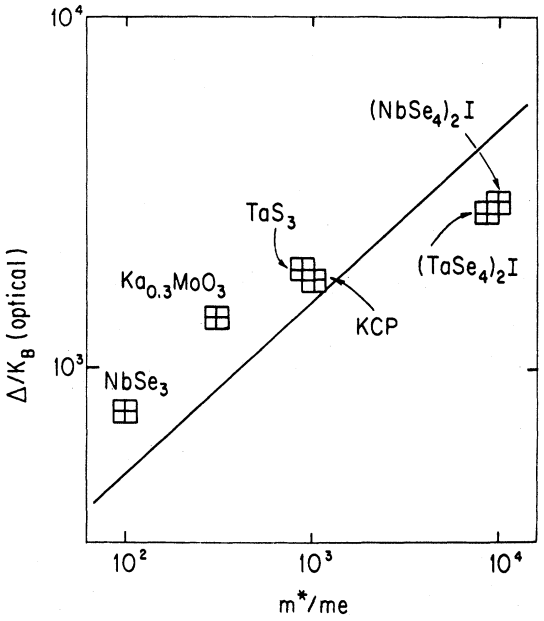

FIG. 29. Effective mass m^*/m_e vs the mean-field single-particle gap Δ for various compounds. The solid line represents the relation $m^*/m_e \sim \Delta^2$.

ties associated with such determination of Δ (Reagor, 1987). In $NbSe_3$, it has been assumed that the BCS relation $\Delta = 3.5 k_B T_c$ is appropriate; this, however, appears to be in disagreement with recent tunneling measurements (Fournel, Sorbier, Konczykowski, and Monseau, 1986). The solid line in Fig. 29 is Eq. (6.5) with $\lambda' = 0.5$ and $\omega_{2k_F} = 50$ K, both reasonable values.

In all cases investigated so far, a Drude-type equation with a single relaxation time describes well the frequency-dependent response at frequencies $\omega > \omega_0$, and the relaxation time τ can be evaluated, both as the function of impurity concentration (where such studies are available). In TaS_3 (Reagor and Grüner, 1986; Sridhar *et al.*, 1986), in $(TaSe_4)_2I$ (Reagor, Sridhar, and Grüner, *et al.*, 1986; Kim *et al.*, 1987), and in $(NbSe_4)_2I$ (Phillip *et al.*, 1987), $1/\tau$ decreases with decreasing temperature and remains finite as $T \to 0$. Experimental results on two $(TaSe_4)_2I$ specimens and on alloys of $(Ta_{1-x}Nb_xSe_4)_2I$ with $x = 0.6\%$ are displayed in Fig. 30. The data can be well represented by the empirical equation

$$\frac{1}{2\pi\tau} = A + BT^2 , \tag{6.6}$$

with A independent of the impurity concentration and B increasing with increasing number of impurities. This is in contrast to what is expected, as the temperature-dependent part should be the result of phonons or uncondensed electrons with the residual damping as $T \to 0$ of impurities. The observation is not explained at present.

The frequency-dependent response in the spectral range $\omega < \omega_0$ cannot be accounted for by a single harmonic oscillator response; the decrease of $\mathrm{Re}\sigma(\omega)$ with decreasing ω is more gradual than what follows from Eq. (6.2). The behavior can be explained by assuming wide distribution pinning frequencies (Sridhar *et al.*, 1986). Such an assumption gives, for a particular distribution, the dotted line of Fig. 31. While such an *ad hoc* assumption accounts for the main qualitative features of both $\mathrm{Re}\sigma(\omega)$ and $\mathrm{Im}\sigma(\omega)$, a different approach has been taken to describe the ω-dependent response in the radio frequency spectral range. At low frequencies both $\mathrm{Re}\sigma(\omega)$ and $\mathrm{Im}\sigma(\omega)$ can be described by a power-law frequency

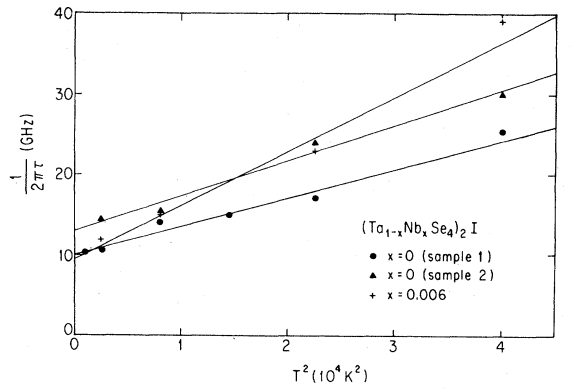

FIG. 30. Inverse relaxation time vs T^2 in two $(TaSe_4)_2I$ specimens (A and B) and an alloy with 0.6% Nb. Samples A and B have a pinning frequency of $\omega_0 = 17$ and 35 GHz, respectively.

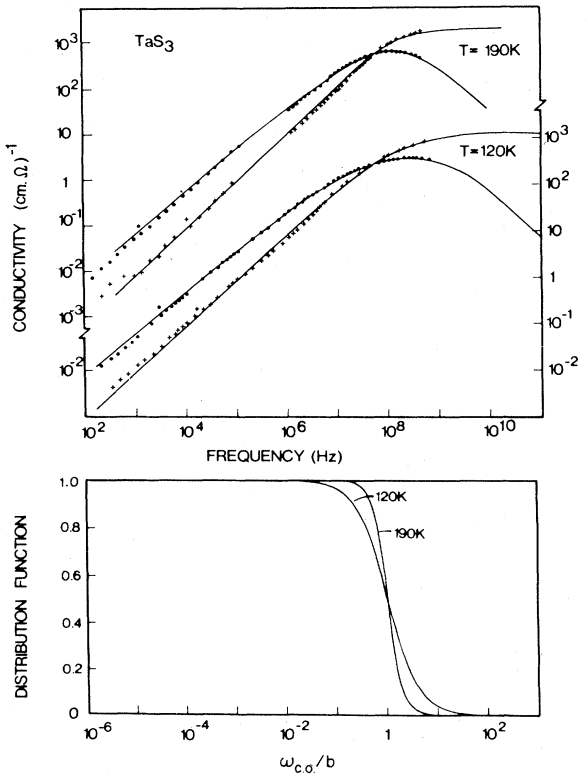

FIG. 31. Real and imaginary parts of the ac conductivity of TaS_3 vs frequency (Wu *et al.*, 1985).

dependence (Wu, Mozurkewich, Mihály, and Grüner, 1986)

$$\sigma(\omega)=A\left[\frac{i\omega}{\omega_0}\right]^{\alpha} \quad \text{with } \alpha=0.8\ . \tag{6.7}$$

Such behavior has been widely observed in various glasses and random systems (Ngai, 1979, 1980). The behavior also leads to a divergent dielectric constant $\varepsilon(\omega)=-4\pi \mathrm{Im}\sigma(\omega)/\omega$ as $\omega\rightarrow 0$, and this is often referred to as zero-field cusp (Fisher, 1985; Littlewood, 1986). At low frequencies deviations from Eq. (6.7) are observed (Cava, Fleming, Littlewood, Rietman, Schneemeyer, and Dunn, 1984; Kalem *et al.*, 1987), and the data are well represented in terms of an equation,

$$\varepsilon(\omega)=\varepsilon_{\mathrm{HF}}+(\varepsilon_0-\varepsilon_{\mathrm{HF}})\frac{1}{[1+(i\omega\tau_0)^{1-\alpha}]^{\beta}}\ , \tag{6.8}$$

where ε_0 and $\varepsilon_{\mathrm{HF}}$ are the zero- and high-frequency dielectric constants, τ_0 is an average relaxation time, and α,β (both less than one) are phenomenological parameters. Similarly to Eq. (6.7), Eq. (6.8) is also extensively used to describe the complex dielectric constant of various random and amorphous solids, and it has been found to account well for $\varepsilon(\omega)$ over a broad frequency range in pure (Cava, Fleming, Dunn, Rietman, and Schneemeyer, 1984) and in doped (Cava *et al.*, 1985) $K_{0.3}MoO_3$, in TaS_3 (Cava *et al.*, 1985; Kalem *et al.*, 1987), in $NbSe_3$ (Cava, Fleming, Littlewood, Rietman, Schneemeyer, and Dunn, 1984), and in $(TaSe_4)_2I$ (Cava *et al.*, 1986). A fit to data taken on $(TaSe_4)_2I$ is displayed in Fig. 32. The average relaxation time increases with decreasing temperature, and in all materials with a semiconducting CDW ground state the temperature dependence

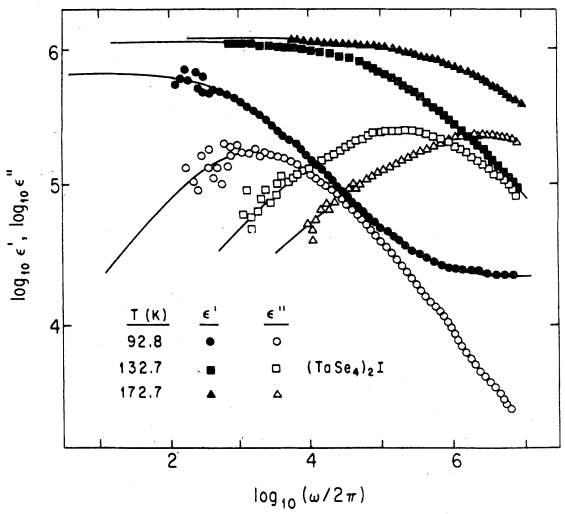

FIG. 32. Frequency dependence of the real (solid symbols) and imaginary (open symbols) parts of the dielectric constant for $(TaSe_4)_2I$ at three representative temperatures. Solid lines are from fits of Eq. (6.8) (from Cava *et al.*, 1986).

$$\frac{1}{\tau_0}\exp\left[-\frac{\Delta_T}{k_BT}\right]\ , \tag{6.9}$$

with Δ_T close to the single-particle gap, suggesting a close relation between the low-frequency CDW relaxation and the resistivity due to uncondensed electrons. The rather different behavior of the relaxation times evaluated from the high- and low-frequency transport data most probably reflects the different role of screening in different spectral regions. At high frequencies the small amplitude response is dominated by the oscillatory notion of the spatially averaged phase with the dynamics of local deformations not playing a significant role. Consequently, screening effects due to the normal electrons are not important. In contrast, at low frequencies Eqs. (6.7) and (6.8) suggest that the dynamics of local deformations are important. These involve the buildup of electric dipoles that have to be screened by the normal electrons. This screening time is often the order of the dc conductivity that rises exponentially with temperature, thus leading to Eq. (6.9) (Sneddon, 1984a, 1984b; Tucker *et al.*, 1986; Littlewood, 1987).

Considerable effort has been made to account for the frequency-dependent response in terms of the tunneling model. The model predicts a scaling relation, given by Eq. (5.19), between $\sigma(E)$ and $\sigma(\omega)$. Early experimental results on $NbSe_2$ (Grüner, Clark, and Portis, 1981) and TaS_3 (Zettl and Grüner, 1982) could indeed be well represented by a scaling relation. No threshold frequency was, however, observed. Subsequently, it was suggested (Miller *et al.*, 1985) that due to polarization effects, no threshold frequency occurs, and a revised scaling between ω and $E-E_T$ was postulated. This leads to an ω-dependent conductivity having the form

$$\sigma(\omega)\sim\exp\left[-\frac{\omega}{\omega_p}\right]\ .$$

Experiments that support this scaling theory have been summarized by Tucker (1986) and by Bardeen (1985a, 1985b). A behavior that can be represented as well as scaling has, however, been derived by Sneddon (1984a, 1984b, 1984c) and has also been shown to hold in the high-field and high-frequency limit (Robbins and Klemm, 1986), both of these on the basis of a classical description of the CDW dynamics.

B. Nonlinear conductivity

Nonlinear conduction has been studied in more detail than the frequency-dependent response, and a variety of nonlinear phenomena have been observed, depending, even for the same material, on the temperature, impurity concentration, crystal perfection, and sample dimensions. In the majority of cases, the onset of nonlinear conduction at E_T is smooth, with a qualitative behavior similar to those displayed in Figs. 10 and 11. The phenomenological equation (5.17), first suggested by Fleming and

Grimes (1979) on the basis of experimental data displayed in Fig. 11, has subsequently been found to account for $\sigma(E)$ in other materials in a semiquantitative way over a broad range of electric fields. The behavior is in clear contrast to the prediction of the single-particle model, Eq. (5.6), which leads to a sharp rise of $\sigma(E)$ at fields close to E_T. The two functional dependences of σ and E are displayed in Fig. 33, together with numerical simulations by Tua and Zawadowski (1984) and by Matsukawa and Takayama (1986), both taking the dynamics of internal deformations into account. Both simulations depend on the parameters, such as the ratio between the elastic energy of the CDW and the interaction energy between the CDW and impurities. The majority of the experimental results reported to date on $NbSe_3$ follow the solid line closely, and this also is appropriate for TaS_3 (Zettl, Grüner, and Thompson, 1982). Due to heating effects, experiments have not been performed in $(TaSe_4)_2I$ in in $K_{0.3}MoO_3$, which would have allowed a close comparison between theory and experiment. Based on Fig. 33, it is clear, however, that both a classical description of the CDW dynamics, with internal degrees of freedom included, and the tunneling model can describe the main features of the nonlinear conduction in various materials over a broad range of electric fields.

Several groups have measured the details of nonlinear conduction, both in the high electric field (or in the high CDW velocity) limit, and at electric fields close to E_T. The perturbation equation of the deformable continuum model leads to a square-root field dependence of the current $\langle j(t)\rangle$ [see Eq. (5.6)], while in the high-velocity limit Eq. (5.17) leads to $\langle j(t)\rangle = \sigma_b E - A\sqrt{E}$. The experimental situation is highly controversial at present. While a $\sqrt{E}$ behavior was found in $NbSe_3$ by Maeda, Naito, and Tanaka (1985), a linear decrease of j with decreasing E was found by Zhang and Ong (1985), Oda and Ido (1982), and Tucker *et al.*, (1981). In contrast, a stronger dependence, which could be described with an exponent of $n = \frac{3}{2}$, was found by Gill (1986c). The reason for these differences is not clear. Furthermore, crystal perfection, temperature, and other factors may also influence the experimental observations, and Joule heating may be difficult to avoid even by applying short electric field pulses.

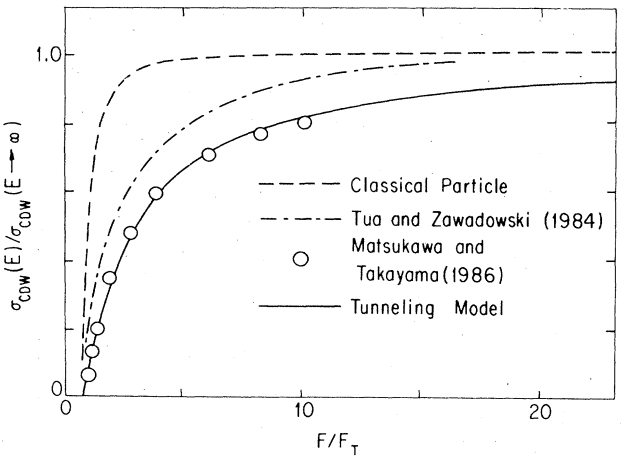

FIG. 33. Electric-field-dependent conductivity that follows from the classical particle model [Eq. (5.6)], from the tunneling model [Eq. (5.17)], and from calculations that take the dynamics of internal degrees of freedom into account. The experimental results follow the solid line closely.

Equally controversial is the experimental state of affairs near threshold, where the mean-field treatment of the dynamics of the many-degrees-of-freedom system leads to a power-law behavior, given by Eq. (5.14). Both the time-average current $\langle j(t)\rangle$ and the oscillation frequency f_0 were studied in various compounds; under ideal circumstances where the current density is uniform, $\langle j(t)\rangle$ is proportional to f_0, the ratio being independent of the applied field. While various groups have found that a power-law dependence can describe the experimental results well, in $NbSe_3$ the exponent is strongly temperature dependent, varying between 1.5 and 2.5 (Monceau *et al.*, 1985). In TaS_3, $\xi = 1.5$ (Gill, 1985), and in $K_{0.3}MoO_3$, the current is a linear function of the applied field (Janossy *et al.*, 1987). No attempt has been made to see whether these differences are due to different sample dimensions and/or whether the exponent varies from specimen to specimen.

In small samples the onset of nonlinear conduction tends to be sharp, and this often leads to well-defined peaks in the differential resistance dV/dI (Monceau *et al.*, 1982; Borodin *et al.*, 1986). An example of this behavior is displayed in Fig. 34, which also demonstrates the different behaviors that can be obtained depending on the temperature. The most likely explanation for the peaks in dV/dI is that they are a finite-size effect due to the phase-phase correlation length becoming comparable to the sample dimensions. This has been investigated in detail by Robbins and Klemm (1986) by using the model proposed originally by Klemm and Schrieffer (1983).

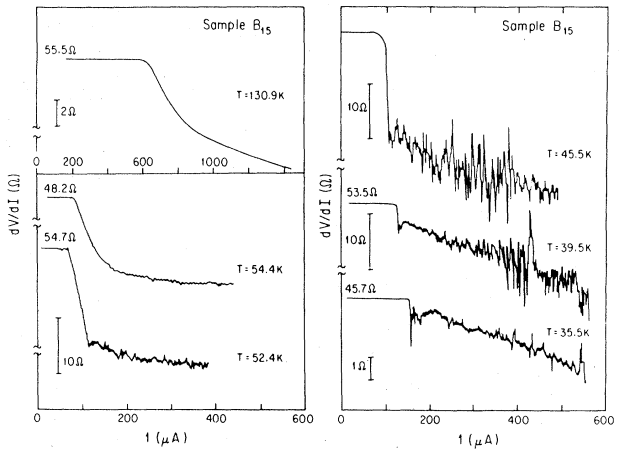

FIG. 34. Differential resistance dV/dI at various temperatures measured in NbS_3. The sudden onset of nonlinear conduction leads to a peak in the derivative (after Monceau *et al.*, 1982a).

Finite-size effects play a particularly important role at low CDW velocities and at low frequencies, due to the divergence of the dynamical phase-phase coherence length in those limits. At high velocities and high frequencies, the dynamics of the internal modes become progressively more important. The effect leads to single-particle-like behavior near threshold, with a peak in dV/dI, with $\sigma(E)$ closely resembling the behavior obtained by Tua and Zawadowski (1984) and by Matsukawa and Takayama (1986). The resulting differential resistance curves, with different ratios $a = l/L_0$ of the sample length l to the phase-phase correlation length L_0, are shown in Fig. 35. The curve labeled by 0.0 corresponds to the classical particle model, and the crosses represent unpublished experimental results obtained on a sample of pure $NbSe_3$, with $l \simeq 1$ mm. As discussed in Sec. V, the behavior near threshold may depend on the experimental conductions: a constant electric-field drive leading to a positive differential resistance (DR) and E_T, with an infinite negative DR for constant applied current. The latter was investigated in detail (Hall *et al.*, 1984b) in $NbSe_3$, and the relation to various dynamical instabilities such as $1/f$ noise and intermittent oscillations between various states has also been established.

Switching and hysteresis effects associated with the onset of nonlinear conduction were observed first in $NbSe_3$ (Zettl and Grüner, 1982b) and have also been found in TaS_3 (Mihály and Grüner, 1984; Kriza *et al.*, 1985), in $(NbSe_4)_{3.33}I$ (Wang, Saint-Lager, Monceau, Renaud, Gressier, Meerschaut, Guemas, and Rouxel, 1983) and in $K_{0.3}MoO_3$ (Dumas *et al.*, 1983). The effect is related to extended pinning centers in the bulk of the specimens; this has been established by experiments where nonperturbative contacts were moved along the chain direction, and the current-voltage characteristics were investigated (Brown and Mihály, 1985; Hall *et al.*, 1986). Models that attempt to account for switching assume that a large pinning center divides the specimen into two coherent regions each characterized by an average phase φ_L and φ_R, on the left- and right-hand side of the barrier. The coupling of the phases through the barrier may occur without the destruction of the CDW order parameter (Mihály, Chen, and Grüner, 1987) or through the development of an amplitude collapse of the pinning site (Hall *et al.*, 1986). The coupled equations of motion, similar in structure to the equations of motion that were proposed to describe coupled Josephson junctions, lead, in certain parameter ranges, to switching and to time delay effects that are associated with the switching (Zettl and Grüner, 1982b; Janossy *et al.*, 1985). The models, however, do not take into account the internal degrees of freedom in the two sides of the barrier; this may be important, in particular, to materials like TaS_3 where the phase coherence is less well established than in $NbSe_3$.

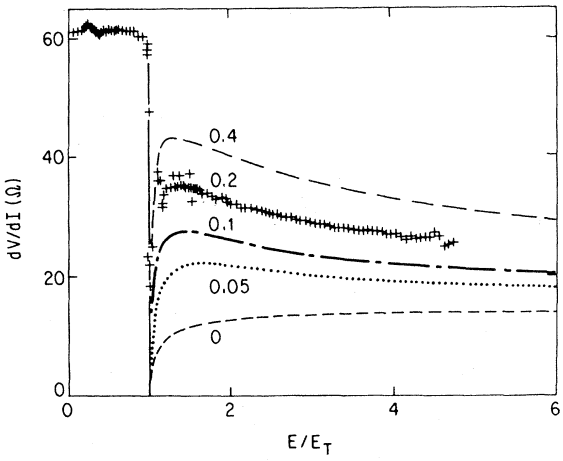

FIG. 35. Differential resistance calculated for finite sample sizes. The parameters shown in the figure are $a = l/L_0$ with l the length of the specimen and L_0 the phase-phase correlation length. Crosses represent experimental results on pure $NbSe_3$, of length $l \sim 1$ mm.

When switching occurs, intermittent chaotic behavior associated with the onset of the current-carrying state is also observed, although the phenomenon has not been investigated in detail. When the onset of the current-carrying state is associated with switching and hysteresis phenomena, apparently random transitions between the two states are also detected (Grüner and Zettl, 1983; Mihály and Grüner, 1984). In this region a dramatic increase of the low-frequency noise is also observed (Hall *et al.*, 1984a, 1984b). Although the random behavior may be due to temperature fluctuations, a more likely explanation is in terms of bistable states (Ben-Jacob *et al.*, 1981). Such bistable configuration follows from the hysteretic nature of the transition, and any effect that leads to hysteretic behavior would also lead to the intermittent route to chaos.

The temperature dependence of the nonlinear conduction has been investigated recently in detail (Zhang and Ong, 1985; Fleming *et al.*, 1986). The temperature dependence of the threshold field was discussed earlier. Close to the transition temperature, the magnitude of the nonlinear response in the large velocity limit was found to be close to the value that would be recovered in the absence of the Peierls transition (Monceau *et al.*, 1976; Ong and Monceau, 1977; Zettl, Jackson, and Grüner, 1982); this has been discussed by Gorkov and Dolgov (1979) in terms of a two-fluid model. With decreasing temperature, the nonlinear current decreases and σ_{CDW} freezes out with a temperature dependence closely following the linear (Ohmic) current due to the electrons excited across the single-particle gap (Fleming *et al.*, 1986). The behavior found for $(TaSe_4)_2I$ is displayed in Fig. 36. Writing the nonlinear current in terms of an electric-field-dependent damping,

$$\sigma_{CDW}(E) = \frac{ne^2\tau(E)}{m^*} , \tag{6.10}$$

suggests that (with n/m^* independent of the temperature) the CDW damping $\tau^{-1}(E)$ observed in moderate electric field diverges as the temperature is decreased.

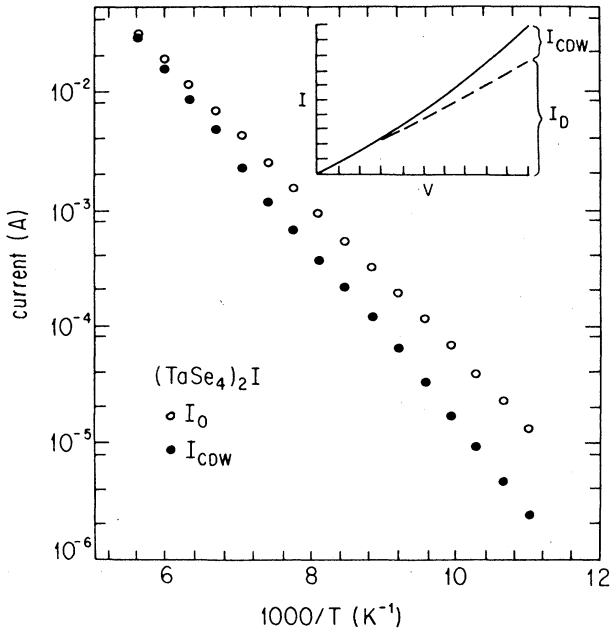

FIG. 36. Temperature dependence of linear and the nonlinear portion of the current in $(TaSe_4)_2I$ (Fleming *et al.*, 1986).

This divergence is closely related to the divergent damping observed in the low-frequency dielectric relaxation. In both effects screening of the internal deformations by the normal electrons appears to be the rate limiting process in the field- and frequency-dependent response (Sneddon, 1984b; Littlewood, 1987).

C. Experiments in the presence of joint dc and ac electric fields

With the conductivity both strongly nonlinear and frequency dependent, a broad variety of experiments can be performed in the presence of both dc and ac applied fields,

$$E = E_{dc} + E_{ac}\cos\omega_{ext}t \ , \tag{6.11}$$

with either the dc or the ac response detected. The experiments lead to additional information on the response of the driven collective mode and, in principle, could also be used to distinguish between the various models proposed. Broadly speaking, the measurements can be divided in two groups: (1) those that test the overall nonlinear response $\sigma(E,\omega)$, and (2) those that focus on interference effects arising as a consequence of mode locking between the intrinsic current oscillation and the applied ac field. These will be discussed in depth in Sec. VII. Here only the nonlinear ac response will be summarized.

Both the ac and dc response have been studied in various materials in the presence of combined electric fields, and both classical approaches and the tunneling model have been extensively used to account for the experiments.

Many of the phenomena that occur in the presence of ac and dc electric fields have been calculated on the basis of the single degree of freedom, the so-called "classical particle," model (Wonneberger, 1979, 1983a, 1983b); Wonneberger and Breymayer, 1981; Breymayer *et al.*, 1982). The model leads to qualitative disagreement with experiments, in particular, near threshold. The reason for this is clear because the model also leads to divergent differential conductivity at E_T, also not observed. Models, which lead to ω- and E-dependent conduction in broad agreement with experiments, are in general also able to describe a variety of observations made in the presence of joint dc and ac fields. This most probably follows from nonlinear circuit theory and suggests that many of these experiments cannot be used to distinguish between the classical and quantum description of CDW dynamics. For other experiments, such as photon-assisted tunneling, the predictions of the models are drastically different. However, other complications often make a direct comparison with the relevant theories difficult, if not impossible.

Experiments involving small applied ac electric fields are in general more straightforward to account for, since in this limit a perturbative treatment of the nonlinear dynamics in terms of the ac drive is appropriate. The first experiments of joint dc and ac fields, however, have been made in the large ac signal limit, where the ac-field-induced dc conduction was detected (Grüner, Zettl, Clark, and Bardeen, 1981). For a purely classical response, the dc conductivity is not modified by an applied ac signal for electric-field strengths $E_{dc}+E_{ac}<E_T$. However, a nonlinear dc response can be induced when $E_{dc}+E_{ac}$ exceeds the dc threshold electric field. The dc current I_{dc} detected for dc fields less than threshold E_T is a strong function of both E_{ac} and ω_{ext} in $NbSe_3$ (Grüner, Clark, and Portis, 1981) and in *o*-TaS_3 (Zettl and Grüner, 1982b).

While detailed calculations on ac-field-induced ac conduction that are based on the classical particle model have not been performed to date, qualitative arguments can be advanced (Grüner *et al.*, 1980; Grüner, Zettl, Clark, and Thompson, 1981) to account for the observations. For a pinned and strongly damped collective mode, the maximum displacement from the equilibrium position is given—for a parabolic potential—by

$$\delta x_0 = \frac{(eE_{ac}/m^*)\omega_0^2}{[1+(\omega/\omega_0^2\tau)^2]^{1/2}} \ . \tag{6.12}$$

If there is a critical displacement x_{crit} that leads to nonlinear dc conduction, then a critical ac field amplitude corresponding to the critical displacement is given by

$$E_{crit}(\omega) = E_{crit}(\omega=0)[1+(\omega/\omega_0^2\tau)^2]^{1/2} \ , \tag{6.13}$$

where $E_{dc}+E_{crit}(\omega=0)=E_T$. The above equation describes well the nonlinear ac behavior of the system as

the function of applied field and of applied frequency, with parameters like E_T and $\omega_0^2\tau$ obtained from the measured dc nonlinear and small amplitudes ac response. The effect can also be described adequately in the framework of the tunneling model. The dc current density in the presence of an ac field is given by (Tucker, 1979; Tucker *et al.*, 1981; Miller *et al.*, 1983)

$$I_{\rm dc}(V_{\rm dc},V_{\rm ac})=\sum_{n=-\infty}^{\infty} J_n'^2\left[\frac{eV_{\rm ac}}{\hbar\omega}\right] I_{\rm dc}\left[V_{\rm dc}+\frac{n\hbar\omega}{e}\right], \tag{6.14}$$

where J_n' is the Bessel function of order n. With $I_{\rm dc}(V_{\rm dc})$ and $\sigma(\omega)$ as input parameters, the $I_{\rm dc}(V_{\rm dc},V_{\rm ac})$ curves generated compare favorably with experiments both in $NbSe_3$ and in TaS_3. Various experiments have also been performed in the small ac signal limit, but in the nonlinear dc conductivity region. Both the ac and dc response can be detected in the presence of joint ac and dc excitation. Moreover, phenomena that arise in the presence of two applied ac fields can also be studied. The applied fields

$$E=E_{\rm dc}+E_{1\rm ac}\cos(\omega_1 t+\varphi)+E_{2\rm ac}\cos\omega_2 t \tag{6.15}$$

and the parameters that are measured are classified as follows.

(a) ac response: differential conductivity. Here $I_{\rm ac}$ is detected for $E_{2\rm ac}=0$ with $E_{\rm dc}$ and ω_1 varied. In the low frequency, $\omega\to 0$ limit, the classical equation

$$I_{\rm ac}=\frac{dI_{\rm dc}}{dE_{\rm dc}}E_{1\rm ac} \tag{6.16}$$

leads to the differential conductivity; $\sigma_{\rm ac}$ gives directly the first derivative of the dc I-V characteristics.

(b) Rectification. The dc response ΔI_r is detected, again with $E_{2\rm ac}=0$. In the $\omega\to 0$ limit

$$\Delta I_r=\tfrac{1}{2}E_{1\rm ac}^2\frac{d^2I_{\rm dc}}{dE_{\rm dc}^2}, \tag{6.17}$$

and at low frequencies the rectified current is proportional to the second derivative of the I-V curve.

(c) Harmonic mixing. The signal is detected at frequencies $\omega_1-2\omega_2$, and this, for $\omega_1=2\omega_2$, corresponds to a dc harmonic mixing current. In the low-frequency limit

$$\Delta I_{\rm nm}=\tfrac{1}{4}E_{1\rm ac}^2E_{2\rm ac}\frac{d^3I_{\rm dc}}{dE_{\rm dc}^3}\cos 2\varphi, \tag{6.18}$$

i.e., the harmonic mixing signal is proportional to the third derivative of the current-voltage characteristics.

The ac conductivity in the presence of a dc field has been studied both in $NbSe_3$ (Longcor, 1981) and in TaS_3 (Miller *et al.*, 1983, 1984; Zettl and Grüner, 1984). In Fig. 37, both the real and imaginary part of the ac conductivity for o-TaS_3 in a broad parameter range is

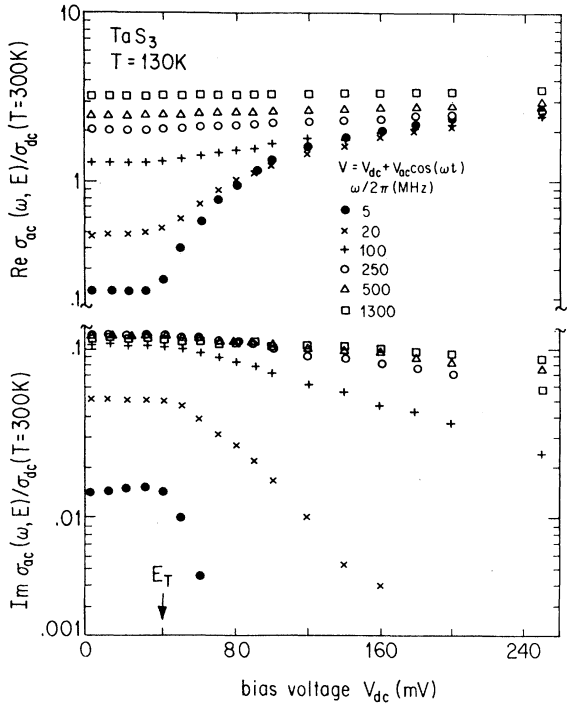

FIG. 37. Real and imaginary parts of the ac conductivity of orthorhombic TaS_3 vs applied dc bias voltage $V_{\rm dc}$. The threshold field for the onset of nonlinear dc conduction is indicated by an arrow (Zettl and Grüner, 1984).

displayed. The ac response is not affected by dc fields $E_{\rm dc}<E_T$, but both the in-phase and the out-of-phase components are enhanced with increasing dc bias in the nonlinear conductivity region. These experimental findings have not been accounted for in terms of the classical particle model, but an extension of the classical dynamics to a model for which coupled particles are considered accounts for the experiments in detail (Sneddon, 1984b, 1984c). In Fig. 38 the results of these calculations are displayed. Here σ' and σ'' refer to the in-phase and out-of-phase components of the ac conductivity; P and HP are parameters, which are related to the threshold field E_T and to a characteristic frequency determining the ω-dependent response in the absence of dc bias. Comparing this figure with Fig. 37, it is clear that all the important features of the experiments are recovered by calculations based on purely classical dynamics. In terms of photon-assisted tunneling theory, the ac current (Miller *et al.*, 1983; Thorne *et al.*, 1984) is

$$\begin{aligned}{\rm Re}I(\omega)&=\frac{1}{2\alpha\omega}[I_{\rm dc}(E_{\rm dc}+\alpha\omega)-I_{\rm dc}(E_{\rm dc}-\alpha\omega)],\\ {\rm Im}I(\omega)&=\frac{1}{2\alpha\omega}[I_{kk}(E_{\rm dc}+\alpha\omega)-2I_{kk}(E_{\rm dc})\\ &\quad+I_{kk}(E_{\rm dc}-\alpha\omega)],\end{aligned} \tag{6.19}$$

where the imaginary part is written in terms of the Kramers-Kronig transform

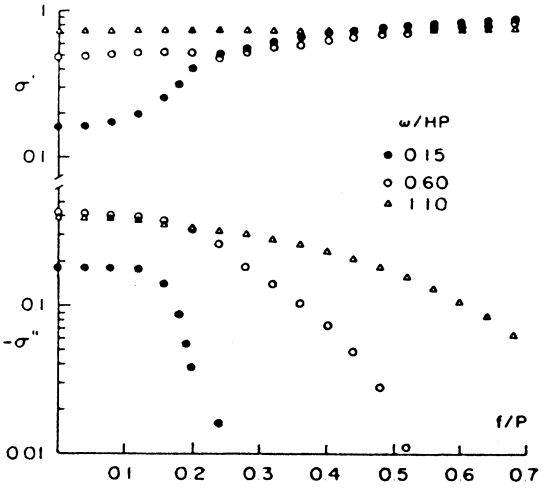

FIG. 38. ac response of an incommensurate chain with infinite-range interactions. HP is defined in the text; f/p refers to the dc field, σ' and σ'' to the real and imaginary ac conductivity (after Sneddon, 1984c).

$$I_{kk}(E_{\rm dc})=P\frac{1}{\pi}\int_{-\infty}^{\infty}\frac{E_{\rm dc}}{\bar{E}_{\rm dc}-E_{\rm dc}}I_{\rm dc}(E_{\rm dc})\ , \tag{6.20}$$

and α is the voltage-frequency scaling parameter $\alpha=h/e$, as given by Eq. (5.44). With α evaluated from the measured $\sigma(\omega)$ and $\sigma(E)$, Eqs. (6.19) and (6.20) can be used to generate ac conductivity curves in the presence of a dc bias. These are shown in Fig. 39, together with experimental results on o-TaS_3 (Thorne *et al.*, 1984).

The most straightforward experiment on rectification is photon-assisted tunneling (PAT). Here the classical and quantum theories lead to fundamentally different predictions. The name PAT refers to an experiment where the specimen is biased below threshold, and a small amplitude ac excitation is used to induce nonlinear conduction. For a purely classical system, no rectified current is obtained for combined dc and ac fields $E_{\rm dc}+E_{\rm ac}<E_T$. In the quantum limit, Tucker's theory (1979) leads to a rectified current

$$\Delta I_r=\left[\frac{e^*E_{\rm ac}}{2\hbar\omega}\right]^2[I_{\rm dc}(E_{\rm dc}+\alpha\omega)-2I_{\rm dc}(E_{\rm dc})-I_{\rm dc}(E_{\rm dc}-\alpha\omega)]\ , \tag{6.21}$$

which for $V_{\rm dc}<V_T$ (and for $V_{\rm dc}-\alpha\omega_{\rm ext}<V_T$) reduces to

$$\Delta I_r=\left[\frac{e^*E_{\rm ac}}{2\hbar\omega}\right]I_{\rm dc}(E_{\rm dc}+\alpha\omega)\ . \tag{6.22}$$

Thus the energy quantum $\alpha\omega$ can span the difference between $V_{\rm dc}$ and V_T even though a classical field amplitude $V_{\rm ac}$ is too small to do so. Early experiments on $NbSe_3$ (Grüner, Zettl, Clark, and Bardeen, 1981) and on o-TaS_3 (Zettl and Grüner, 1982a, 1982b) failed to detect photon-assisted tunneling for specimens biased below E_T and at frequencies where [on the basis of scaling relation between $\sigma(\omega)$ and $\sigma(E)$ the tunneling theory suggests significant ΔI_r. The reason for this is not entirely clear at present; if the tunneling model is appropriate, then a likely explanation lies in complicated low-frequency and long-time phenomena, which are associated with the development of the current-carrying CDW state (Lyons *et al.*, 1985).

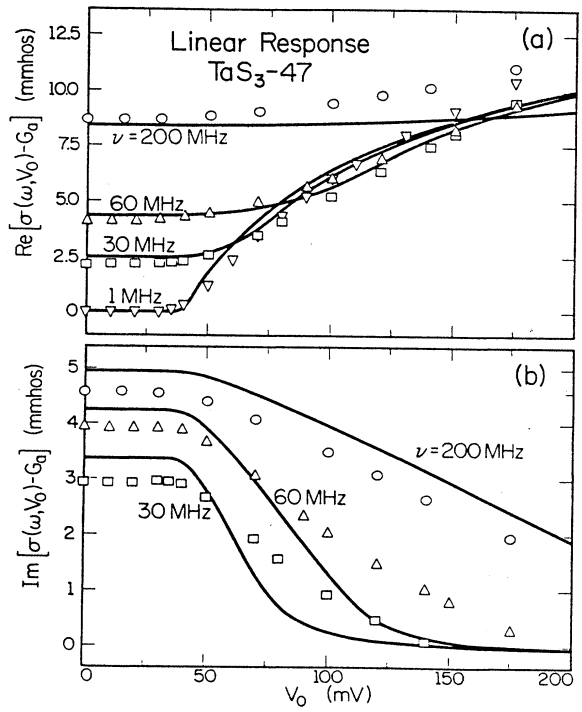

FIG. 39. Real and imaginary parts of the ac conductivity in o-TaS_3 vs applied dc voltage. The solid lines are calculated curves, using the tunneling model prediction Eq. (6.19) with parameters given in the text (Miller *et al.*, 1985).

Detailed rectification experiments in the dc nonlinear conductivity region have been performed both in $NbSe_3$ (Richard *et al.*, 1984) and in o-TaS_3 (Miller *et al.*, 1983; Thorne, 1984; Miller *et al.*, 1985). Harmonic mixing has also been investigated in detail both in the radio frequency spectral region (Miller *et al.*, 1983) and at microwave frequencies (Seeger *et al.*, 1982, 1984a, 1985), and has been accounted for within the framework of the tunneling model. In particular, the experimental result that was observed is principal evidence for tunneling in the absence of phase shift in the small difference-frequency harmonic response (Miller *et al.*, 1983, 1985; Thorne *et al.*, 1986). Similar, small phase shifts were, however, obtained on the basis of the classical particle model by Wonneberger (1983a, 1983b), and detailed calculations by Liu and Sneddon (1987) on the basis of the Fukuyama-Lee-Rice model lead to a rather good agreement with all

of the essential features of the experiment conducted in a broad range of frequencies and electric field.

It appears therefore that both a classical description and the tunneling model can account for all the essential findings concerning the small amplitude ac response, the nonlinear dc response, and a wide class of experiments performed in the presence of the ac and dc fields. Detailed comparison between theory and experiments that often are claimed as clear evidence for one or another model are often not reproduced in other laboratories; consequently, the matter whether classical or quantum models are required to describe the dynamics of the collective mode remains controversial.

VII. CURRENT OSCILLATIONS AND INTERFERENCE EFFECTS

Since the discovery of Fleming and Grimes (1979) of the current oscillations in the nonlinear conductivity region a variety of experiments have been performed where interference effects between this intrinsic oscillation and the externally applied ac field have been studied. The experiments, similar in many respects to those performed in Josephson junctions, display a variety of phenomena that are of general interest (such as the possibility of various routes to chaos; see, for example, Zettl and Grüner, 1986). They also have been used to distinguish between the various models of charge-density-wave transport.

A. Current oscillations

Questions as to whether the current oscillations are a bulk effect and whether they are generated at the contacts or also at other pinning centers have been addressed in Sec. III. While the question is not fully resolved, the existence of these oscillations, indicating a high degree of coherence, particularly in $NbSe_3$, is well established. In carefully prepared specimens the quality factor of the oscillations is high, and a fundamental with several harmonics with decreasing intensity is observed. An example is shown in Fig. 40 (Mozurkewich and Grüner, 1983b).

In recent experiments in $NbSe_3$ (Thorne *et al.*, 1987) extremely coherent current oscillations were detected. In certain cases $Q \sim 30\,000$ was observed in the upper CDW state. The measured spectral width is a sensitive function of crystal perfection, and in samples of average quality the spectral width is significantly larger. The quality factors also depends strongly on temperature, and as a rule it decreases with decreasing T. In other materials, Q is significantly smaller; in good quality TaS_3 specimens $Q \sim 10$, while in $(TaSe_4)_2I$ the value is of the order of 1 (Mozurkewich *et al.*, 1983).

It also tends to be smaller in specimens with larger cross sections (Mozurkewich *et al.*, 1983), as expected for loss of perpendicular dynamical coherence with an increased cross-sectional area. The above observations clearly establish the intimate relation between the quality

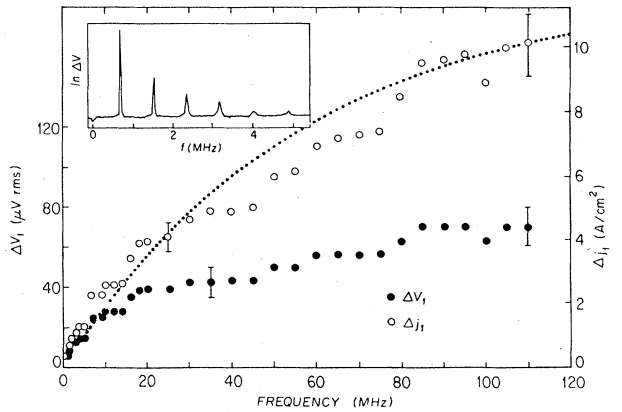

FIG. 40. Amplitude of the fundamental oscillation in $NbSe_3$ at 42.5 K vs oscillation frequency. The amplitude is plotted both as a voltage ΔV_1 (solid symbols, left-hand scale) and as an equivalent current density Δj_1 (open symbols, right-hand scale). The inset shows a typical spectrum. The dotted line is Eq. (6.25). From Mozurkewich and Grüner (1983).

factor of current oscillations and dynamical coherence throughout the specimens. Whether normal electron screening is important in establishing such coherence in $NbSe_3$, and also in other materials near to T_p, remains to be seen.

Another fact that plays an important role in the generation of oscillating current is the existence of macroscopic defects. These have been studied by employing nonperturbative contacts (Brown and Mihály, 1985). For large extended defects, the amplitude fluctuations of the order parameter are also expected to be important, and several models have been suggested (see, for example, Maki, 1985, 1986). Because of the nonlinear response a mode locking is expected between the intrinsic current oscillation and an externally applied field. This was first detected by Monceau *et al.* (1980). The locking leads to a frequency pulling and, consequently, to a modification of the dc I-V characteristic in the form of well-defined steps. The ac response is also influenced by mode locking, leading to inductive dips in the dielectric constant.

B. Interference effects

While interference phenomena have been reported in various materials (Brown and Grüner, 1985; Brown *et al.*, 1985a; Fleming, Dunn, and Schneemeyer, 1985; Wu *et al.*, 1985; Latyshev *et al.*, 1986), most of the experiments have been performed in $NbSe_3$. In this compound the phase-phase correlation length appears to be long, comparable to the dimensions of the specimens (Fleming *et al.*, 1984), and, consequently, the response to external drives is highly coherent. This is responsible for the extremely coherent current oscillations observed in pure specimens in both CDW states, in contrast to the weak and broad Fourier components of the oscillating current in other material CDW states. The high degree

of dynamical coherence also suggests that internal degrees of freedom may be of less importance in this material than in others, and these can be included perturbatively when the observations are accounted for by any particular model.

In order to discuss these phenomena in detail, it is useful to recall the formal correspondence between the equation of motion, Eq. (5.2), and the Stewart-McCumber model of the resistively shunted Josephson junction (see, for example, Barone and Paterno, 1982), and to use the vast literature on the Josephson effects to account for observations associated with the dynamics of charge-density waves. (The equation of motion is also equivalent to that of a damped, driven pendulum and of a phase-locked loop.) Including the inertial terms, Eq. (5.2) in dimensionless form reads

$$\frac{d^2\varphi}{dt^2}+\Gamma\frac{d\varphi}{dt}+\sin\varphi=\frac{E}{E_T}\ , \tag{7.1}$$

where $\theta=(\omega_0\tau)^{-1}$ and time is measured in units of ω_0^{-1}. The equation of motion of the resistively shunted Josephson junction is

$$\frac{d^2\theta}{dt^2}+G\frac{d\theta}{dt}+\sin\theta=\frac{I}{I_j}\ , \tag{7.2}$$

where Γ is the phase difference across the junction, I is the current, $G=(RC\omega_j)^{-1}$, with R and C the junction resistance and capacitance and $\omega_j=2eI_\tau/Ch$. Time is measured in units of ω_j^{-1}, and I_j is the critical current. The threshold electric field for CDW conduction corresponds to the critical Josephson current, and the pinned CDW state to the zero-resistance state in Josephson junctions. Current oscillations in the current-carrying CDW with $j_{\rm CDW}/f_0=2e$ per chain correspond to the ac Josephson effect with the voltage-frequency relation $V/f_0=2e/\hbar$. The latter was first demonstrated by detecting a change of the dc current-voltage characteristics in the presence of applied ac radiation. Steps in the I-V curve when $f_0=f_{\rm ext}$ were first found by Shapiro (hence the name "Shapiro steps"), and, consequently, similar ac interference effects found in CDW systems will also be called Shapiro steps. Experiments of this kind were first performed in $NbSe_3$ by Monceau *et al.* (1982), who measured the differential resistance dV/dI in the presence of ac fields. Their results, obtained for keeping the dc current constant and varying the frequency of the applied ac field, are displayed in Fig. 41. Peaks in the derivative correspond to applied frequencies for which $\omega_{\rm ext}=n\omega_0$ with ω ranging from 1 to 4, as indicated in the figure. Various sequences called F_1, F_2, and F_3 are detected, and this may be due either to the fibrous nature of the material or to the contact configuration used in the experiments. In small and highly uniform specimens, the interference is more dominant and shows up in direct I-V curves (Zettl and Grüner, 1983b, 1984). Interference effects have also been observed recently in the elastic properties (Bourne *et al.*, 1986). In Fig. 42, dc I-V traces are shown in the presence of an applied field at constant

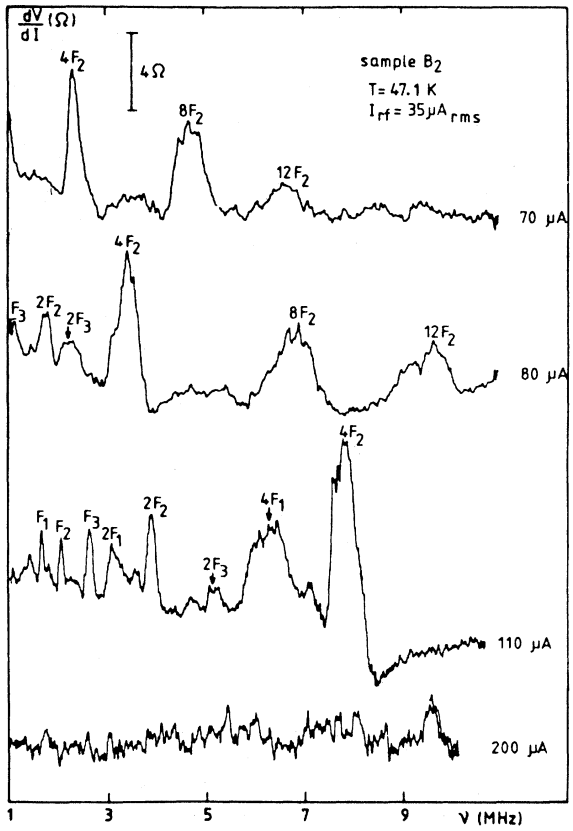

FIG. 41. Differential resistance dV/dI in $NbSe_3$ observed by sweeping the frequency of the rf current, for a constant dc current. The various sets of interference peaks are labeled by F_1, F_2 and F_3 (Monceau *et al.*, 1982).

frequency $f_{\rm ext}=100$ MHz. For $V_{\rm ac}=0$, a smooth nonlinear I-V curve is obtained with a well-defined threshold voltage V_T for the onset of nonlinear conduction. Increasing $V_{\rm ac}$ results in the appearance of broad peaks at certain dc currents, and these become sharper with increasing ac amplitude. The position of the $n=1$ step, indicated on the figure, corresponds to a dc current $I_{\rm dc}$ which, in the absence of ac fields, yields an intrinsic oscillation frequency $f_0=100$ MHz, as established by direct measurements of the current oscillations. There are also harmonic steps corresponding to $n=2$ (where the intrinsic oscillation frequency couples to the first harmonics of the external frequency), and a subharmonic step corresponding to $n=\frac{1}{2}$ is also visible in the figure. The step height δV first increases and then decreases with increasing $V_{\rm ac}$, while the threshold voltage V_T is strongly reduced by the applied ac fields. The step height and threshold field can be calculated by solving Eq. (7.1) directly [Fack and Kose (1971); Clark and Lindelof (1976); Lindelof (1981)]. In the high-frequency ($\omega\gg\omega_0^2\tau$) limit,

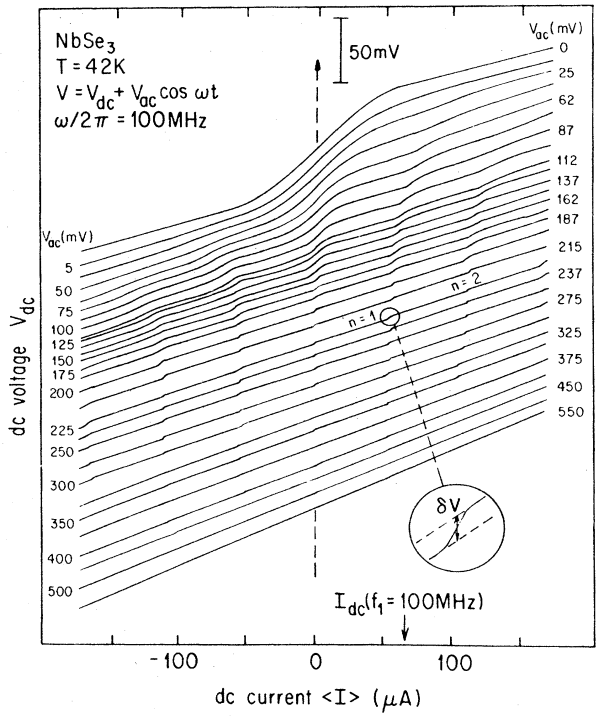

FIG. 42. Shapiro steps in the dc I-V traces for $NbSe_3$ when rf field is applied at frequency $\omega/2\pi=100$ MHz and of amplitude V_{ac}. The step height δV is defined in the figure. No Shapiro steps are observed for $V_{ac}=0$, while the maximum step height is at approximately $V_{ac}=100$ mV. The arrow indicates the dc current that yields a fundamental noise frequency $f_1=100$ MHz. The step index is n (Zettl and Grüner, 1984).

$$\delta V=\beta 2V_T(\omega=0)J_n'(V_{\text{eff}}) ,$$
$$V_T=V_T(\omega\to 0)J_0'(V_{\text{eff}}) , \tag{7.3}$$

where J_n' is the Bessel function of order n, and

$$V_{\text{eff}}=\frac{V_{ac}\omega_0^2\tau}{V_T(\omega\to 0)} . \tag{7.4}$$

The parameter β is phenomenological, representing the volume fraction of the specimen that responds coherently to the applied dc and ac fields. In Fig. 43 the $n=1$ step height is shown as a function of the ac amplitude V_{ac}. The solid line is Eq. (7.3) with parameters $\omega_0^2\tau/2\pi=170$ MHz and $\beta=0.17$. The characteristic Bessel function behavior is clearly recovered by experiment; furthermore, the crossover frequency $\omega_0^2\tau$ is in approximate agreement with that derived from the low-field ac conductivity measurements. The value $\beta=0.17$ indicates that a large fraction of the specimen is responding coherently to the external perturbations. While analytical solutions are not available in the low-frequency $\omega<\omega_0^2\tau$ limit, computer simulations (Fack and Kose, 1971; Clark and Lindelof, 1976) also lead to Bessel function behavior with step heights strongly dependent on the frequency. The frequency dependence of the maximum step height (Zettl

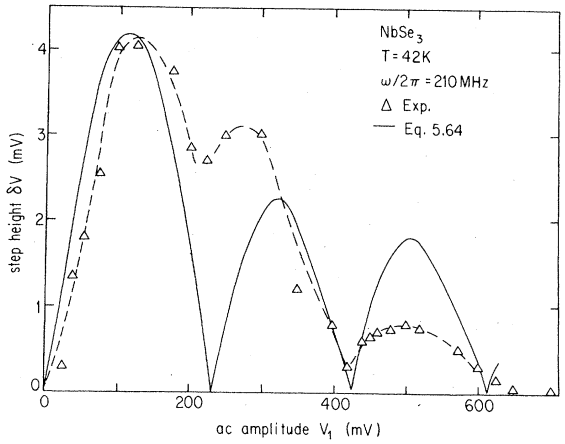

FIG. 43. Step height δV vs ac amplitude V_{ac} for Shapiro steps in $NbSe_3$. The rf frequency is 310 MHz and the step index is $n=1$. The solid line is the prediction of the classical model, Eq. (7.3), with parameters $\omega_0^2\tau/2\pi=80$ MHz. $V_T=24$ mV, $\beta=0.17$ (Zettl and Grüner, 1984).

and Grüner, 1984) can be analyzed in terms of the model leading to a crossover frequency, in agreement with the values quoted above. While the threshold voltage decreases with increasing V_{ac}, the Bessel function behavior predicted by Eq. (7.1) is not recovered by early experiments, and instead of displaying oscillations, V_T goes to zero smoothly with increasing V_{ac}. Subsequent experiments by Latyshev *et al.* (1987) and by Thorne *et al.* (1987) on carefully prepared specimens displayed oscillations in E_T, in full agreement with predictions based on Eq. (7.1).

Interference phenomena also influence the frequency-dependent response, leading to steps in $\mathrm{Re}\sigma(\omega)$ and inductive dips in $\varepsilon(\omega)$ at currents for which $f_0\sim f_{\text{ext}}$. The dielectric constant ε and conductivity $\mathrm{Re}\sigma$, both measured at fixed frequency $\omega_0/2\pi=3.2$ MHz, are shown in Fig. 44 as a function of dc bias voltage. The large step and strong inductive response at $V_{dc}\sim 2.3$ mV correspond to currents where $f_0=f_{\text{ext}}$, and similar to the Shapiro-type steps, both a harmonic and subharmonic interference are evident. Although no calculations based on Eq. (7.1) are available, the interference effect can be accounted for by qualitative arguments that use mode locking between the intrinsic oscillation and the externally applied ac field (Zettl and Grüner, 1984). Not surprisingly, interference effects are observed also when $V_{dc}=$const and the ac frequency is varied; these, however, have not been analyzed in detail. Frequency modulation effects related to interference phenomena have also been measured and analyzed (Stokes *et al.*, 1987).

Interference effects have also been observed in TaS_3 (Brown and Grüner, 1985) and in $K_{0.3}MoO_3$ (Fleming, Dunn, and Schneemeyer, 1985), but, similar to the current oscillations, their magnitude is much weaker than those observed in $NbSe_3$. As discussed before, this may reflect a smaller degree of coherence in TaS_3, leading

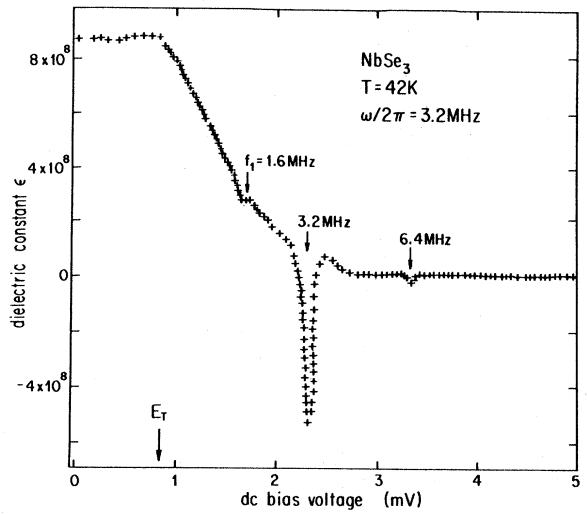

FIG 44. Real part of the ac conductivity $\mathrm{Re}\sigma(\omega)$ and dielectric constant $\varepsilon(\omega)$ measured at $\omega/2\pi=3.2$ MHz as a function of applied dc bias voltage. The threshold field is indicated by an arrow (Zettl and Grüner, 1984).

to smaller values of β in Eq. (7.3). In these cases, the interference peaks are also much broader than those observed in $NbSe_3$, suggesting a distribution of CDW velocities in the specimens. Such effects cannot be accounted for by models where the internal dynamics of the collective mode are neglected. Experiments where the derivative dV/dI is recorded instead of direct I-V curves (Brown *et al.*, 1984) show, aside from the harmonic locking structure, a rich subharmonic structure. In Fig. 45 the differential resistance, measured with and without an externally applied rf voltage at $\omega_{ext}=25$ MHz, is displayed. For the low ac voltage used, the threshold for the onset of nonlinearity is not reduced significantly, but peaks (which correspond to steps in the direct I-V curves) develop for a whole series of dc currents for which

$$p\omega_{ext}=q\omega_0 , \tag{7.5}$$

where p and q are integers. The ratio of p/q can be evaluated by plotting the frequency associated with a given peak versus the current J_{CDW} and comparing the slope J_{CDW}/ω_{ext} with that corresponding to the main Shapiro step, labeled by 1/1 in the figure. The steps $q=1$ and $p\geq 1$ correspond to frequency locking between the internal frequency $f_0=\omega_0/2\pi$ and all harmonics $p\omega_{ext}$ of the applied rf field, as studied before (Zettl and Grüner, 1984), while steps that occur when $p/q<1$ are called the subharmonic steps. Interference effects corresponding to subharmonic steps have been observed in the ac response (Zettl and Grüner, 1984; Fleming, Dunn, and Schneemeyer, 1985), and have also been detected in o-TaS_3 (Brown *et al.*, 1985b). As the intrinsic oscillation contains many harmonics, and also the response of the nonlinear system to a sinusoidal ac field $E_{ac}\cos\omega_{ext}t$ is highly nonsinusoidal, it is natural to interpret the peaks as regions in which any harmonic of the internal frequency locks to any harmonic of the external field. Such behavior is in general referred to as a "devil's staircase" (Bak, 1982b). The interference peaks shown in Fig. 45 do not reflect complete mode locking, for which the differential resistance is the same as the ohmic resistance below E_T, and are usually referred to as "interference features." Complete mode locking and serveral subharmonics were first detected by Hall and Zettl (1984a, 1984b), and were subsequently observed by applying low frequencies and larger drive amplitude (Sherwin and Zettl, 1985; Thorne *et al.*, 1987); an example for this behavior is displayed in Fig. 46. The condition under which complete mode locking is observed has not been completely settled, but most probably it is related to the extent of phase coherence throughout the specimens,

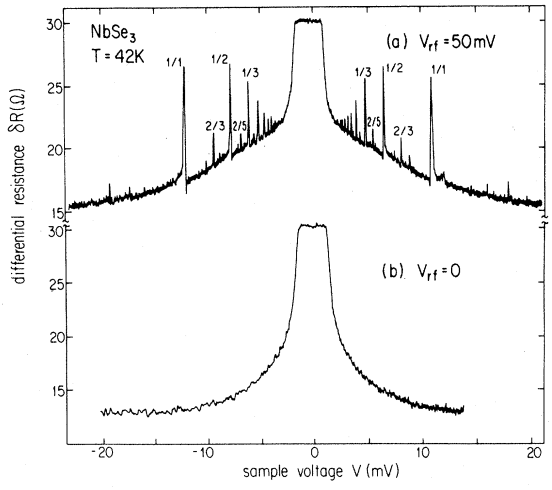

FIG. 45. Differential resistance of $NbSe_3$ with and without an applied rf voltage V_{rf}. The numbers indicate the various subharmonic steps (Brown *et al.*, 1984).

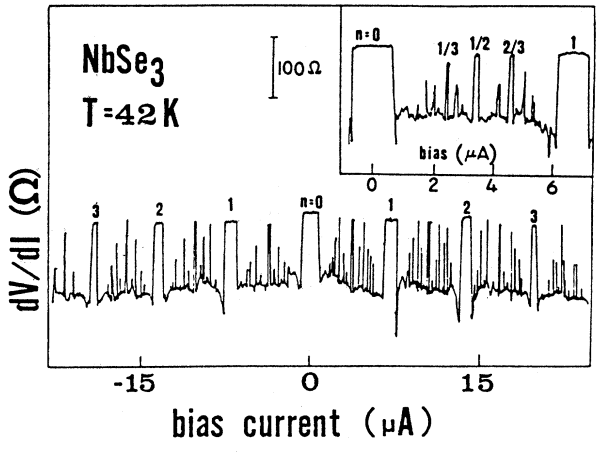

FIG. 46. Mode-locked Shapiro steps in $NbSe_3$. Over the mode-locked region, dV/dI is independent of dc bias. The inset shows the subharmonic structure in detail, with corresponding p/s values (Sherwin and Zettl, 1985).

since, as a rule, smaller samples with careful handling (and, consequently, less defects introduced during the contact preparation, etc.) display complete mode locking more readily. The effect of driven amplitude has been directly demonstrated by Sherwin and Zettl (1985) by performing broadband noise measurements in the presence of dc and ac drive. Broadband noise results from internal dynamics of the collective mode (Bhattacharya *et al.*, 1985); consequently, its presence or absence clearly indicates the importance of internal dynamics of freedom. It was found that during mode locking the broadband noise is absence for complete mode locking, which is achieved for increasing ac drive; for small amplitude ac fields, only partial mode locking is observed.

Several dramatically different explanations have been advanced to account for the existence of the subharmonic steps. While an overdamped classical response, such as that given by Eq. (5.2), does not lead to subharmonic mode locking, inertial effects described by Eq. (7.1) restore subharmonic mode locking (Bak, 1982a, 1982b; Azbel and Bak, 1984). Furthermore, the main features of the mode-locking phenomenon can be studied by using a return map, which describes the time evolution of the CDW phase sampled at discrete times $t_m = 2\pi m/\omega_{ex}$. Assuming that $\dot{\theta}_m$ is determined only by θ_m, due to dissipation, a "circle map"

$$\theta_{m+1} = \theta_m + \Omega + K \sin(2\pi\theta_m)/2\pi \tag{7.6}$$

results, where $\Omega = 2\pi f_0/\omega_{ex}$, and K describes the strength of the coupling between the system and the external perturbation—and is consequently assumed proportional to E_{ac}. The circle map is the return map appropriate to Eq. (7.1), as demonstrated by detailed numerical integrations (Bohr *et al.*, 1984; Jensen *et al.*, 1984). For finite-coupling K, mode locking occurs for certain values of ω_{ex} and f_0, i.e., f_0 remains fixed at $(p/s)\omega_{ex}$ over a finite range of E_{dc}. From Eq. (7.1) the time-averaged CDW current [and hence $(\partial\varphi/\partial t)$] is then dictated strictly by ω_{ex}. The mode-locked regions are separated by regions corresponding to free-running solutions of the phase.

The extent of the mode lock, i.e., the completeness of the devil's staircase, can in principle be determined directly from the subharmonic interference structure. Instrumental noise sets a lower limit to the size of the step that can be observed experimentally; consequently, the completeness of the staircase cannot be confirmed directly. The completeness of the staircase can, however, be examined by the following test: Choosing a discrimination level r, one adds up to the total width $S(r)$ of steps wider than r. If $N(r) = [I - S(r)]/r$ in an interval of unit length, then rN is the fraction of interval unoccupied by steps larger than r. For a complete staircase, $rN \to 0$ as $r \to 0$, and

$$N(r) = r^{-d}, \tag{7.7}$$

with d defining the fractal dimension of the complementary Cantor set. As mentioned previously, the circle map, Eq. (7.6), leads to $d = 0.87$, for $K = 1$. This univeral behavior has been confirmed by analog computer simulations and by studying a two-dimensional dissipative map (Alstrom *et al.*, 1984). An analysis as described above, for experiments performed on $NbSe_3$ (Brown *et al.*, 1984), gives a dimension $d = 0.91$, in striking agreement with theory.

There are, however, several serious problems with such an interpretation. First, one expects, on the basis of the circle map and corresponding simulations of Eq. (7.1), that the value of d depends critically on E_{ac} and on the selected range of p/s. Such behavior has not been observed in $NbSe_3$, and indeed a critical line cannot be clearly identified. Equally important, subharmonic steps are predicted by Eq. (7.4) only in the underdamped limit, and therefore should not exist in an overdamped system as determined from the frequency dependence of the low-field ac response. Furthermore, in the underdamped limit where Eq. (7.4) does predict subharmonic interference steps, chaos is also predicted on mode-locked steps. In contrast to this, for the samples displayed in Figs. 3 and 5, chaos is not observed for any combination of ac and dc drive parameters. In the language of the circle map, the fractal dimension $d \approx 0.91$ indicate that the system is at criticality ($K = 1$), yet the absence of chaos suggests $K = 1$ cannot be exceeded, irrespective of the magnitude of E_{ac}.

A conceptually simpler explanation has been advanced by Thorne *et al.* (1986, 1987) by assuming that the periodic potential is nonsinusoidal, but inertial effects and the effects of internal degrees of freedom are neglected. The magnitude of the subharmonic steps can be directly related to the components of the Fourier transform of the potential, and a good agreement has been obtained between experiment and theory for a potential

$$V(\theta) = \begin{cases} -\cos\theta & \text{for } -\dfrac{\pi}{2} < \theta < \dfrac{\pi}{2}, \\ \cos\theta & \text{for } \dfrac{\pi}{2} < \theta < \dfrac{3\pi}{2} \pmod{2\pi}. \end{cases} \tag{7.8}$$

Such potential is assumed for the tunneling model (Bardeen, 1986). The subharmonic step height, calculated and measured for the parameters given in the caption, are displayed in Fig. 47. The agreement is remarkable, suggesting that the above simple approach may be appropriate. One should note, however, that the detailed form of the potential is probably not very important, as any potential with cusps [such as $V(\theta)$ given by Eq. (7.8) as a triangle potential-potential, for example] leads to subharmonic mode locking with a smaller locking region for larger p and q values. More detailed experiments (Thorne *et al.*, 1986) on $NbSe_3$ were also analyzed in detail, with a periodic potential such as that given by Eq. (7.8), which is completely adequate to account for all the features of the interference experiments.

A rather different approach has been taken by Tua and Ruvalds (1985) and by Coppersmith and Littlewood (1986), who assume that internal degrees of freedom are

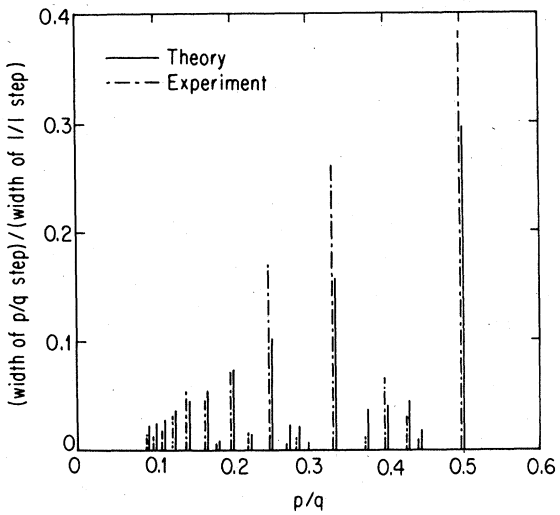

FIG. 47. Normalized step size $\delta V(p/q)\delta V(1/1)$ vs p/q. The solid lines are for a NbSe sample at $T=42$ K with $V_T(V_{ac}=0)=2.0$ mV, $\omega_{ac}/2\pi=25$ MHz, and $V_{ac}=30$ mV peak to peak. The dotted lines are calculated by use of Eq. (10) and the pinning potential of Fig. 1(b), on assumption that $\omega_1/\omega=1.6$. All 18 steps between $p/q=\frac{1}{11}$ and $\frac{1}{2}$ for which $q\leq 11$ are shown (Thorne *et al.*, 1986).

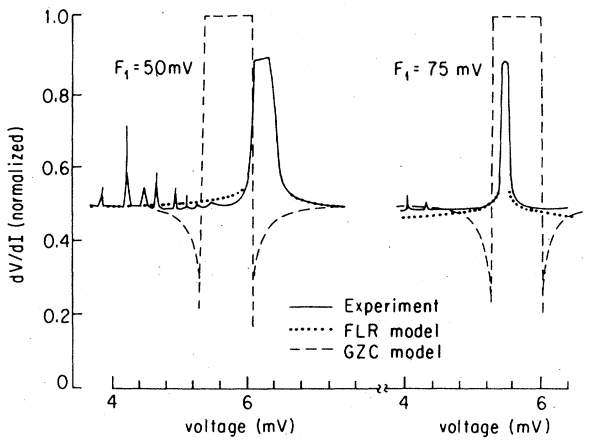

FIG. 48. Differential resistance dV/dI vs dc voltage V_0 near the first harmonic feature $Q\cdot v\sim\omega_{ac}$ for $NbSe_3$ with ac frequency $\omega_{ac}=25$ MHz and ac voltage amplitudes $V_1\sim 50$ and 75 mV (Brown and Grüner, 1988) for a sample with $V_T\sim 2$ mV. Also shown are theoretical fits using the Fukuyama-Lee-Rice (FLR) deformable CDW model (dotted line) and the Grüner-Zawadowski-Chaikin (GZC) one-degree-of-freedom result (dashed line). For FLR, both curves are fitted by use of a single parameter of order unity, as discussed in the text. The tops of the peaks are not calculated because the perturbation theory breaks down when the change in dV/dI is large (Coppersmith and Littlewood, 1986).

essential in obtaining subharmonic steps. In a model of coupled domains (Tua and Ruvalds, 1985), a rich subharmonic structure is recovered in qualitative agreement with the experiments. The amplitude of the subharmonic disappears in the thermodynamic limit, in parallel with the disappearance of the current oscillations in this limit. Internal degrees of freedom, when treated perturbatively in the large CDW velocity limit, also lead to the emergence of subharmonics, with an increasing number of mode-locking regions having an increasing number of perturbative steps (Coppersmith and Littlewood, 1986). Such an approach leads to mode locking in the thermodynamic limit and allows a detailed calculation of the shape of the mode-locking curves. The results of such a calculation are displayed in Fig. 48, together with unpublished experimental results of Brown and Grüner (1988). The classical single-particle model (Grüner, Zawadowski, and Chaikin, 1981) leads to well-defined "wings" that accompany the mode-locked region. In contrast, the mode locking obtained by the model whose internal degrees of freedom are included (called the FLR, or Fukuyama-Lee-Rice, model on the figure) leads to no such wings, in agreement with experiment. In contrast to the experimental results displayed on the figure, substantial wings are also often observed (see, for example, Thorne *et al.*, 1987), and the experimental state of affairs is far from being clear at present. The details of the mode locking appears to depend on several factors, such as sample quality, contact geometry, sample purity, and temperature, and a systematic investigation of these factors has not been performed as yet. Such experiments, however, appear to be essential in order to distinguish between the various proposed models. It is also conceivable that internal degrees of freedom are important under some circumstances and are negligible in different situations.

As discussed earlier, in certain specimens of $NbSe_3$ the onset of the current-carrying state is not smooth, and the current-voltage characteristics display well-defined switching and hysteresis behavior. When subjected to combined ac and dc electric drive fields, such specimens again display dramatic mode locking with hysteretic structure (Hall *et al.*, 1984b). The dc response is like that predicted by the circle map and similar to that displayed in Fig. 46. However, the range of mode lock for the harmonic Shapiro steps, i.e., for $p=1,2,3,\ldots$, $s=1$, is substantially larger, and the harmonic steps virtually fill all of Ω space, as shown in Fig. 49(a). The simultaneously measured ac response is a complicated function of ac amplitude E_{ac} and frequency ω_{ex}, and dc bias E_{dc}. With fixed E_{ac} and ω_{ex}, increasing E_{dc} leads, on each mode-locking step, to a period doubling route to chaos. This is displayed schematically in Fig. 49(a), which shows vertical windows, each corresponding to a partiuclar period (or chaos) for the response. The corresponding frequency response spectra are displayed in Fig. 49(b). Period-doubling bifurcations and a chaotic behavior, distinguished by large broadband noise, are clearly observed. A period doubling route to chaos can also be observed by keeping the dc bias constant and smoothly changing E_{ac} or ω_{ex}. By systematic variation of all three parameters, i.e., E_{dc}, E_{ac}, and ω_{ex}, the response boundary between period 1,2,4,. . . and chaotic solutions may

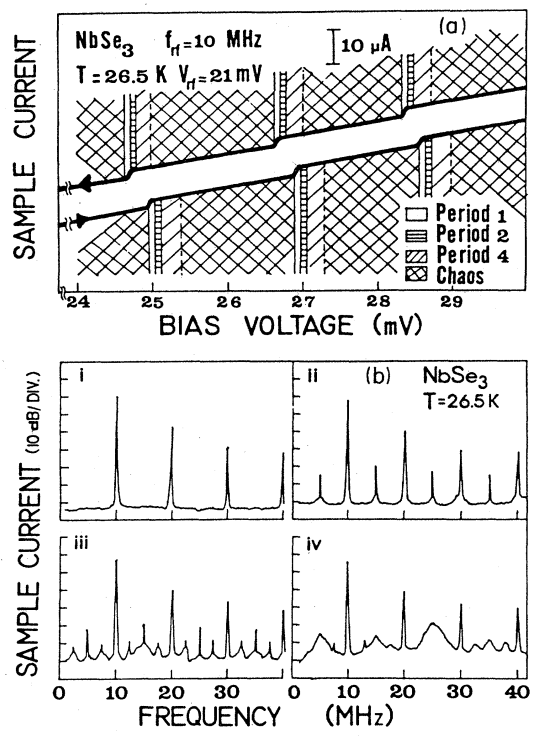

FIG. 49. (a) Schematic representation of the current response in the Shapiro step region of $NbSe_3$, for forward and reverse bias voltage sweeps. The heavy lines are the direct I-V traces, offset vertically for clarity; (b) frequency spectrum of the current response in the Shapiro step region. External rf drive frequency and amplitudes as in (a). (i) $V_{dc}=25.0$ mV, period 1; (ii) $V_{dc}=25.1$ mV, period 2; (iii) $V_{dc}=25.2$ mV, period 4; (iv) $V_{dc}=25.5$ mV, chaos (Hall *et al.*, 1985).

be mapped out. In general, repetitive (hysteretic) period-doubling routes to chaos can be induced by varying all three parameters monotonically through a limited range of phase space.

A repetitive period-doubling route to chaos on each mode-locked Shapiro step suggests a modulo 1 variable for the CDW phase, such as θ_m in Eq. (7.6). This equation is identically recovered by changing Ω to $\Omega+n$, with n an integer. The periodicity of the bifurcation sequence in dc bias is thus consistent with the periodicity of the behavior predicted by the circle map. Similarly, period-doubling routes to chaos on mode-locked Shapiro steps are predicted by Eq. (7.2) if the inertial term is retained (Kantz, 1981).

VIII. DISORDER AND METASTABLE STATES

The observation of current oscillations and the pronounced interference effects in the presence of ac and dc excitations are suggestive of a highly coherent response in the current-carrying state, with a phase-phase correlation length L_0 comparable to the dimensions of the specimens. Such a high degree of coherence can be achieved only in relatively pure $NbSe_3$ specimens where the small threshold fields E_T for nonlinear conduction suggest through Eqs. (4.16) and (4.12) that L_0 is substantial, of the order of 1μ. This is confirmed directly by x-ray studies (Fleming *et al.*, 1978, 1984). Consequently, the dynamics of internal modes may be largely neglected (for rather pure and small specimens), or can be included perturbatively by considering first the dynamics of the average phase $\langle\varphi\rangle$. The situation is somewhat different in TaS_3 where the small amplitude of the current oscillations and the relatively weak interference effects suggest that disorder and/or sample inhomogeneity play an important role. In the materials $(TaSe_4)_2I$ and $K_{0.3}MoO_3$ the current oscillations, when Fourier analyzed, give a substantial distribution of CDW velocities within the specimen, and interference effects are either not observed or are extremely weak. For these materials, the phase-phase correlation length is presumably small. This, together with the relatively large sample dimensions both parallel and perpendicular to the chains, $L_\parallel$ and $L_\perp$, leads to a situation where the number of degrees of freedom, or number of metastable states, is of the order $(L_{\text{sample}}/L_0)^3$, where $L_{\text{sample}}=(L_\parallel L_\perp^2)^{1/3}$, an "average" sample dimension, is large and can, for all practical purposes, be regarded as close to the thermodynamic limit. Under such circumstances, the dynamics of internal degrees of freedom are important. This may lead to observations similar to those made in spin-glass random-field magnets.

The close relation between the observations on low-frequency and long-time relaxation phenomena in materials with a charge-density-wave ground-state and random-field systems is not surprising. Equation (5.13) is formally identical to the random-field X-Y model,

$$H=\sum_{i,j} J_{ij}\mathbf{S}_i\cdot\mathbf{S}_j+\sum_i (h_i\mathbf{S}_i)^2 ,$$

in the limit where the angle θ between the neighboring spin direction is small. Arguments on the absence of long-range order and the behavior of the various correlation functions are appropriate for both systems, and it is expected that the dynamical behavior displays strong similarities for small amplitude driving fields. H_e in Eq. (5.13), however, corresponds to an applied torque in the random-field X-Y model, and the electric polarization P_e corresponds to a rotational magnetization. The difference between the coupling to external fields leads to fundamentally different behavior in the large amplitude response: In the random X-Y model the magnetization saturates in the infinite magnetic field limit, while for an applied torque there is a phase transition to a "phase-winding" state where all spins rotate under the influence of the applied torque. This transition corresponds to the transition from the pinned to the current-carrying CDW state. Furthermore, because of the large polarizability (related to the large length scale L_0) nonlinear response phenomena may become important even for moderate applied fields. Effects associated with metastable states

are also expected to be temperature dependent because of the possibility of temperature-driven transitions between the various metastable configurations.

The small amplitude ac response of various materials has been discussed in detail in Sec. VI. In the full frequency range, from dc to millimeter wave frequencies, the response can be described by a distribution of pinning frequencies (Wu *et al.*, 1985). Alternatively, phenomenological equations, such as (6.7) and (6.8), have been used extensively to describe both $\mathrm{Re}\sigma(\omega)$ and $\mathrm{Im}\sigma(\omega)$; both are suggestive of "glassy dynamics", i.e., of the importance of internal degrees of freedom. Certain features, such as the anomalous low-frequency response of the dielectric constant, have been recovered by calculations (Fisher, 1985; Littlewood, 1986) based on the FLR model. The experimentally found behavior for various materials is displayed in Fig. 50. The strongly divergent response as $\omega \rightarrow 0$ is in clear conflict with single-degree-of-freedom dynamics, which would suggest a leading low-frequency behavior of

$$\varepsilon(\omega) \sim \varepsilon(\omega=0) - B\omega^2 \ . \tag{8.1}$$

Linked, as $\omega \rightarrow 0$, the behavior can be described as

$$\varepsilon(\omega) = \varepsilon(\omega=0) - B'\omega^{\alpha'} \tag{8.2}$$

with $\alpha' < 1$. The behavior is usually referred to as the zero-frequency cusp. Whether $\varepsilon(\omega=0)$ is finite and whether there is a crossover to a behavior given by Eq. (8.1) for very small frequencies and small excitation amplitudes is not clear. The behavior most probably depends on factors like sample dimensions or temperature.

A. The nonlinear ac response

Dielectric constant measurements in the small amplitude $E_{ac} \rightarrow 0$ limit sample the relaxation effects around the state, which has been reached prior to the excitation applied. This state is, in general, expected to be frozen in a metastable state (Fisher, 1983; Littlewood and Rice, 1982; Matsukawa and Takayama, 1984). Other metastable states close in energy to the "frozen-in" metastable state, but presumably far from its configuration space, can, however, be excited by the application of finite-amplitude dc or ac drives. The effect was first demonstrated by Cava, Fleming, Dunn *et al.* (1984) in $K_{0.3}MoO_3$, by measuring the dielectric response at various ac signal amplitudes. The data have been analyzed using

$$\varepsilon(\omega) = (\varepsilon_0 - \varepsilon_{HF}) \frac{1}{[1+(i\omega\tau_0)^{1-\alpha}]^{\beta}} + \varepsilon_{HF} \ , \tag{8.3}$$

where ε_0 and ε_{HF} are the static dielectric constant and τ_0 is a characteristic relaxation time. Both α and τ_0 were found to be dependent on the applied ac amplitude, suggesting a strong modification of the long-time response of the system by finite-amplitude ac fields. The effect was found to be less pronounced at higher frequencies, as expected for internal modes the dynamics of which is described by relaxational dynamics. Similar amplitude-dependence ac response was found by Ong *et al.* (1985) in *o*-TaS_3.

The nonlinear ac response was further studied by monitoring the higher harmonic generation (Chen *et al.*, 1988; Mihály and Grüner, 1987). For a linear system, the response to an excitation $V = V_0 \sin\omega_{ext}$ is purely sinusoidal, and no harmonics at frequencies $n\omega_{ext}$ are observed. In general, for a simple nonlinear system, the dielectric constant can be expressed in terms of powers of the excitation amplitude V_0 and $\varepsilon = \varepsilon^{(1)} + \varepsilon^{(3)}V_0^2 + \varepsilon^{(5)}V_0^4 + \cdots$ where $\varepsilon^{(2n+1)}$ represents the response of the system at frequency $(2n+1)\omega_{ext}$. Experimentally, the third harmonic response measured at frequencies $3\omega_{ext}$ was found to be both amplitude V_0 and frequency ω_{ext} dependent, and the observations can be described as (Chen *et al.*, 1987)

$$\varepsilon(\omega) = A \frac{V_0^{\nu}}{\omega^{\eta}} \tag{8.4}$$

with both ν and η less than one and $A = \text{const}$. This behavior, which is similar to the nonlinear susceptibilities observed in spin glasses both below and slightly above the glass transition temperature, is unexplained at present. The behavior is most probably related to the apparent inductive response observed in low-frequency large-amplitude measurements in a Lissajous representation (Tessema and Ong, 1985).

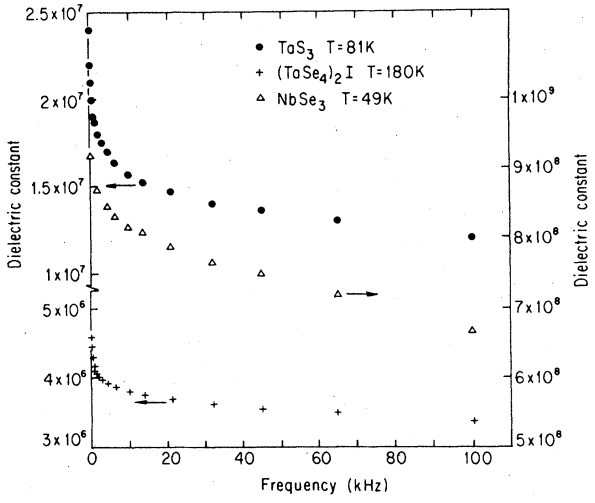

FIG. 50. Frequency-dependent dielectric constant in various materials (Wu *et al.*, 1984).

B. Time domain studies and remanent polarizations

The highly anomalous frequency and electric-field-dependent response is strongly related to anomalous time-dependent effects and also to remanent polarization phenomena, the latter observed at low temperatures.

The response to steplike electric field excitations of the form of $V(t)=V_0\delta(t-t_0)$, where δ is a step function, is in general nonexponential and displays long-time tails. The functional form observed depends on various factors, such as temperature and drive amplitude. For small excitation amplitude the response appears to be exponential, but for large step excitations, the observed time-dependent polarization was found to be well described by the so-called Kohlrausch equation (Kohlrausch, 1947; Jonscher, 1977),

$$P(t)=P_0\left\{1-\exp\left[-\left[\frac{t}{\tau}\right]\alpha\right]\right\}, \tag{8.5}$$

with $\alpha<1$ (Mihály and Tessema, 1986). Typical time-dependent polarizations, obtained after various pulse excitations, are displayed in Fig. 51 (Mihály and Tessema, 1986). Here P_0 is the remanent polarization, τ and average relaxation time and the exponential $\alpha<1$. Equation (8.4) has been used extensively to describe long-time relaxational phenomena in spin glasses and various random-field systems (Chamberlin, 1984; Chamberlin *et al.*, 1984). Logarithmic time dependencies, in the form

$$P(t)=A\ln\frac{t}{\tau}, \tag{8.6}$$

have also been observed (Mihály and Mihály, 1984; Ong *et al.*, 1985; Mihály *et al.*, 1985). The above observations are clearly related to the frequency-dependent response, which is also described by fractional powers of frequency [see Eq. (8.4)]. In Eq. (8.5) P_0 refers to a remanent polarization. Because of the long-time response P_0 cannot be directly measured, and, in general, it is assumed that the polarization measured on substantial time after the pulse is applied is close to P_0. In addition, the remanent polarization can be detected only at low temperatures, where thermally induced transitions between the various metastable states are not significant. P_0, i.e., a polarization close to P_0 has been measured in detail in $K_{0.3}MoO_3$ by applying a sequence of electric field excitations with successively larger amplitude. A typical hysteresis loop shown in Fig. 52 is recovered by such experiments.

At low temperatures, where the conductivity due to the normal electrons is small, the polarization can be measured directly. At higher temperatures this is not possible because of screening currents shown to the uncondensed electrons. The CDW polarization, however, is the result of frozen-in local distortions of the collective mode, and this leads to changes in the small-field (ohmic) resistance of the specimens. Although the detailed mechanism is not clear, the effect can be used to monitor the buildup of CDW polarizations at higher temperatures. This method was employed to establish the existence of remanent polarizations in $NbSe_3$ and in TaS_3 (Brown, Grüner, and Mihály, 1986). Furthermore, the polarization observed was shown to be a bulk effect and the result of long-range remanent deformations of the collective mode, which leads to the breakdown of translational invariance in the bulk (Tessema *et al.*, 1985; Brown, Grüner, and Mihály, 1986). This has been directly demonstrated by measuring the polarization as the function of distance along the long axis of the specimens, which also corresponds to the chain direction. Furthermore, metastable states induced by the application of electric fields have been directly observed by x-rays (Fleming, Dunn, and Schneemeyer, 1985; Tamegai *et al.*, 1985; Mihály, Lee, and Stephens, 1987). The remanent polarization increases dramatically with increasing applied voltage V_0, and the experimental results displayed on the figure are suggestive for a divergent polarization when the threshold field E_T is approached from below. This has been studied in detail (Wang and Ong, 1987; Mihály and Grüner, 1987), and the observations have been described in terms of a polarization catastrophe with critical exponents that describe the divergence of

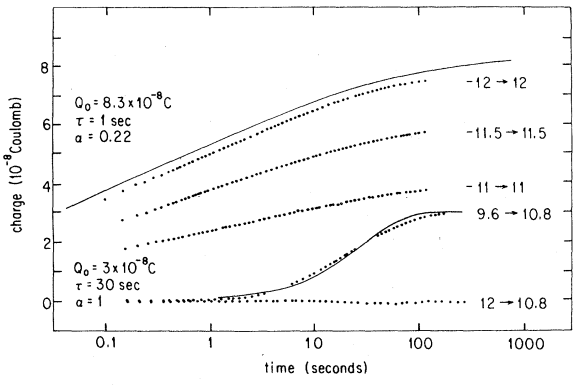

FIG. 51. Relaxation processes in response to a steplike external voltage drive measured on a blue bronze sample at $T=4.2$ K. The numbers on the right-hand side indicate the voltage before and after the step. The continuous lines were obtained by using the stretched exponential formula (8.7) with parameters shown on the left-hand side.

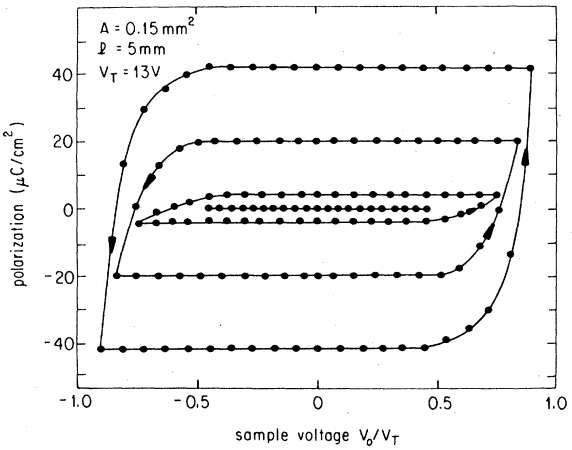

FIG. 52. Dielectric polarization loops observed in $K_{0.3}MoO_3$ at low temperatures. V_T refers to the threshold voltage for the onset of nonlinear conduction (Mihály and Tessema, 1986).

P_0. Because of the extremely long time scales involved, and because of the ambiguities as far as the detailed time dependences involved (whether logarithmic or stretched exponential), a clear-cut analysis of this novel type of critical phenomenon has not been possible to date. The behavior displayed in Fig. 52 is, however, well reproduced by numerical simulations (Matsukawa and Takayama, 1986) that are based on the Fukuyama-Lee-Rice model of impurity pinning. Numerical simulations have not yet been extended to treat the behavior near the threshold field. The problem has been treated by a simplified model (Mihály, Chen, and Grüner, 1987) that indeed leads to critical exponents for the divergent polarization and for the relaxation time τ, which appears in Eq. (8.5). The remanent polarization effects also suggest that special procedures, similar to those that lead to demagnetization for ferromagnets, are required to arrive at an unpolarized CDW state. Such procedures, along with temperature-induced depolarization effects, have been discussed by Wang and Ong (1987).

At higher temperature, thermally induced transitions between the various metastable states destroy the remanent polarization and lead to the so-called thermally stimulated currents; the relaxation back to the unpolarized state is well described by a stretched exponential or by logarithmic (Mihály and Mihály, 1984) time dependence. These have been investigated by measuring the Ohmic resistance R of the specimens, assuming that changes in the CDW polarization lead to changes in the single-particle gap and thus to R.

Detailed studies performed on TaS_3 (Kriza and Mihály, 1986) over a broad time domain demonstrate that the time-dependent depolarization currents can be well described by the stretched exponential form. Moreover, the average relaxation time τ obeys the empirical form

$$\tau(T)=\tau_0 \exp\left[-\frac{\Delta}{kT}\right], \tag{8.7}$$

with 2Δ close to the single-particle gap in this material. The behavior is most probably related to the strongly temperature-dependent relaxation time obtained from the analysis of the low-frequency dielectric constant (Cava *et al.*, 1985) and from the analysis of the temperature dependence of the nonlinear conduction (Fleming *et al.*, 1986). Similar temperature- (and also field-) dependent relaxation time was observed in $K_{0.3}MoO_3$ for the field-activated relaxation (Wang and Ong, 1987) in $(TaSe_4)_2I$ (Tucker *et al.*, 1986).

These studies, along with thermal and electric field cycling experiments (Wang and Ong, 1986; Duggan and Ong, 1986), raise interesting questions about the approach toward the ground state and about the dynamics near the ground state. Various distinct routes to equilibrium were found, and the extreme sensitivity of the ground state to small temperature changes was also established (Wang and Ong, 1986).

C. Transitions from below to above threshold

A variety of interesting phenomena occur when the pinned CDW is driven through E_T to the current-carrying state and back by the application of a sequence of various pulses. These are usually referred to as memory effects because the response to an applied pulse depends on the history polarization and deviation of the previous pulse. The observations are clearly metastable states in the pinned configuration, and their rearrangement under the influence of applied electric field.

The so-called pulse sign memory effect refers to the phenomenon where the response of the system to a pulse depends on the direction of the polarization of the previous pulse. When the electric field applied is the same direction as the preceding pulse, the response is fast, while a sluggish response is detected for a reverse polarization. The phenomenon was first observed in TaS_3 (Gill, 1981b; Gill and Higgs, 1983), and has subsequently been found in $K_{0.3}MoO_3$ and $NbSe_3$ (Fleming and Schneemeyer, 1983; Fleming, 1985b). The observations are shown in Fig. 53 for both $NbSe_3$ and $K_{0.3}MoO_3$.

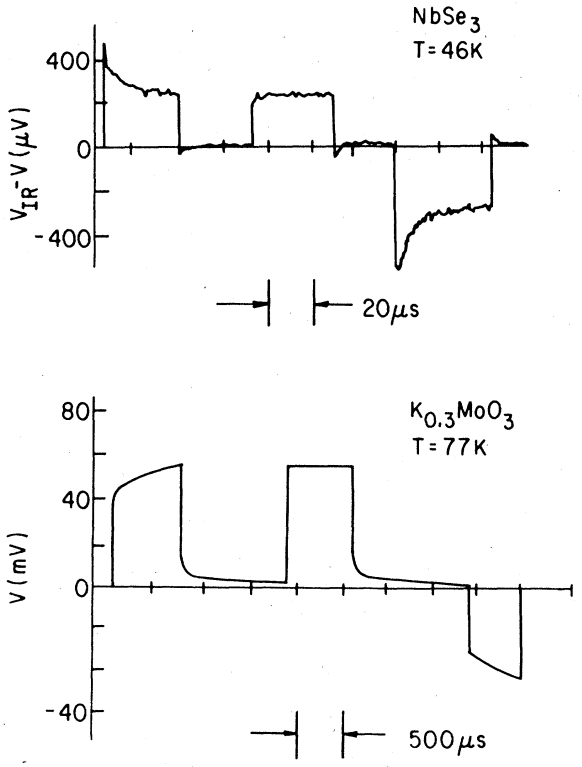

FIG. 53. Pulse sign memory effect. Response of $NbSe_3$ and $K_{0.30}MoO_3$ to a repetitive series of constant-current pulses consisting of two positive pulses followed by one negative pulse. The amplitude of the pulses are in excess of threshold. When the current direction is reversed, the response becomes very slow. (a) for $NbSe_3$; the linear response is subtracted so that only $IR_{linear}-V(t)$ is plotted as a function of time; (b) the total signal $V(t)$ is plotted.

Both types of response phenomena—the so-called overshoot observed in $NbSe_3$ and the smooth gradual buildup of the response observed in $K_{0.3}MoO_3$, both for applied pulses in the reverse direction from the preceding pulse—are reproduced by numerical simulations based on the treatment of the Fukuyama-Lee-Rice model (Littlewood, 1986; Coppersmith and Littlewood, 1985a, 1985b). The explanation of the phenomenon is relatively straightforward. When the applied electric field is suddenly removed, the charge-density wave does not relax back to the equilibrium configuration, but remains in a polarized state (see, for example, Fig. 52). This polarized state is a metastable state with remanent local configurations of the CDW deformation, similar to those that characterize the current-carrying state in a particular current direction. Consequently, with these configurations already established before the next electric field pulse, the response to this pulse will be fast. This is the case when the pulse polarities are identical. Different local configurations represent the current-carrying state in the opposite current direction, and a sluggish response or overshoot results because the long-range correlations have to be "unwound" and then "rewound" in the opposite direction (Littlewood, 1986).

The notion of pulse deviation memory effect refers to features found in the transient voltage or current oscillations observed in the current-carrying state after the application of a sudden electric field pulse. The transient oscillations occur at the fundamental frequency of the current oscillations, but their amplitude decreases slowly with increasing time (Fleming, 1981; Zettl and Grüner, 1982a, 1982b) saturating at a constant value as $t \rightarrow \infty$. The initial phase of the oscillations is adjusted to the leading edge of the applied pulse, and, more important, at the end of the pulse the phase of the oscillations is also the same. The phenomenon is shown in Fig. 54. This so-called pulse duration memory effect (Brown, Mihály, and Grüner, 1986; Fleming and Schneemeyer, 1986) is clearly related to the mode-locking phenomena discussed in the previous section. However, it should not occur for a single-degree-of-freedom system (Coppersmith and Littlewood, 1986). Reasons why a many-degrees-of-freedom system should display pulse duration memory effects have been discussed recently (Tang *et al.*, 1987), and concepts such as phase organization and dynamical selection of states have emerged from models that mimic the dynamics of charge-density waves. These effects are discussed in detail by Littlewood (1987).

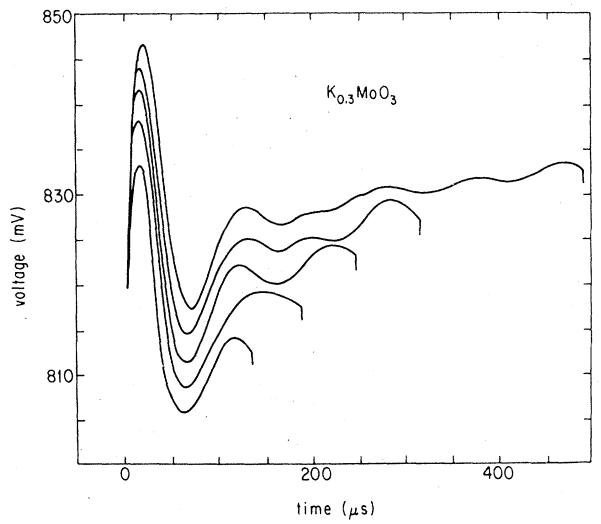

FIG. 54. Voltage response to repetitive pulse drive. For repetitive pulses of constant amplitude, the phase of the last transient oscillation is fixed relative to the end of the pulse for arbitrary pulse width (Fleming *et al.*, 1986).

IX. FINAL REMARKS

During the past decade the field has advanced considerably, and the basic notions on the dynamics of charge-density waves are well documented by a broad range of experimental studies. Most of the important features of this novel type of collective transport phenomenon are well established.

Several questions remain, however. Experiments on properties other than electrical conduction, such as Hall effect, thermoelectric power, and acoustic properties, clearly require an underlying microscopic theory, and the same is true for the high-frequency damping and for the temperature-dependent low-frequency damping processes. Little is known about the effects associated with the dynamics of the amplitude mode. While this may not be important at low temperatures, in most materials the gap associated with the amplitude excitations is less than kT_p, and also less than the temperatures where the experiments are conducted, and, consequently, should be important. In contrast, Coulomb effects are important at low temperatures because they can lead to long-range order, even in the presence of impurities, and lead to a gap in the phason spectrum (Fukuyama and Lee, 1978). Both effects (Wong and Takada, 1988) are expected to influence the dynamics of the collective mode. The question of whether quantum-mechanical concepts are required to describe the dynamics of charge-density waves is still hotly debated (Thorne *et al.*, 1987, and references cited therein), and a broad variety of experiments involving joint ac and dc excitations have been interpreted in terms of quantum and classical models. Experiments on effects where the predictions of the two models are different, such as photon-assisted tunneling from the pinned to the current-carrying state, have not been successful to date.

Charge-density waves have also served in the past as models for the study of the dynamics of driven nonlinear systems. Mode locking and interference phenomena (similar in many respects to those observed in Josephson junctions) were used to study the possibility of transitions to chaos, but because of the complexity of material problems (associated with pinning effects) most of the issues remain unresolved. Charge-density waves have also been

used to study relaxation effects in random systems, with analogies to spin glasses and random field magnets. The effect of an applied electric field in CDW transport is analogous to an applied torque in random field magnets; this leads to a phase transition (in terms of the analogy to random-field systems), and then to a phase-winding state. Only initial attempts have been made to measure the various parameters near this novel type of driven phase transition, in particular, below E_T.

Practically nothing has been said in this review about the nonlinear and frequency-dependent transport, which is observed at low temperatures (Maeda, Furayama, and Tanaka, 1986; Mihály and Tessema, 1986; Mihály *et al.*, 1988). The phenomenon, which is also accompanied by polarization divergences (Chen *et al.*, 1988) and changes in the CDW deformations (Mihály, Crommie, and Grüner, 1987), appears to be rather different from the nonlinear and frequency-dependent response observed at high temperatures. The difference between the two regimes most probably is due to the effects associated with screening (Wong and Takada, 1987). At high temperatures, screening by the normal electrons leads to a gapless phason spectrum and, consequently, to the possibility of long-range deformations around impurities. In the absence of normal electrons, at low temperatures such screening is not possible. This results in a gap in the phason spectrum and, possibly, also long-range order even in the presence of random impurities. Charge transport where the dynamics of local deformations are important cannot occur with the nonlinearity determined by the translational motion of the rigid condensate (Littlewood, 1988). This low-temperature regime, with the possibility of true Fröhlich superconductivity, clearly deserves further investigation.

Relatively little is known about the various nonlinear excitations of the collective mode, which may occur at energies below the single-particle gap. Various solitonlike modes may occur, in particular, in systems that are close to commensurability, and higher harmonic phason modes (Sherwin *et al.*, 1984; Travaglini and Wachter, 1984) have also been discussed.

Whether features in the observed optical spectra can be clearly identified with the fundamental features of the dynamics of the collective mode remains to be seen. Experiments on different materials and on alloys may clarify this aspect of CDW dynamics.

Nonlinear and frequency-dependent phenomena have also been reported recently in systems other than discussed in this review. In the organic linear-chain compound TTF-TCNO, the nonlinear response is clearly due to charge-density waves (Lacoe *et al.*, 1986), with added complications that two charge-density waves are present where the nonlinear conduction was observed. Less clear is the situation in intercalated graphite (Iye and Dresselhaus, 1985) and on the material Hg-Cd-Te, which is assumed to undergo a phase transition to a Wigner-crystal state. The electrical conductivity is a nonlinear (Osada *et al.*, 1987) and a frequency- (Javadi *et al.*, 1986) dependent organic linear-chain conductor with a spin-density-wave ground state. The question whether spin-density-wave dynamics is similar to the dynamics of charge-density waves deserves further investigation.

ACKNOWLEDGMENTS

This review is the result of many useful discussions with several colleagues. I am most grateful to John Bardeen for many comments concerning this paper, to W. Wonneberger and L. Sneddon for reading the paper, and to D. Fisher and N. P. Ong for constructive remarks. Part of this review was written when the author was a guest scientist at the Max Planck Institut für Festkorperforschung, Stuttgart. Support by the National Science Foundation Grant No. DMR 86-20340 is also acknowledged.

REFERENCES

Allender, D., J. W. Bray, and John Bardeen, 1974, Phys. Rev. B **9**, 119.
Allgeyer, R., B. H. Suits, and F. C. Brown, 1982, Solid State Commun. **43**, 207.
Alstrom, P., M. H. Jensen, and M. T. Levinsen, 1984, Phys. Lett. A **103**, 171.
Ambegaokar, V., and B. I. Halperin, 1969, Phys. Rev. Lett. **22**, 1364.
Aronov, A. G., and V. L. Gurevich, 1974, Fiz. Tverd. Tela (Leningrad) **16**, 2656 [Sov. Phys.-Solid State **16**, 1722 (1975)].
Artemenko, S. N., E. N. Dolgov, A. N. Krugov, Y. I. Latyshev, Y. S. Savitskaya, and V. V. Frolov, 1984, Pis'ma Zh. Eksp. Teor. Fiz. **39**, 258 [JETP Lett. **39**, 308].
Artemenko, S. N., and A. F. Volkov, 1981a, Pis'ma Zh. Eksp. Teor. Fiz. **33**, 155 [JETP Lett. **33**, 147].
Artemenko, S. N., and A. F. Volkov, 1981b, Zh. Eksp. Teor. Fiz. **81**, 1872 [Sov. Phys.—JETP **54**, 992].
Artemenko, S. N., A. F. Volkov, and A. N. Kruglov, 1986, Physica B **143**, 146.
Azbel, M. Ya., and Per Bak, 1984, Phys. Rev. B **30**, 3722.
Bak, Per, 1982a, Phys. Rev. Lett. **48**, 692.
Bak, Per, 1982b, Rep. Prog. Phys. **45**, 587.
Bak, Per, 1983, Proceedings of the International Symposium on Nonlinear Transport in Inorganic Quasi-One-Dimensional Conductors, Sapporo, Japan (unpublished).
Bardeen, John, 1979, Phys. Rev. Lett. **42**, 1498.
Bardeen, John, 1980, Phys. Rev. Lett. **45**, 1978.
Bardeen, John, 1982, Mol. Cryst. Liq. Cryst. **81**, 719.
Bardeen, John, 1984, Physica B **126**, 342.
Bardeen, John, 1985a, in *Proceedings of the International School of Physics "Enrico Fermi,"* Vol. 89 (North-Holland, Amsterdam), p. 349.
Bardeen, John, 1985b, Phys. Rev. Lett. **55**, 1010.
Bardeen, John, 1986, Physica B **143**, 14.
Bardeen, John, 1987, Z. Phys. **67**, 427.
Bardeen, John, E. Ben-Jacob, A. Zettl, and G. Grüner, 1982, Phys. Rev. Lett. **49**, 493.
Bardeen, John, J. W. Lyding, W. G. Lyons, J. H. Miller, Jr., R. E. Thorne, and J. R. Tucker, 1987, Synth. Met. **19**, 1.
Bardeen, John, and J. R. Tucker, 1985, in *Charge Density Waves*

in Solids, Proceedings of the International Conference Held in Budepest, Hungary, 1984, Lecture Notes in Physics Vol. 217, edited by Gy. Hutiray and J. Sólyom (Springer, Berlin), p. 155.
Barisic, S., 1986, in *Electronic Properties of Inorganic Materials with Quasi-One-Dimensional Structures,* edited by P. Monceau (Reidel, Dordrecht/Boston/Lancaster), Part 1, p. 1.
Barnes, S. E., and A. Zawadowski, 1983, Phys. Rev. Lett. **51**, 1003.
Barone, A., and G. Paterno, 1982, *Physics and Applications of the Josephson Effect* (Wiley, New York).
Batistic, I., A. Bjelis, and L. P. Gorkov, 1984, J. Phys. (Paris) **45**, 1049.
Beasley, M. R., and B. A. Huberman, 1982, Comments Solid State Phys. **10**, 155.
Ben-Jacob, E., 1983, Solid State Commun. **47**, 603.
Ben-Jacob, E., Y. Braiman, R. Shainsky, and Y. Imry, 1981, Appl. Phys. Lett. **38**, 822.
Berlinski, J., 1979, Rep. Prog. Phys. **42**, 1243.
Berthier, C., and P. Ségranson, 1987, in *Low Dimensional Conductors and Superconductors,* NATO Advanced Study Institute, Series B, Vol. 155, edited by D. Jerome and L. G. Carol (Plenum, New York), p. 455.
Beyermann, W. P., L. Mihály, and G. Grüner, 1986, Phys. Rev. Lett. **56**, 1489.
Bhattacharya, S., J. P. Stokes, M. J. Higgins, and R. A. Klemm, 1987, Phys. Rev. Lett. **59**, 1849.
Bhattacharya, S., J. P. Stokes, M. O. Robbins, and R. A. Klemm, 1985, Phys. Rev. Lett. **54**, 2453.
Birgenau, R. J., K. Yoshizava, R. A. Covely, G. Shirane, and K. Ikeda, 1983, Phys. Rev. B **28**, 1438.
Bjelis, A., 1987, in *Low Dimensional Conductors and Superconductors,* NATO Advanced Study Institute, Series B, Vol. 155, edited by D. Jerome and L. G. Carol (Plenum, New York/London), p. 409.
Bohr, T., P. Bak, and M. H. Jensen, 1984, Phys. Rev. A **30**, 1970.
Borodin, D. V., F. Y. Nad, Y. S. Savitskaya, and S. V. Zaitsev-Zotov, 1986, Physica B **143**, 73.
Bouffard, S., M. Sanguer, H. Mutka, J. Dumas, and C. Schlenker, 1985, unpublished.
Bourne, L. C., M. S. Sherwin, and A. Zettl, 1986, Phys. Rev. Lett. **56**, 1952.
Brazovskii, S. A., and I. E. Dzyaloshinskii, 1976, Zh. Eksp. Teor. Fiz. **71**, 2338 [Sov. Phys.—JETP **44**, 1233].
Breymayer, H.-J., H. Risken, H. D. Vollmer, W. Wonneberger, 1982, Appl. Phys. B **28**, 335.
Brill, J. W., 1982, Solid State Commun. **41**, 925.
Brill, J. W., and S. L. Herr, 1983, Phys. Rev. B **27**, 3916.
Brill, J. W., and N. P. Ong, 1978, Solid Commun. **25**, 1075.
Brill, J. W., N. P. Ong, J. C. Eckert, J. W. Savage, S. K. Khanna, and R. B. Somoano, 1981, Phys. Rev. B **23**, 1517.
Brill, J. W., and W. Roark, 1984, Phys. Rev. Lett. **53**, 846.
Brill, J. W., W. Roark, and G. Minton, 1986, Phys. Rev. B **33**, 6831.
Brown, S. E., and G. Grüner, 1985, Phys. Rev. B **31**, 8302.
Brown, S. E., and G. Grüner, 1988, unpublished.
Brown, S. E., G. Grüner, and L. Mihály, 1986, Solid State Commun. **57**, 165.
Brown, S. E., A. Janossy, and G. Grüner, 1985, Phys. Rev. B **31**, 6869.
Brown, S. E., and L. Mihály, 1985, Phys. Rev. Lett. **55**, 742.
Brown, S. E., L. Mihály, and G. Grüner, 1986, Solid State Commun. **58**, 231.
Brown, S. E., G. Mozurkewich, and G. Grüner, 1984, Phys. Rev. Lett. **52**, 2277.
Brown, S. E., G. Mozurkewich, and G. Grüner, 1985a, Solid State Commun. **54**, 23.
Brown, S. E., G. Mozurkewich, and G. Grüner, 1985b, in *Charge Density Waves in Solids, Proceedings of the International Conference Held in Budapest, Hungary, 1984,* Lecture Notes in Physics Vol. 217, edited by Gy. Hutiray and J. Sólyom (Springer, Berlin), p. 318.
Bruinsma, R., and L. Mihály, 1985, Bull. Am. Phys. Soc. **30**, 364.
Burkov, S. E., and V. L. Pokrowsky, 1984, Solid State Commun. **46**, 609.
Butaud, P., P. Ségranson, C. Berthies, J. Dumas, and C. Schlenker, 1985, Phys. Rev. Lett. **55**, 253.
Cava, R. J., R. M. Fleming, R. G. Dunn, and E. A. Rietman, 1985, Phys. Rev. B **31**, 8325.
Cava, R. J., R. M. Fleming, R. G. Dunn, E. A. Rietman, and L. F. Schneemeyer, 1984, Phys. Rev. B **30**, 7290.
Cava, R. J., R. M. Fleming, P. Littlewood, E. A. Rietman, L. F. Schneemeyer, and R. G. Dunn, 1984, Phys. Rev. B **30**, 3228.
Cava, R. J., P. Littlewood, R. M. Fleming, R. G. Dunn, and E. A. Rietman, 1986, Phys. Rev. B **33**, 2439.
Challener, W. A., and P. L. Richards, 1984, Solid State Commun. **52**, 117.
Chamberlin, R. V., 1984, Phys. Rev. B **30**, 5393.
Chamberlin, R. V., G. Mozurkewich, and R. Orbach, 1984, Phys. Rev. Lett. **52**, 867.
Chen, C. H., and R. M. Fleming, 1983, Solid State Commun. **48**, 777.
Chen, C. H., L. F. Schneemeyer, and R. M. Fleming, 1984, Phys. Rev. B **29**, 8765.
Chen, T., L. Mihály, and G. Grüner, 1987, Phys. Rev. B **36**, 2931
Chen, T., L. Mihály, and G. Grüner, 1988, Phys. Rev. Lett. **60**, 464.
Clark, T. D., and P. E. Lindelof, 1976, Phys. Rev. Lett. **37**, 368.
Coppersmith, S. N., 1984, Phys. Rev. B **30**, 410.
Coppersmith, S. N., and P. B. Littlewood, 1985a, Phys. Rev. B **31**, 4049.
Coppersmith, S. N., and P. B. Littlewood, 1985b, in *Charge Density Waves in Solids, Proceedings of the International Conference Held in Budapest, Hungary, 1984,* Lecture Notes in Physics Vol. 217, edited by Gy. Hitiray and J. Sólyom (Springer, Berlin), p. 236.
Coppersmith, S. N., and P. B. Littlewood, 1986, Phys. Rev. Lett. **57**, 1927.
Coppersmith, S. N., and C. M. Varma, 1984, Phys. Rev. B **30**, 3566.
Dee, R. H., P. M. Chaikin, and N. P. Ong, 1979, Phys. Rev. Lett. **42**, 1234.
Devreese, J. T., R. P. Evrard, and V. E. van Doren, 1979, in *Highly Conducting One-Dimensional Solids,* edited by J. T. Devreese (Plenum, New York/London).
Devreux, F., 1982, J. Phys. (Paris) **43**, 1489.
Dolgov, E. N., 1984, Solid State Commun. **50**, 405.
Douglass, D. C., L. M. Schneemeyer, and S. E. Spengler, 1985, Phys. Rev. B **32**, 1813.
Duggan, D. D., T. W. Jing, N. P. Ong, and P. M. Lee, 1985, Phys. Rev. B **32**, 1397.
Duggan, D. D., and N. P. Ong, 1986, Phys. Rev. B **34**, 1375.
Dumas, J., C. Schlenker, J. Marcus, and R. Buder, 1983, Phys. Rev. Lett. **50**, 757.
Efetov, K. B., and A. I. Larkin, 1977, Zh. Eksp. Teor. Fiz. **72**, 2350 [Sov. Phys.—JETP 45, 1236].

Everson, M. P., and R. V. Coleman, 1983, Phys. Rev. B **28**, 6659.
Everson, M. P., G. Eiserman, A. Johnson, and R. V. Coleman, 1984, Phys. Rev. B **30**, 3582.
Fack, H., and V. Kose, 1971, J. Appl. Phys. **42**, 320.
Feigelman, M. V., and V. M. Vinokur, 1983, Solid State Commun. **45**, 603.
Feinberg, D., and J. Dumas, 1986, Physica B **143**, 111.
Fisher, B., 1976, J. Phys. C **9**, 1201.
Fisher, B., 1978, J. Appl. Phys. **49**, 5339.
Fisher, B., 1983, Solid State Commun. **46**, 227.
Fisher, B., 1984, Phys. Rev. B **30**, 1073.
Fisher, D., 1983, Phys. Rev. Lett. **50**, 1486.
Fisher, D., 1984, Physica B **126**, 409.
Fisher, D., 1985, Phys. Rev. B **31**, 1396.
Fleming, R. M., 1980, Phys. Rev. B **22**, 5606.
Fleming, R. M., 1981, in *Physics in One Dimension,* Springer Series in Solid-State Sciences Vol. 23, edited by J. Bernasconi and T. Schneider (Springer, New York), p. 253.
Fleming, R. M., 1982, Solid State Commun. **43**, 167.
Fleming, R. M., 1985, Physica B **143**, 86.
Fleming, R. M., R. J. Cava, L. F. Schneemeyer, E. A. Rietman, and R. G. Dunn, 1986, Phys. Rev. B **33**, 5450.
Fleming, R. M., R. G. Dunn, and L. F. Schneemeyer, 1985, Phys. Rev. B **31**, 4099.
Fleming, R. M., and C. C. Grimes, 1979, Phys. Rev. Lett. **42**, 1423.
Fleming, R. M., D. E. Moncton, J. D. Axe, and G. S. Brown, 1984, Phys. Rev. B **30**, 1877.
Fleming, R. M., D. E. Moncton, and D. B. McWhan, 1978, Phys. Rev. B **18**, 5560.
Fleming, R. M., and L. F. Schneemeyer, 1983, Phys. Rev. B **28**, 6996.
Fleming, R. M., and L. F. Schneemeyer, 1984, Bull. Am. Phys. Soc. **29**, 470.
Fleming, R. M., and L. F. Schneemeyer, 1986, Phys. Rev. B **33**, 2930.
Fleming, R. M., L. F. Schneemeyer, and R. J. Cava, 1985, Phys. Rev. B **31**, 1181.
Fleming, R. M., L. F. Schneemeyer, and D. E. Moncton, 1985, Phys. Rev. B **31**, 899.
Fogle, W., and H. Perlstein, 1972, Phys. Rev. B **6**, 1402.
Forró, L., J. R. Cooper, A. Jánossy, and K. Kamaras, 1985, Phys. Rev. B **34**, 9047.
Fournel, A., J. P. Sorbier, M. Konczykowski, and P. Monceau, 1986, Phys. Rev. Lett. **57**, 2199.
Fournel, A., J. P. Sorbier, M. Konczykowski, P. Monceau, and F. Levy, 1986, Physica B **143**, 177.
Frenkel, Y. I., and T. Kontorova, 1939, J. Phys. USSR **1**, 139.
Fröhlich, H., 1954, Proc. R. Soc. London, Ser. A **223**, 296.
Fujishita, H., M. Sato, and S. Hoshino, 1984, Solid State Commun. **49**, 313.
Fukuyama, H., 1976, J. Phys. Soc. Jpn. **41**, 513.
Fukuyama, H., 1978, J. Phys. Soc. Jpn. **45**, 1474.
Fukuyama, H., and P. A. Lee, 1978, Phys. Rev. B **17**, 535.
Fuller, W. W., G. Grüner, P. M. Chaikin, and N. P. Ong, 1981, Phys. Rev. B **23**, 6259.
Fung, K. K., and J. W. Steeds, 1980, Phys. Rev. Lett. **45**, 1696.
Geserich, H. P., G. Scheiber, M. Dürrler, F. Levy, and P. Monceau, 1986, Physica B **143**, 198.
Gill, J. C., 1981a, Solid State Commun. **37**, 459.
Gill, J.C., 1981b, Solid State Commun. **39**, 1203.
Gill, J. C., 1982a, Solid State Commun. **44**, 1041.
Gill, J. C., 1982b, Mol. Cryst. Liq. Cryst. **81**, 73.
Gill, J. C., 1985, in *Charge Density Waves in Solids, Proceedings of the International Conference Held in Budapest, Hungary, 1984,* Lecture Notes in Physics Vol. 217, edited by Gy. Hutiray and J. Sólyom (Springer, Berlin), p. 377.
Gill, J. C., 1986a, Contemp. Phys. **27**, 37.
Gill, J. C., 1986b, J. Phys. C **19**, 6589.
Gill, J. C., 1986c, Physica **143B**, 49.
Gill, J. C., and A. W. Higgs, 1983, Solid State Commun. **48**, 709.
Gleisberg, F., and W. Wonneberger, in *Charge Density Waves in Solids, Proceedings of the International Conference Held in Budapest, Hungary, 1984,* Lecture Notes in Physics Vol. 217, edited by Gy. Hutiray and J. Sólyom (Springer, Berlin), p. 254.
Gorkov, L. P., 1977, Pis'ma Zh. Eksp. Teor. Fiz. **25**, 384 [JETP Lett. **25**, 358].
Gorkov, L. P., 1983, Pis'ma Zh. Eksp. Teor. Fiz. **38**, 76 [JETP Lett. **38**, 87].
Gorkov, L. P., and E. N. Dolgov, 1979, Zh. Eksp. Teor. Fiz. 77, 396 [Sov. Phys.—JETP **50**, 203].
Grüner, G., 1982, Mol. Cryst. Liq. Cryst. **81**, 17.
Grüner, G., 1983a, Proceedings of the International Symposium on Nonlinear Transport in Inorganic Quasi-One-Dimensional Conductors, Sapporo, Japan (unpublished).
Grüner, G., 1983b, Physica D **296**, 1.
Grüner, G., 1983c, Comments Solid State Phys. **10**, 183.
Grüner, G., 1983d, Physica D **8**, 1.
Grüner, G., 1984, Physica B **126**, 400.
Grüner, G., W. G. Clark, and A. M. Portis, 1981, Phys. Rev. B **24**, 3641.
Grüner, G., L. C. Tippie, J. Sanny, W. G. Clark, and N. P. Ong, 1980, Phys. Rev. Lett. **45**, 935.
Grüner, G., A. Zawadowski, and P. M. Chaikin, 1981, Phys. Rev. Lett. **46**, 511.
Grüner, G., and A. Zettl, 1983, J. Phys. (Paris) Colloq. **44**, C3-1745.
Grüner, G., and A. Zettl, 1985, Phys. Rep. **119**, 117.
Grüner, G., A. Zettl, W. G. Clark, and John Bardeen, 1981, Phys. Rev. B **24**, 7247.
Grüner, G., A. Zettl, W. G. Clark, and A. H. Thompson, 1981, Phys. Rev. B **23**, 6813.
Haen, P., P. Monceau, B. Tissier, G. Waysand, A. Meerschaut, P. Moline, J. Rouxel, 1975, in *Low Temperature Physics—LT14,* edited by M. Krusius and V. Vuorio (North-Holland, Amsterdam), p. 445.
Hall, R. P., M. F. Hundley, and A. Zettl, 1986, Physica B **143**, 152.
Hall, R. P., M. Sherwin, and A. Zettl, 1984a, Phys. Rev. B **29**, 7076.
Hall, R. P., M. Sherwin, and A. Zettl, 1984b, Phys. Rev. Lett. **52**, 2293.
Hall, R. P., M. Sherwin, and A. Zettl, 1985, in *Charge Density Waves in Solids, Proceedings of the International Conference Held in Budapest, Hungary, 1984,* Lecture Notes in Physics Vol. 217, edited by Gy. Hutiray and J. Sólyom (Springer, Berlin), p. 314.
Hall, R. P., and A. Zettl, 1984a, Phys. Rev. B **30**, 2279.
Hall, R. P., and A. Zettl, 1984b, Phys. Rev. B **30**, 2279.
He, Da Ren, W. J. Yeh, and Y. H. Kao, 1982, Phys. Rev. B **30**, 172.
Heeger, A. J., 1979, in *Highly Conducting One-Dimensional Solids,* edited by J. T. Devreese *et al.* (Plenum, New York/London).
Herr, S. L., G. Minton, and J. W. Brill, 1986, Phys. Rev. **33**, 8851.

Horovitz, B., 1986, in *Solitons,* Modern Problems in Condensed Matter Sciences, Vol. 17, edited by S. E. Trullinger, V. E. Zakharov, and V. L. Pokrovsky (North-Holland, Amsterdam), p. 691.
Horowitz B., A. Bishop, and P. S. Lombdale, 1986 Synth. Met. **13**, 231.
Horowitz B., and J. Krumhansl, 1984, Phys. Rev. B **29**, 2109.
Hsieh, P. L., F. de Czito, A. Janossy, and G. Grüner, 1983, J. Phys. (Paris), Colloq. **44**, C3-1753.
Huberman, B. A., and J. P. Crutchfield, 1979, Phys. Rev. Lett. **43**, 1743.
Huberman, B. A., J. P. Crutchfield, and N. Packard, 1980, Appl. Phys. Lett. **37**, 750.
Humieres, D. D., M. R. Beasley, B. A. Huberman, and A. Liebchaber, 1982, Phys. Rev. A **26**, 3483.
Hundley, M., R. P. Hall, and A. Zettl, 1985, Bull. Am. Phys. Soc. **30**, 212.
Hutiray, Gy., G. Mihály, and L. Mihály, 1983, Solid State Commun. **48**, 227.
Hutiray, Gy., and J. Sólyom, 1985, Eds., *Charge Density Waves in Solids, Proceedings of the International Conference Held in Budapest, Hungary, 1984* (Lecture Notes in Physics, Vol. 217) (Springer, Berlin).
Imry, Y., and S. Ma, 1975, Phys. Rev. Lett. **35**, 1399.
Inui, M., and S. Doniach, 1987, Phys. Rev. B **35**, 6244.
Iye, Y., and G. Dresselhaus, 1985, Phys. Rev. Lett. **54**, 1182.
Janossy, A., G. Mihály, and G. Kriza, 1984, Solid State Commun. **51**, 63.
Janossy, A., G. Mihály, and L. Mihály, 1985, in *Charge Density Waves in Solids, Proceedings of the International Conference Held in Budapest, Hungary, 1984,* Lecture Notes in Physics Vol. 217, edited by Gy. Hutiray and J. Sólyom (Springer, Berlin), p. 412.
Janossy, A., G. Mihály, G. Pekker, and S. Roth, 1987, Solid State Commun. **61**, 33.
Javadi, H. H., S. Sridhar, G. Grüner, L. Chiang, and F. Wudl, 1986, Phys. Rev. Lett. **55**, 1216.
Jensen, M. H., P. Bak, and T. Bohr, 1984, Phys. Rev. A **30**, 1960.
Johnston, D., 1984, Phys. Rev. Lett. **52**, 2049.
Johnston, D., M. Maki, and G. Grüner, 1985, Solid State Commun. **53**, 5.
Johnston, D. C., J. P. Stokes, P. L. Hsieh, and G. Grüner, 1983, J. Phys. (Paris), Colloq. **44**, C3-1749.
Jonscher, A. K., 1977, Nature (London) **267**, 673.
Joos, B., and D. Murray, 1984, Phys. Rev. B **29**, 1094.
Kalem, C. B., N. P. Ong, and J. C. Eckert, 1987, unpublished.
Kantz, R. L., 1981, J. Appl. Phys. **52**, 6241.
Kawabata, K., M. Ido, and T. Sambongi, 1981, J. Phys. Soc. Jpn. **50**, 739.
Kim, T. W., W. P. Beyermann, and G. Grüner, 1987, unpublished.
Kinzel, W., 1983, Phys. Rev. Lett. **51**, 1787.
Klemm, R. A., and M. O. Robbins, 1986, Physica B **143**, 76.
Klemm, R. A., and J. R. Schrieffer, 1983, Phys. Rev. Lett. **51**, 47.
Klemm, R. A., and J. R. Schrieffer, 1984, Phys. Rev. Lett. **52**, 482.
Kogoj, M., S. Zumer, and R. Brinz, 1984, J. Phys. C **17**, 2415.
Kohlrausch, R., 1947, Ann. Phys. (Leipzig) **12**, 393.
Kriza, G., A. Janossy, and G. Mihály, 1985, in *Charge Density Waves in Solids, Proceedings of the International Conference Held in Budapest, Hungary, 1984,* Lecture Notes in Physics Vol. 217, edited by Gy. Hutiray and J. Sólyom (Springer, Berlin), p. 426.
Kriza, G., and G. Mihály, 1986, Phys. Rev. Lett. **56**, 2529.
Kriza, G., S. Pekker, and K. Kamaras, 1987, Europhys. Lett. **3**, 1027.
Kuper, C. G., 1955, Proc. R. Soc. London, Ser. A **227**, 214.
Lacoe, R., H. J. Schulz, D. Jerome, K. Bechgaard, and J. Johannsen, 1986, Phys. Rev. Lett. **55**, 2351.
Latyshev, Yu. T., V. E. Mihakova, Ya. S. Savitshaya, and V. V. Frolov, 1986, Physica B **143**, 155.
Latyshev, Yu. T., V. E. Minakova, and Yu. A. Rzhakov, 1987, Pis'ma Zh. Eksp. Teor. Fiz. **46**, 31 [JETP Lett. **46**, 37].
Latyshev, Yu. T., and Ya. S. Savitskaya, 1986, Physica B **143**, 180.
Latyshev, Yu. I., Ya. S. Savitskaya, and V. V. Frolov, 1984, Pis'ma Zh. Eksp. Teor. Fiz. **40**, 72 [JETP Lett. **40**, 807 (1984)].
Lee, P. A., and H. Fukuyama, 1972, Phys. Rev. B **17**, 542.
Lee, P. A., and T. M. Rice, 1979, Phys. Rev. B **19**, 3970.
Lee, P. A., T. M. Rice, and P. W. Anderson, 1973, Phys. Rev. Lett. **31**, 462.
Lee, P. A., T. M. Rice, and P. W. Anderson, 1974, Solid State Commun. **14**, 703.
Lindelof, P. E., 1981, Rep. Prog. Phys. **44**, 949.
Link, B., and G. Mozurkewich, 1988, unpublished.
Littlewood, P. B., 1986, Phys. Rev. B **33**, 6694.
Littlewood, P. B., 1987, Phys. Rev. B **36**, 3108.
Littlewood, P. B., 1988, Solid State Commun. **65**, 1347.
Littlewood, P. B., S. Coppersmith, and D. Fisher, 1988, unpublished.
Littlewood, P. B., and T. M. Rice, 1982, Phys. Rev. Lett. **48**, 44.
Liu, S., and L. Sneddon, 1987, Phys. Rev. B **35**, 7745.
Longcor, S., 1981, Ph.D. thesis (University of California, Berkeley).
Lyding, J. W., J. S. Hubacek, G. Gammie, and R. E. Thorne, 1986, Phys. Rev. B **33**, 4341.
Lyons, W. G., R. E. Thorne, J. H. Miller, and J. R. Tucker, 1985, Phys. Rev. B **31**, 6797.
MacDonald, A. H., and M. Plisbke, 1983, Phys. Rev. B **27**, 201.
Maeda, A., T. Furuyama, and S. Tanaka, 1985, Solid State Commun. **55**, 8156.
Maeda, A., T. Furuyama, and S. Tanaka, 1986, Solid State Commun. **55**, 951.
Maeda, A., T. Furuyama, K. Uchinokura, and S. Tanaka, 1986, Physica B **143**, 123.
Maeda, A., M. Naito, and S. Tanaka, 1983, Solid State Commun. **47**, 1001.
Maeda, A., M. Naito, and S. Tanaka, 1985, J. Phys. Soc. Jpn. **54**, 1912.
Maki, K., 1977, Phys. Rev. Lett. **39**, 46.
Maki, K., 1978, Phys. Rev. B **18**, 1641.
Maki, K., 1985, in *Electronic Properties of Inorganic Quasi-One-Dimensional Compounds,* Part I, edited by P. Monceau (Reidel, Dordrecht/Boston/Lancaster), p. 125.
Maki, K., 1986, Physica B **143**, 59.
Maki, K., and A. Virosztek, 1987, Phys. Rev. B **36**, 2910.
Matsukawa, H., and H. Takayama, 1984, Solid State Commun. **50**, 283.
Matsukawa, H., and H. Takayama, 1986, Physica B **143**, 80.
Meerschaut, A., 1983, J. Phys. (Paris), Colloq. **44**, C3-1615.
Mihály, G., P. Beauchene, J. Marcus, J. Dumas, and C. Schlenkas, 1988, Phys. Rev. B **37**, 1097.
Mihály, G., Gy. Hutiray, and L. Mihály, 1983, Phys. Rev. B **28**, 4896.
Mihály, G., G. Kriza, and A. Janossy, 1984, Phys. Rev. B **30**, 3578.

Mihály, G., and L. Mihály, 1984, Phys. Rev. Lett. **52**, 149.
Mihály, G., L. Mihály, and H. Mutka, 1984, Solid State Commun. **49**, 1009.
Mihály, L., Ting Chen, B. Alavi, and G. Grüner, 1985, *Charge Density Waves in Solids, Proceedings of the International Conference Held in Budapest, Hungary, 1984,* Lecture Notes in Physics Vol. 217, edited by Gy. Hutiray and J. Sólyom (Springer, Berlin), p. 455.
Mihály, L., T. Chen, and G. Grüner, 1987, Solid State Commun. **61**, 751.
Mihály, L., M. Crommie, and G. Grüner, 1987, Europhys. Lett. **4**, 103.
Mihály, L., and G. Grüner, 1984, Solid State Commun. **50**, 807.
Mihály, L., and G. Grüner, 1987, in *Nonlinearity in Condensed Matter,* Springer Series in Solid-State Sciences Vol. 69, edited by A. R. Bishop, D. K. Campbell, P. Kumar, and S. E. Trullinger (Springer, Berlin), p. 308.
Mihály, L., Ki-Bong Lee, and P. W. Stephens, 1987, Phys. Rev. B **36**, 1793.
Mihály, L., G. Mihály, and A. Janossy, 1985, in *Charge Density Waves in Solids, Proceedings of the International Conference Held in Budapest, Hungary, 1984,* Lecture Notes in Physics Vol. 217, edited by Gy. Hutiray and J. Sólyom (Springer, Berlin), p. 404.
Mihály, L., and G. Y. Tessema, 1986, Phys. Rev. B **33**, 5858.
Miller, J. H., J. Richard, R. E. Thorne, W. G. Lyons, J. R. Tucker, and John Bardeen, 1984, Phys. Rev. B **29**, 2328.
Miller, J. H., J. Richard, J. R. Tucker, and John Bardeen, 1983, Phys. Rev. **51**, 1592.
Miller, J. H., R. E. Thorne, W. G. Lyons, J. R. Tucker, and John Bardeen, 1985, Phys. Rev. B **31**, 5229.
Monceau, P., 1980, in *Electronic Properties of Inorganic Quasi-One-Dimensional Materials,* edited by P. Monceau (Reidel, Dordrecht/Boston/Lancaster).
Monceau, P., 1982, Physica B **109**, 1890.
Monceau, P., 1985, in *Electronic Properties of Inorganic Quasi-One-Dimensional Compounds, Part II,* edited by P. Monceau (Reidel, Dordrecht/Boston/Lancaster), p. 139
Monceau, P., 1986, in *Properties of Inorganic Quasi-One-Dimensional Materials,* Vol. II, edited by P. Monceau (Reidel, Holland).
Monceau, P., N. P. Ong, A. M. Portis, A. Meerschaut, and J. Rouxel, 1976, Phys. Rev. Lett. **37**, 6902.
Monceau, P., M. Renard, J. Richard, and M. C. Saint-Lager, 1986, Physica B **143**, 64.
Monceau, P., M. Renard, J. Richard, M. C. Saint-Lager, H. Salva, and Z. Z. Wang, 1983, Phys. Rev. B **28**, 1646.
Monceau, P., M. Renard, J. Richard, M. C. Saint-Lager, and Z. Z. Wang, 1985, in *Charge Density Waves in Solids, Proceedings of the International Conference Held in Budapest, Hungary, 1984,* Lecture Notes in Physics Vol. 217, edited by Gy. Hutiray and J. Sólyom (Springer, Berlin), p. 279.
Monceau, P., J. Richard, and M. Renard, 1980, Phys. Rev. Lett. **45**, 43.
Monceau, P., J. Richard, and M. Renard, 1982, Phys. Rev. B **25**, 931.
Moses, D., and R. M. Boysel, 1985, Phys. Rev. B **31**, 3202.
Mozurkewich, G., P. M. Chaikin, W. G. Clark, and G. Grüner, 1985a, Solid State Commun. **56**, 421.
Mozurkewich, G., P. M. Chaikin, W. G. Clark, and G. Grüner, 1985b, in *Charge Density Waves in Solids, Proceedings of the International Conference Held in Budapest, Hungary, 1984,* Lecture Notes in Physics Vol. 217, edited Gy. Hutiray and J. Sólyom (Springer, Berlin), p. 353.
Mozurkewich, G., and G. Grüner, 1983a, Phys. Rev. Lett. **51**, 2206.
Mozurkewich, G., and G. Grüner, 1983b, unpublished.
Mozurkewich, G., M. Maki, and G. Grüner, 1983, Solid State Commun. **48**, 5.
Mutka, H., S. Bouffard, J. Dumas, and C. Schlenker, 1984, J. Phys. Lett. **45**, L729.
Mutka, H., S. Bouffard, and L. Zuppiroli, 1985, in *Charge Density Waves in Solids, Proceedings of the International Conference Held in Budapest, Hungary, 1984,* Lecture Notes in Physics Vol. 217, edited by Gy. Hutiray and J. Sólyom (Springer, Berlin), p. 55.
Nad, F. Ya., 1985, in *Charge Density Waves in Solids, Proceedings of the International Conference Held in Budapest, Hungary, 1984,* Lecture Notes in Physics Vol. 217, edited by Gy. Hutiray and J. Sólyom (Springer, Berlin), p. 286.
Nerenberg, M. A., T. A. Blackburn, and S. Vik, 1984, Phys. Rev. B **30**, 5084.
Ng, H. K., G. A. Thomas, and L. F. Schneemeyer, 1986, Phys. Rev. B **33**, 8755.
Ngai, K. L., 1979, Comments Solid State Phys. **9**, 127.
Ngai, K. L., 1980, Comments Solid State Phys. **9**, 141.
Nomura, K., T. Sambongi, K. Kume, and M. Sato, 1986, Physica B **143**, 117.
Oda, M., and M. Ido, 1982, Solid State Commun. **44**, 1535.
Oda, M., and M. Ido, 1985, Solid State Commun. **50**, 879.
Ong, N. P., 1982, Can. J. Phys. **60**, 757.
Ong, N. P., 1983, J. Phys. (Paris), Colloq. **44**, C3-1659.
Ong, N. P., and J. W. Brill, 1978, Phys. Rev. B **18**, 5265.
Ong, N. P., J. W. Brill, J. C. Eckert, J. W. Savage, S. K. Khanna, and R. B. Somoano, 1979, Phys. Rev. Lett. **42**, 811.
Ong, N. P., D. D. Duggan, C. B. Kalem, T. W. Jing, and P. A. Lee, 1985, in *Charge Density Waves in Solids, Proceedings of the International Conference Held in Budapest, Hungary, 1984,* Lecture Notes in Physics Vol. 217, edited by Gy. Hutiray and J. Sólyom (Springer, Berlin), p. 387.
Ong, N. P., and C. Gould, 1981, Solid State Commun. **37**, 25.
Ong, N. P., C. B. Kalem, and J. C. Eckert, 1984, Phys. Rev. B **30**, 2902.
Ong, N. P., and K. Maki, 1985, Phys. Rev. B **32**, 6582.
Ong, N. P., and P. Monceau, 1977, Phys. Rev. B **16**, 3443.
Ong, N. P., and P. Monceau, 1978, Solid State Commun. B **26**, 487.
Ong, N. P., G. X. Tessema, G. Varma, J. C. Eckert, J. Savage, and S. K. Khanna, 1982, Mol. Cryst. Liq. Cryst. **81**, 41.
Ong, N. P., and G. Verma, 1983, Phys. Rev. B **27**, 4495.
Ong, N. P., G. Verma, and M. Maki, 1984, Phys. Rev. Lett. **52**, 663.
Osada, T., N. Miura, and G. Saito, 1987, Solid State Commun. **60**, 441.
Palmer, R. G., D. L. Stein, E. Abrahams, and P. W. Anderson, 1984, Phys. Rev. Lett. **53**, 958.
Peierls, R. E., 1955, *Quantum Theory of Solids* (Oxford University, New York/London).
Phillip, A., A. Mayr, T. W. Kim, and G. Grüner, 1987, Solid State Commun. **62**, 521.
Pietronero, L., and S. Strässler, 1983, Phys. Rev. B **28**, 5863.
Portis, A. M., 1982, Mol. Cryst. Liq. Cryst. **81**, 59.
Pouget, J. P., S. Kagoshima, C. Schlenker, and J. Marcus, 1983, J. Phys. (Paris) Lett. **44**, L-113.
Pouget, J. P., A. H. Moudden, R. Moret, C. Escribe-Filippini, B. Mannion, J. Marcus, and C. Schlenker, 1985, in *Charge Density Waves in Solids, Proceedings of the International Conference Held in Budapest, Hungary, 1984,* Lecture Notes in

Physics, Vol. 217, edited by Gy. Hutiray and J. Sólyom (Springer, Berlin).
Prester, M., 1985, Phys. Rev. B **32**, 2621.
Reagor, D., 1987, Ph.D. thesis (University of California, Los Angeles).
Reagor, D., and G. Grüner, 1986, Phys. Rev. Lett. **56**, 659.
Reagor, D., and G. Mozurkewich, 1988, unpublished.
Reagor, D., S. Sridhar, and G. Grüner, 1985, in *Charge Density Waves in Solids, Proceedings of the International Conference Held in Budapest, Hungary, 1984,* Lecture Notes in Physics Vol. 217, edited by Gy. Hutiray and J. Sólyom (Springer, Berlin), p. 308.
Reagor, D., S. Sridhar, and G. Grüner, 1986, Phys. Rev. B **34**, 2212.
Reagor, D., S. Sridhar, M. Maki, and G. Grüner, 1985, Phys. Rev. B **32**, 8445.
Rice, M. J., 1975, in *Low Dimensional Cooperative Phenomena,* edited by J. Keller (Plenum, New York).
Rice, M. J., and S. Strässler, 1973, Solid State Commun. **13**, 1389.
Richard, J., P. Monceau, M. Popoular, and M. Renard, 1982, J. Phys. C **15**, 7157.
Richard, J., P. Monceau, and M. Renard, 1982, Phys. Rev. B **25**, 948.
Richard, J., R. E. Thorne, W. G. Lyons, J. H. Miller, and J. R. Tucker, 1984, Solid State Commun. **52**, 183.
Robbins, M., and R. M. Klemm, 1986, Phys. Rev. B **34**, 8496.
Ross, J. H., Z. Wang, and C. P. Slichter, 1986, Phys. Rev. Lett. **56**, 663.
Roucau, C., 1983, J. Phys. (Paris), Colloq. **44**, C3-1725.
Rouxel, J., 1982, Mol. Cryst. Liq. Cryst. **81**, 31.
Salva, H., Z. Z. Wong, P. Monceau, J. Richard, and M. Renard, 1984, Philos. Mag. **49**, 385.
Saso, T., Y. Suzumura, and H. Fukuyama, 1984, in *Proceedings of the 17th International Conference on Low Temperature Physics,* edited by V. Eckern, A. Schmid, W. Weber, and H. Wühl (North-Holland, Amsterdam), p. 1345.
Sato, M., H. Fujishita, and S. Hoshino, 1983, J. Phys. C **16**, L877.
Schlenker, C., and J. Dumas, 1986, in *Crystal Chemistry and Properties of Materials with Quasi-One-Dimensional Structures,* edited by J. Rouxel (Reidel, Dordrecht/Boston/Lancaster).
Schlesinger, M. I., and E. W. Montroll, 1984, Proc. Nat. Acad. Sci. U.S.A. **81**, 1280.
Schneemeyer, L. F., R. M. Fleming, and S. E. Spengler, 1984, Bull. Am. Phys. Soc. **29**, 357.
Schneemeyer, L. F., R. M. Fleming, and S. E. Spengler, 1985, Solid State Commun. **53**, 505.
Seeger, K., 1985, Solid State Commun. **53**, 219.
Seeger, K., W. Mayr, and A. Phillip, 1982, Solid State Commun. **43**, 113.
Seeger, K., A. Phillip, and W. Mayr, 1984, Solid State Commun. **50**, 223.
Seeger, K., A. Phillip, and W. Mayr, 1985, Mol. Cryst. Liq. Cryst. **120**, 55.
Ségranson, P., A. Jánossy, C. Berthier, J. Marcus, and P. Butaud, 1986, Phys. Rev. Lett. **56**, 1854.
Sham, L. J., and B. R. Patton, 1976, Phys. Rev. B **13**, 2151.
Shapiro, S., 1963, Phys. Rev. Lett. **11**, 80.
Sherwin, M., R. Hall, and A. Zettl, 1984, Phys. Rev. Lett. **53**, 1387.
Sherwin, M., and A. Zettl, 1985, Phys. Rev. B **32**, 5536.
Sneddon, L., 1984a, Phys. Rev. B **30**, 2979.
Sneddon, L., 1984b, Phys. Rev. B **29**, 719.
Sneddon, L., 1984c, Phys. Rev. Lett. **52**, 65.
Sneddon, L., 1986, Phys. Rev. Lett. **55**, 1194.
Sneddon, L., M. Cross, and D. Fisher, 1982, Phys. Rev. Lett. **49**, 292.
Sneddon, L., and K. Lox, 1987, Phys. Rev. Lett. **58**, 1903.
Sokoloff, J.B., 1981, Phys. Rev. B **23**, 1992.
Sokoloff, J. B., and B. Horovitz, 1983, J. Phys. (Paris), Colloq. **44**, C3-1667.
Sólyom, J., 1979, Adv. Phys. **28**, 201.
Sridhar, S., D. Reagor, and G. Grüner, 1986, Phys. Rev. B **34**, 2223.
Stokes, J. P., S. Bhattacharya, and A. N. Bloch, 1987, Phys. Rev. B **34**, 8944.
Stokes, J. P., A. N. Bloch, and G. Grüner, 1983, Bull. Am. Phys. Soc. **28**, 426.
Stokes, J. P., A. N. Bloch, A. Janossy, and G. Grüner, 1984, Phys. Rev. Lett. **52**, 372.
Stratonovich, R. L., 1958, Radiotekh. Elektron. **3**, 497.
Suzuki, A., H. Mizubayashi, S. Okuda, and M. Doyama, 1986, Physica B **143**, 161.
Takada, S., M. Wong, and T. Holstein, 1985, in *Charge Density Waves in Solids, Proceedings of the International Conference Held in Budapest, Hungary, 1984,* Lecture Notes in Physics Vol. 217, edited by Gy. Hutiray and J. Sólyom (Springer, Berlin), p. 227.
Talopov, A. L., 1981, Zh. Eksp. Teor. Fiz. **81**, 1890 [JETP Lett. **54**, 1001 (1981)].
Tamegai, T., K. Tsutsumi, S. Kagoshima, Y. Kanai, M. Tani, H. Tomozawa, M. Sato, K. Tsuji, J. Harada, M. Sakata, and T. Nakajima, 1985, Solid State Commun. **56**, 13.
Tami, M., Y. Nogami, and M. Sato, 1985, Solid State Commun. **56**, 13.
Tanaka, S., and K. Uchinokura, 1986, Eds., *Physics and Chemistry of Quasi-One-Dimensional Conductors,* Proceedings of the Yamada Conference XV (Physica B **143**).
Tang, C., K. Wisenfeld, Per Bak, S. Coppersmith, and P. Littlewood, 1987, Phys. Rev. Lett. **58**, 1161.
Teranishi, N., and R. Kubo, 1979, J. Phys. Soc. Jpn. **47**, 720.
Tessema, G. X., B. Alavi, and L. Mihály, 1985, Phys. Rev. B **31**, 6878.
Tessema, G. X., and L. Mihály, 1987, Phys. Rev. B **35**, 7680.
Tessema, G. X., and N. P. Ong, 1981, Phys. Rev. B **23**, 5607.
Tessema, G. X., and N. P. Ong, 1983, Phys. Rev. B **27**, 1427.
Tessema, G. X., and N. P. Ong, 1985, Phys. Rev. B **31**, 1055.
Testardi, J., 1975, Phys. Rev. B **12**, 3849.
Thompson, A. N., A. Zettl, and G. Grüner, 1981, Phys. Rev. Lett. **47**, 64.
Thorne, R. E., W. G. Lyons, J. H. Miller, Jr., J. W. Lyding, and J. R. Tucker, 1986, Phys. Rev. B **34**, 5988.
Thorne, R. E., W. G. Lyons, J. H. Miller, Jr., J. Richard, and J. R. Tucker, 1984, Solid State Commun. **50**, 833.
Thorne, R. E., J. R. Tucker, and John Bardeen, 1987, Phys. Rev. Lett. **58**, 828.
Travaglini, G., I. Mörkee, and P. Wachter, 1983, Solid State Commun. **45**, 289.
Travaglini, G., and P. Wachter, 1984, Phys. Rev. B **30**, 1971.
Tsang, J. C., C. Herman, and M. W. Shafer, 1978, Phys. Rev. Lett. **40**, 1528.
Tsutsumi, K., T. Sambongi, S. Kagoshima, and T. Ishiguro, 1978, J. Phys. Soc. Jpn. **44**, 1735.
Tua, P. F., and J. Ruvalds, 1984, Solid State Commun. **51**, 293.
Tua, P. F., and J. Ruvalds, 1985, Solid State Commun. **54**, 471.
Tua, P. F., and A. Zawadowski, 1984, Solid State Commun. **49**, 19.

Tucker, J. R., 1979, IEEE J. Quantum Electron. **15**, 1234.
Tucker, J. R., 1986, Phyisca B **143**, 19.
Tucker, J. R., W. G. Lyons, J. M. Miller, R. E. Thorne, and J. W. Lyding, 1986, Phys. Rev. B **34**, 9038.
Tucker, J. R., J. M. Miller, K. Seeger, and John Bardeen, 1981, Phys. Rev. B **25**, 2979.
Tüttő, I., and A. Zawadowski, 1985, Phys. Rev. B **32**, 2449.
Underweiser, M., M. Maki, B. Alavi, and G. Grüner, 1987, Solid State Commun. **64**, 181.
Verma, G., N. P. Ong, S. K. Khanna, J. C. Eckert, and J. W. Savage, 1983, Phys. Rev. B **28**, 910.
Voss, R. F., and R. A. Webb, 1981, Phys. Rev. Lett. **47**, 265.
Wada, S., R. Aoki, and O. Fujita, 1984, J. Phys. F **14**, 1515.
Wang, Z. Z., P. Monceau, M. Renard, P. Gressier, L. Guemas, and A. Meerschaut, 1983, Solid State Commun. **47**, 439.
Wang, Z. Z., and N. P. Ong, 1986, Physica B **143**, 100.
Wang, Z. Z., and N. P. Ong, 1987, Phys. Rev. B **34**, 5967.
Wang, Z. Z., M. C. Saint-Lager, P. Monceau, M. Renard, P. Gressier, A. Meerschaut, L. Guemas, and J. Rouxel, 1983, Solid State Commun. **46**, 325.
Wang, Z. Z., K. Salva, P. Monceau, M. Renard, C. Roucau, R. Ayroles, F. Levy, L. Guemas, and A. Meerschaut, 1983, J. Phys. (Paris) Lett. **44**, L311.
Weger, M., W. G. Clark, and G. Grüner, 1983, J. Phys. (Paris), Colloq. **44**, C3-1673.
Weger, M., G. Grüner, and W. G. Clark, 1980, Solid State Commun. **35**, 243.
Weger, M., G. Grüner, and W. G. Clark, 1982, Solid State Commun. **44**, 1179.
Weisz, J. F., J. B. Sokoloff, and J. E. Sacco, 1979, Phys. Rev. B **20**, 4713.
Williams, G., and D. C. Watts, 1970, Trans. Faraday Soc. **66**, 80.
Wilson, J. A., 1979, Phys. Rev. B **19**, 6456.
Wilson, J. A., F. J. DiSalvo, and S. Mahajan, 1975, Adv. Phys. **24**, 117.
Wong, K. Y. M., and S. Takada, 1987, Phys. Rev. B **36**, 5476.
Wonneberger, W., 1979, Solid State Commun. **30**, 511.
Wonneberger, W., 1983a, Z. Phys. B **50**, 23.
Wonneberger, W., 1983b, Z. Phys. B **53**, 167.
Wonneberger, W., 1985, Solid State Commun. **54**, 317.
Wonneberger, W., and H.-J. Breymayer, 1981, Z. Phys. B **43**, 329.
Wonneberger, W., and H.-J. Breymayer, 1984, Z. Phys. B **56**, 241.
Wu, Wei-yu, A. Janossy, and G. Grüner, 1984, Solid State Commun. **49**, 1013.
Wu, Wei-yu, L. Mihály, and G. Grüner, 1985, Solid State Commun. **55**, 663.
Wu, Wei-yu, L. Mihály, G. Mozurkewich, and G. Grüner, 1986, Phys. Rev. B **33**, 2444.
Wu, Wei-yu, G. Mozurkewich, L. Mihály, and G. Grüner, 1984, Phys. Rev. Lett. **52**, 2382.
Wu, Wei-yu, G. Mozurkewich, L. Mihály, and G. Grüner, 1986, Phys. Rev. B **33**, 2444.
Xiang, X. D., and J. W. Brill, 1987, Phys. Rev. B **36**, 2969.
Xiang, X. D., and J. W. Brill, 1988, unpublished.
Yeh, W. J., Da-Rem He, and Y. H. Kao, 1984, Phys. Rev. Lett. **52**, 480.
Zawadowski, A., I. Tüttő, S. E. Barnes, P. F. Tua, and J. Ruvalds, 1985, in *Charge Density Waves in Solids, Proceedings of the International Conference Held in Budapest, Hungary, 1984,* Lecture Notes in Physics Vol. 217, edited by Gy. Hutiray and J. Sólyom (Springer, Berlin), p. 240.
Zeller, H. R., 1974, in Low-Dimensional Cooperative Phenomena, NATO Advanced Study Institutes Series, Vol. 7, edited by H. J. Keller (Plenum, New York), p. 215.
Zettl, A., 1983a, Ph.D. thesis (University of California, Los Angeles).
Zettl, A., 1983b, Proceedings of the International Symposium on Nonlinear Transport in Inorganic Quasi-One-Dimensional Conductors, Sapporo, Japan (unpublished).
Zettl, A., and G. Grüner, 1982a, Phys. Rev. B **26**, 2298.
Zettl, A., and G. Grüner, 1982b, Phys. Rev. B **25**, 2081.
Zettl, A., and G. Grüner, 1983a, Phys. Rev. B **28**, 2091.
Zettl, A., and G. Grüner, 1983b, Solid State Commun. **46**, 501.
Zettl, A., and G. Grüner, 1983c, Solid State Commun. **46**, 29.
Zettl, A., and G. Grüner, 1984, Phys. Rev. B **29**, 755.
Zettl, A., and G. Grüner, 1986, Comments Condens. Matter Phys. **12**, 265.
Zettl, A., G. Grüner, and A. H. Thompson, 1982, Phys. Rev. B **26**, 5760.
Zettl, A., C. M. Jackson, and G. Grüner, 1982, Phys. Rev. B **26**, 5773.
Zettl, A., M. B. Kaiser, and G. Grüner, 1984, Bull. Am. Phys. Soc.
Zettl, A., M. B. Kaiser, and G. Grüner, 1985, Solid State Commun. **53**, 649.
Zeyher, R., 1988, unpublished.
Zhang, X. J., and N. P. Ong, 1985, Phys. Rev. Lett. **55**, 2919.
Zhang, X. J., N. P. Ong, and J. C. Eckert, 1986, Phys. Rev. Lett. **56**, 1206.